

Standardisierung der Energieertrags- prognose für solarthermische Kraftwerke (SESK)

AP 7300 MATCH model based aerosol information

Marion Schroedter-Homscheidt, Andreas Hartmann

April 15, 2009

**Gefördert durch das Bundesministerium für Umwelt,
Naturschutz und Reaktorsicherheit (BMU)**



DLR

**Deutsches Zentrum
für Luft- und Raumfahrt e.V.**
in der Helmholtz-Gemeinschaft



Table of Content

1	SUMMARY	5
2	INTRODUCTION	9
3	MODEL DESCRIPTION MATCH V4.2.....	9
3.1	Aerosol physics and chemistry	9
3.2	Input data.....	11
3.3	Transport scheme	15
3.4	Emission data bases.....	16
3.4.1	SOx emission data base.....	16
3.4.2	DMS emissions	18
3.4.3	Carbonaceous emissions	18
3.4.4	Sea salt	24
3.5	Dust emissions and model	24
3.6	Stratospheric aerosols	26
3.7	Aerosol optical depth.....	27
4	AVAILABLE DATASETS.....	27
4.1	NCAR/MATCH-MODIS	27
4.2	DLR/MATCH 2004	28
4.3	AERONET validation data.....	28
5	VALIDATION OF AEROSOL OPTICAL DEPTH	28
5.1	NCAR/MATCH-MODIS	28
5.1.1	General validation	28
5.1.2	High sulfate AOD value problem.....	29
5.1.3	Mediterranean Region	32
5.1.4	Overestimation in dust AOD.....	33
5.1.5	Africa	38
5.1.6	Asia	40
5.1.7	Post processing.....	42
5.1.8	Comparison with GACP climatology.....	45
5.2	DLR/MATCH 2004	50
5.2.1	Assimilation impact	50
5.2.2	Post processing.....	54
5.2.3	Hourly variability	55

5.3	DLR/MATCH 2004 Regional Validation	57
5.3.1	Central Europe	58
5.3.2	Mediterranean Region	58
5.3.3	Arabian Peninsula	63
5.3.4	Africa	66
5.3.5	Asia	68
6	REFERENCES.....	72
7	ABBREVIATIONS.....	75
8	ANNEX A – AERONET STATIONS.....	76

1 Summary

Previous work shows, that the atmospheric aerosol extinction can reach up to 30% of the incoming direct irradiance. Therefore, accurate knowledge about the variable aerosol concentration and composition in high temporal and spatial resolution is needed for the yield assessment of solar thermal power plants. Today, climatological monthly means in approx. $4 \times 5^\circ$ spatial resolution are used typically in satellite-based irradiance calculation schemes.

In the aerosol community, numerical modelling of the aerosol composition is a state of the art approach. Even if exact modelling remains an ongoing question of research, it is the objective of this report to evaluate the existing state of the art for solar energy purposes.

Therefore, this report analyses the capabilities of the Model of Atmospheric Transport and Chemistry (MATCH, Collins et al., 2001), provides a description of the model structure, summarizes the physical and chemical processes, and visualizes all emission data bases used. Special focus is laid on the Dust Entrainment and Deposition model (DEAD, Zender et al., 2003).

MATCH provides the modelling of column aerosol optical depth of several aerosol types as sulfate, organics, soot, dust, and sea salt. It includes emission databases for seasonal sulfur emissions on 0 and 100 m height for 1990 and 2005, monthly mean surface DMS emissions, monthly mean biomass burning black and organic carbon fluxes, monthly mean natural organic carbon fluxes from terpene emissions, fossil fuel black and organic carbon surface fluxes and an explicit dust mobilisation scheme (DEAD). The DEAD model describes dust emissions produced by the saltation process as a function of surface layer wind speed and an erodibility which depends spatially, is reduced in case of seasonal vegetation and modified according to the clay fraction in the underlying ground. Physical and chemical processes include a flux-form Semi-Lagrange advection description, convective and turbulent transport, dry and wet deposition, cloud-aerosol interactions, the sulfur cycle, ageing, particle size transformation, and hygroscopic growth. It is a global offline model with a spatial resolution driven by meteorological input fields (1.9° Gaussian grid used in this study, up to 0.7° was tested at NCAR). The temporal resolution is set to 30 minutes and even 2 minutes in the sulfur chemistry sub-cycle. It can be applied both for long-term data set generation (analysis) and forecasting.

The report deals with two different data sets. The NCAR/MATCH-MODIS dataset was derived by Fillmore (2005) and provided by NCAR to DLR for further use in solar energy activities. It provides daily global 12 UTC aerosol fields for the period 2000-2005 on the 1.9° Gaussian grid used by the NCEP reanalysis project. This dataset provides AOD at 550 nm and is based on the assimilation of MODIS level 3 daily gridded AOD. The DLR/MATCH dataset was processed within this study. It covers the period from 1.1. to 31.12.2004. It uses DLR/MATCH v4.2 in a 1.9° spatial resolution and provides AOD at 550 nm in hourly temporal resolution. There was no assimilation scheme applied for this dataset. This data set will act as a reference dataset for further DLR internal development on MATCH.

First, this summary reports on the validation of the NCAR/MATCH-MODIS dataset. A total number of 10800 coincidences are analysed from 79 stations in Europe and Africa. Additionally, 21 stations in Asia are available. The overall MBD is 0.06 with a RMSD of 0.24 and a Pearson correlation coefficient $r = 0.62$. Generally, a good agreement within 0.1 is observed for a majority of all cases. A remarkable scatter can be observed as well and is analysed deeper. In Central Europe a peak-like structured overestimation of AOD caused by the sulfate component can be observed. This seems to be an artefact caused by the MODIS assimilation scheme. For the western Mediterranean region (Spain, Portugal) a good agreement is found, while stations in the eastern Mediterranean region and Italy frequently show also a peak-like overestimation, but in the dust component. This occurs also on the Arabian Peninsula, but is not observed at the Afri-

can stations. Case studies show that these overestimations result from a few large scale long-range transport cases in the Eastern Mediterranean, while on the Arabian Peninsula overestimations are observed typically in short-range transport cases. A further validation based on several years is needed to decide if this is a general issue in these regions or if a few extreme cases show up in 2004. The regional dependency of overestimations and the lack of such effects in other regions like Western Africa or the Western Mediterranean point towards deficiencies in the underlying erodibility databases, while the general transport and deposition parameterisation seem to be appropriate.

A post processing was empirically developed based on 2003 data to detect and eliminate these peak-like overestimations automatically. Suspicious dust events are removed if a strong temporal gradient in the dust component from day to day above 0.7 is observed or if the AOD value is above 1.0 with at least a 95% dust contribution. Suspicious sulfate events are removed, if a temporal gradient in the sulfate component from day to day above 0.4 is detected. Flagged values are replaced by linearly interpolated values and finally, a 3 days low pass filter is applied. The post processing procedure is developed on the basis of 2003 data and reduces the RMSD from 0.21 to 0.17 and improves the correlation coefficient from 0.57 to 0.63. For 2004 the MBD is reduced from 0.06 to 0.04, the RMSD is reduced from 0.24 to 0.2 and the correlation coefficient increases from 0.62 to 0.67. Similar improvements can also be found for 2005. In Europe a general reduction in MBD and RMSD can be observed at all stations. In the Mediterranean, several stations show a positive impact, while the remaining stations are not influenced. This is mainly due to missing AERONET measurements in cases of removed peaks. On the Arabian Peninsula, a positive impact can be observed at 5 stations. For most stations, AERONET data is missing on those days with eliminated peaks. It can be speculated, that these peaks are realistic dust events leading to a false removal of the AERONET measurement by its own cloud detection. Such problems are well known for AERONET measurements and dust validation studies. Therefore, it cannot be decided if MATCH overestimates these peaks or not. Also, in Africa a positive impact can only be shown in Agoufou, while the other stations lack AERONET measurements in the relevant days.

Analysing AERONET measurements with a dust criterion following Dubovik et al. (2002) provides a statistic of dust cases reaching the Iberian Peninsula, the Mediterranean Islands and the North African coast. The maximum number of 34 days is observed in Blida, while Italy shows only between 2 and 5 dust days. On the Arabian Peninsula the maximum occurrence of dust events is 63 days, while values between 20 and 50 are common.

The work package aims at improved aerosol information compared to currently used aerosol climatologies as e.g. the GACP data base used for the SOLEMI database. Therefore, a validation of GACP versus AERONET is compared with this validation of NCAR/MATCH-MODIS versus AERONET. The GACP dataset shows large underestimations with MBD up to -0.5, while NCAR/MATCH-MODIS remains in a MBD between -0.1 and 0.1 for most stations. Generally, NCAR/MATCH-MODIS tends to slightly overestimate in the MBD. Especially, the correlation coefficient of NCAR/MATCH-MODIS is significantly higher than for the GACP dataset. Values above 0.7 are reached frequently, while GACP shows correlations coefficients below 0.5 or even negative.

A comparison of NCAR/MATCH-MODIS and DLR/MATCH versus AERONET allows assessing the impact of the MODIS assimilation. Generally, European stations show a negative assimilation impact as a result of the sulfate peaks discussed above. Some stations affected by dust outbreaks in the Mediterranean show a positive impact of the assimilation. The same holds for all African stations. On the Arabian Peninsula the MBD values are smaller in the 'no assimilation' case, but RMSD and correlation coefficient show also a positive assimilation impact.

Aerosol variability on the hourly scale is mainly related to hygroscopic growth and spatio-temporal gradients. A quantitative analysis of differences between minimum and maximum daily values in DLR/MATCH shows the value of hourly resolved aerosol modelling.

A further validation of the DLR/MATCH dataset for 2004 uses daily mean values based on the hourly output resolution chosen for DLR/MATCH.

The post processing scheme is still applied to remove suspicious dust events, while the sulfate criteria are not applied for this data set.

A dependency of validation results on station height can not be found.

Finally, it can be concluded that MATCH validation results show a clear improvement compared to the nowadays used GACP climatology. Europe, the Mediterranean and Africa have been modelled with sufficient accuracy. Further investigations on dust emission regions are also recommended to increase data quality on the Arabian Peninsula. The provision of a long-term data set for the SOLEMI database is recommended. A positive impact of the MODIS assimilation can be found in several regions, even if the approach used in the NCAR/MATCH-MODIS dataset results in a reduced data quality in Europe. Therefore, another approach should be applied to exclude sulfate overestimations.



2 Introduction

Concentrating solar power plants require sophisticated knowledge on direct normal irradiance reaching the surface. It is known from previous work (e.g. Wittmann et al., 2008; Gueymard, 2003) that atmospheric aerosol extinction can reach up to 30% of the incoming direct irradiance. Therefore, an accurate knowledge about the horizontal and temporal variability of aerosols is needed. Standard climatologies providing a 4 x 5° spatial resolution (approx. 400 x 500 km²) and monthly temporal resolution (as e.g. Tegen, 1997, Kinne et al. 2005, Schmidt et al. 2006) are not sufficient for this task. The horizontal scale length of aerosols is between 10 and 100 km and a significant variability in the range of hours to single days is typical.

Therefore, an enhanced modelling of atmospheric aerosols is needed. Numerical aerosol models have been developed by the air quality community in recent years. Among these, the NCAR-MATCH (Model of Atmospheric Transport and Chemistry, Collins et al., 2001) model provides

- column aerosol optical depth and not only aerosol mass concentrations at the ground level
- modelling of several aerosol types as sulfate, organics, soot, dust, and sea salt
- global modelling with a spatial resolution driven by the meteorological input fields and emission databases
- both a long-term analysis and options for forecasting
- a 30 minutes model time step

During a guest scientist visit at the National Center of Atmospheric Research (NCAR) a first evaluation of the MATCH model was performed. The model results available at NCAR (named NCAR/MATCH-MODIS dataset in this report) were originally used only to derive monthly averages for climate modelling purposes. It turned out, that they seem promising also for a daily analysis of the atmospheric aerosol state as needed for direct irradiance modelling purposes. A more detailed evaluation of this model is the purpose of this report.

DLR intends to include the output from a long-term MATCH model run covering 1984 – today as enhanced aerosol information into its SOLEMI (Solar Energy Mining) database providing global and direct normal irradiance in Europe, Africa, and Asia according to the METEOSAT satellite field of views (Meteosat prime and east mission).

3 Model Description MATCH v4.2

3.1 Aerosol physics and chemistry

Aerosol types

The **NCAR/MATCH** (Model of Atmospheric Transport and Chemistry, Collins et al., 2001; Fillmore, 2005; Rasch et al., 1997) is a three-dimensional global transport model predicting an external aerosol mixture containing sulfate, black and organic carbon, and mineral aerosols. Sea salt aerosols are treated only in the diagnosis mode without any transport. Nitrate aerosols are not taken into account.

Aerosols are treated as **external mixtures** of the basic aerosol types.

Sulfate, sea salt and carbonaceous aerosols are treated with a constant lognormal **aerosol size distribution**. Only the dust model operates with 4 dust bin sizes from 0.01-1, 1-20, 10-20, 20-

50 μm effective particle radius and a lognormal size distribution in each of the bins (tab. 3.1, section 3.7).

Dry **sulfate aerosols** are modelled with a geometric mean radius of 0.05 μm and a standard deviation of 2.03 μm .

Sea salt aerosols are modelled as an external mixture of the OPAC (Hess et al. 1998) coarse and accumulation mode sea salt particles with a mass ratio of 6:1. The coarse mode is described with a geometric mean radius of 1.75 μm and a standard deviation of 2.03 μm , while the accumulation mode has a geometric mean radius of 0.21 μm and the same standard deviation of 2.03 μm .

Organic carbonaceous aerosols are modelled with the size distribution of the OPAC water soluble component (geometric mean radius of 0.02 μm and a standard deviation of 2.24 μm), while **black carbon** is modelled with the size distribution of the OPAC soot component (geometric mean radius of 0.01 μm and a standard deviation of 2.0 μm).

Soluble aerosols as sulfate, sea-salt and organic carbon are a subject of **hygroscopic growth** which is modelled during the calculation of aerosol optical depths as a function of relative humidity and following the OPAC database.

An issue of growing concern in the solar energy community is the so called **'Atmospheric brown cloud'** – a layer of air pollution covering large areas e.g. in South Asia but also in other areas world wide affected by industrial production and human activities. Strong aerosol layers are well known in industrial areas as the Po valley in Italy or in US cities like Denver – mostly they occur due to a combination of **local emissions** and stationary **temperature inversion situations** blocking the turbulent mixture in the boundary layer.

After the Indian Ocean Experiment (INDOEX) it was realised that such a brown cloud can be observed not only regionally, but also on the **continental scale** in South Asia covering the Indian Ocean, India, Pakistan and large areas in China. An impact study by UNEP in 2002 raised attention towards this so called **'Asian brown cloud'**. A further impact study by UNEP in 2008 points out, that the problem of atmospheric brown clouds has regional hotspots in Eastern China, Pakistan, India, Bangladesh and Myanmar, Cambodia, Indonesia, Thailand and Vietnam as well as Southern Africa from sub-Saharan Africa into Angola, Zambia and Zimbabwe as well as the Amazon Basin in South America. Bangkok, Beijing, Dhaka, Karachi, Kolkata, Lagos, Mumbai, New Delhi, Seoul, Shanghai, Shenzhen as well as Cairo and Teheran have been identified as hot spots. In Karachi, Beijing, Shanghai and New Delhi a **dimming of solar irradiance** between 10 and 25% is observed. For China and India, an annual mean surface dimming of about 14-16 W/m^2 (-6%) is estimated for the period 2000 – 2007 as a direct aerosol effect. For India a trend of 2% per decade (-4.2 W/m^2) of dimming between 1960 and 2000 was observed, while the trend between 1980 and 2004 was accelerated up to -8 W/m^2 per decade. For China a dimming trend from the 1950s to the 90s of 3-4% per decade was recorded (Ramanathan et al., 2008). Indirect effects on increased cloudiness, reduced rain fall, increased air temperature, changes in regional weather systems like the monsoon and extreme rainfall, food production and health impacts are expected and further analysed in this report.

Recent research investigates emission sources for this large scale atmospheric pollution. **Sources from increased fossil fuel use, traffic, fertilizers used in agriculture, traditional bio-energy use (wood, dung) and industrial emissions are under investigation.** Nevertheless, a clear picture has not been reached, yet. Emission data bases used e.g. in MATCH show strongly increased emissions both in sulfate and carbonaceous aerosols in South Asia, but the validation in section 5.2.4.5 reveals that these databases cover the recent changes in the Asian economic development not appropriately.

Aerosol processes

Sources are described in section 3.4 (emission databases) and section 3.5 (dust model).

Besides advection, physical processes treated are convective and turbulent transport together with dry and wet deposition. Chemical processes as ageing and transformation are treated as well.

Dry deposition for sulfate and both, hydrophilic and hydrophobic carbonaceous aerosols is modelled with a constant deposition velocity of 0.2 cm/s for sulfate and 0.1 cm/s for carbon, while dust deposition by gravity and turbulent deposition is modelled as a function of dust bin size (Collins et al., 2001).

Wet deposition is modelled as below-cloud (through precipitation) and in-cloud scavenging (Rasch and Kristjansson, 1998). Particles can be re-emitted in case of an evaporating cloud or raindrop. Cloud amount is diagnosed from humidity, vertical motion, static stability and precipitation following the CCM3 scheme (Kiehl et al., 1998).

Cloud-aerosol interactions include aqueous-phase reactions for sulfate and a hygroscopic growth.

Boundary layer, turbulent eddy transport schemes and the hydrological cycle are the same as in the NCAR Community Atmosphere Model (CAM).

The **sulfur cycle** (Barth et al., 2000 and Rasch et al., 2000) includes sulfur emissions from biogenic and industrial sources (see below). Dimethyl sulfide (DMS, CH_3SCH_3) is produced in oceans by phytoplankton. Sulfur dioxide (SO_2) from fossil-fuel combustion and other industrial processes are described in an emission data base together with emissions of hydrogen sulphide (H_2S) from plants and soils, carbon disulfide (CS_2) from oceans and wetlands and carbonyl sulfide (OCS) from oceans and biomass burning. Sulfate is produced in an oxidation process from DMS and SO_x . A

Carbonaceous aerosols consist of black and organic carbon. Biomass burning sources (wood fuel, charcoal burning, dung, charcoal production, agricultural, savannah and forest fires) and fossil fuel burning sources are described for both black and organic carbon particles. Natural organic aerosols resulting from terpene emissions are included additionally. Following Cooke and Wilson, 1996, the carbonaceous aerosols are emitted in a hydrophobic form and age with a 1.2 day e-folding time to a hydrophilic form which can be washed out by wet deposition. There is no size bin resolved modelling of carbonaceous aerosols.

The **model time step** is set to 30 min for the advection, all physical and all chemical processes with exception of the sulfur sub-cycle time step of 2 minutes.

Computational demand

The model needs approx. 30 min cpu time per model day (1 model month = 15 hours cpu time, 1 model year = 8 cpu days, 10 model years = 76 cpu days, 25 model years (1984-2009) = 190 cpu days).

3.2 Input data

MATCH is an **offline transport model** using NCEP operational or reanalysis meteorological fields as meteorological driver every 6 hours, but not at each time step like an online model. The model has been operated in a 0.7, 1.4 or 1.9 deg resolution according to the NCEP operational model spectral resolution of T62L28 (1.9°), T126L42 (1.4°), or T170L42 (0.7°).

For the long-term datasets the **NCEP/NCAR reanalysis** (<http://dss.ucar.edu/pub/reanalysis/>) meteorological fields are used. The NCEP/NCAR reanalysis provides data back to 1.1.1948.

The NCEP/NCAR reanalysis dataset is available only as **T62L28** spectral truncation which refers to a resolution of 1.875° in longitudinal and approx. 1.9° in latitudinal direction (Gaussian grid with 192 x 94 grid points, fig. 3.1).

All three-dimensional parameters are given on 28 sigma levels at .9950, .9821, .9644, .9425, .9159, .8838, .8458, .8014, .7508, .6943, .6329, .5681, .5017, .4357, .3720, .3125, .2582, .2101, .1682, .1326, .1028, .0782, .0580, .0418, .0288, .0183, .0101, and .0027.

All values are instantaneous values at a specified time every 6 hours.

Tab. 3.1. NCEP/NCAR reanalysis model vertical structure (Kalnay et al., 1996)

TABLE 1. Model levels, midlevel sigma value, sigma thickness, geopotential thickness (m), and approximate location of the mandatory pressure levels (hPa).

Model level	Midlevel sigma	Delta sigma	Thickness	Mandatory pressure level
28	2.73	6.57	∞	3.0
27	10.06	7.29	5599	10.0
26	18.34	9.23	3828	20.0
25	28.75	11.60	3053	30.0
24	41.79	14.51	2621	
23	58.05	18.03	2342	50.0
22	78.15	22.22	2142	70.0
21	102.78	27.09	1984	100.0
20	132.61	32.62	1851	
19	168.23	38.67	1729	150.0
18	210.06	45.03	1612	200.0
17	258.23	51.35	1495	250.0
16	312.48	57.16	1376	300.0
15	372.05	61.97	1260	400.0
14	435.68	65.26	1139	
13	501.68	66.69	1017	500.0
12	568.09	66.06	895	
11	632.90	63.47	776	
10	694.26	59.19	664	700.0
9	750.76	53.72	560	
8	801.42	47.54	466	
7	845.79	41.15	384	850.0
6	883.84	34.93	313	
5	915.92	29.19	253	925.0
4	942.55	24.05	203	
3	964.37	19.59	162	
2	982.08	15.82	129	
1	995.00	10.00	80	1000.0

A short description following http://dss.ucar.edu/pub/reanalysis/rean_model.html (Kalnay et al., 1996): "The reanalysis is done at NCEP (formerly NMC) using T62 (209 km) global spectral model of 28 vertical levels. This is the same model used in the assimilation system, as implemented in the NCEP operational system in December 1994. The model has 5 levels in the boundary layer and about 7 levels above 100 hPa. The lowest model level is about 5 hPa from the surface, and the top level is at about 3 hPa. This vertical structure was chosen so that the boundary layer is reasonably well resolved and the stratospheric analysis at 10 hPa is not much affected by the top boundary conditions.

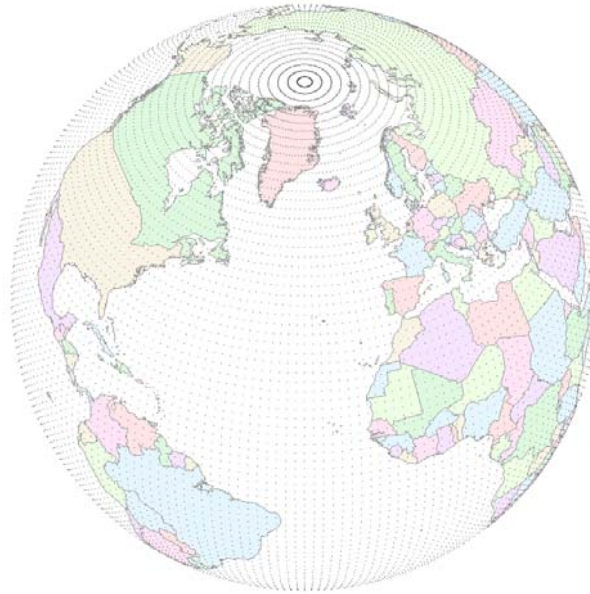


Fig. 3.1: Gaussian grid as used in NCEP/NCAR reanalysis T62L28 model (Source: Wikipedia)

The details of the model dynamics and physics are described in Development Division (1988), Kanamitsu (1989), and Kanamitsu et al (1991). The model includes parameterizations of all major physical processes, i.e., convection, large scale precipitation, shallow convection, gravity wave drag, radiation with diurnal cycle and interaction with clouds, boundary layer physics, an interactive surface hydrology, and vertical and horizontal diffusion processes.

A major difference with the model as described by Kanamitsu et al (1991) is the use of a simplified Arakawa-Schubert convective parameterization scheme developed by Pan and Wu (1994) based on Grell (1993). Pre-implementation experiments showed that the simplified Arakawa-Schubert scheme results in much better prediction of precipitation than the previous Kuo scheme over the continental US, as measured by equitable threat scores over North America. In addition, the precipitation patterns over the tropics are more realistic, with a smoother distribution, and less concentration over tropical orographic features.

Two other recent improvements were also implemented into the reanalysis model. The first is a better diagnostic cloud scheme (Campana et al, 1994) which has resulted in model generated outgoing long-wave radiation (OLR) in much better agreement with observations. The second is a new soil model, based on Pan and Mahrt (1987), which has also resulted in much more realistic surface temperature, and more skilful predictions of precipitation over North America in the summer. These changes to the model were systematically tested by running two months of assimilations in the summer and in the winter together with 25 forecasts from each assimilation run. Some tuning of the cloudiness and cloud optical properties were performed to correct systematic temperature and cloudiness errors. The final version of the model also produced good 5-day forecast scores."

Meteorological input parameters

Meteorological model output is used every 6 hours and interpolated linearly towards the actual time step. The following parameters are used:

- zonal wind component (West to East, m/s)
- meridional wind component (South to North, m/s)
- surface pressure (Pa)

- orography (land/ocean) flag
- surface geopotential height (m^2/s^2)
- temperature (K)
- specific humidity (kg/kg)
- surface skin temperature (K)
- surface zonal stress (N/m^2), stress in x direction
- surface meridional stress (N/m^2), stress in y direction
- surface sensible heat flux (W/m^2)
- surface water vapour flux ($kg/m^2/s$)
- downward solar flux at surface (W/m^2)
- upward solar flux at surface (W/m^2)
- downward longwave flux at surface (W/m^2)
- water equivalent snow depth (m)
- volumetric soil water content at surface (frac)

Three-dimensional properties of cloud and precipitation fields are required for the calculation of in-cloud oxidation of SO₂ and wet deposition rates. They are constructed using prognostic cloud-water parameterizations from the CCM3 model (Rasch and Kristjansson, 1998; Hack, 1998] also inside MATCH:

- vertical wind component ($d(\eta)/dt$, 1/s, eta coordinate system)
- vertical wind component ($\omega = d(\text{pressure})/dt$, Pa/s, pressure coordinate system)
- turbulent vertical diffusion coefficient
- counter-gradient coefficient
- Moist convection scheme (Zhang and McFarlane, 1995 deep convection and Hack, 1994 shallow convective transport scheme)
 - Zhang cloud updraft mass flux, μ_2 parameter, $kg/m^2/s$
 - Zhang cloud downdraft mass flux, md_2 parameter, $kg/m^2/s$
 - Zhang total entrainment rate, eu_2 parameter, 1/s
 - Hack convective mass flux ($kg/m^2/s$)
 - Hack overshoot parameter (fraction)
- radiative heating tendency (K/s)
- dq/dt due to convective rainout ($kg/kg/s$)
- convective in-cloud water mixing ratio (kg/kg)
- total cloud fraction
- convective cloud fraction
- rate of condensation/evaporation within the cloud ($kg/kg/s$)
- dq/dt due to stratiform precipitation ($kg/kg/s$)
- rate of evaporation of stratiform precipitation ($kg/kg/s$)
- grid box cloud water (kg/kg)

3.3 Transport scheme

Offline transport model

Online transport models are coupled directly with a numerical weather prediction model. They get a meteorological input update for each time step of e.g. 30 minutes. On the contrary, the MATCH model is an offline transport model, which means that meteorological input is used only every few hours (e.g. every 6 hours) and interpolated to the half hourly time steps in between.

Advection

Atmospheric advection can basically be described in an Eulerian as well as in a Lagrangian approach. The Lagrange approach uses a moving coordinate system following the trajectory of each air parcel. Air parcels have to be modelled sufficiently small to allow the assumption of a point volume which is following the surrounding wind fields. A species concentration of an air parcel is changed only by sources and sinks in the area the parcel is travelling through.

The Euler approach assumes a fixed coordinate system which divides a certain region on the globe in grid boxes. Grid boxes are typically chosen with borders parallel to latitudes and longitudes or in an icosahedral-hexagonal structure to avoid the pole problem. A species concentration is modelled as the sum of incoming and outgoing species in the atmospheric flow direction and sources and sinks inside the grid box. Eulerian approaches suffer from the intrinsic problem of an artificial numerical diffusion. Generally, diffusion describes the temporal and spatial leveling of a species concentration. The grid box modelling approach describes a species as concentrated equally within the grid box during a time step. Even a small point source is described as a peak with the grid box size as spatial extension. Therefore, an artificial diffusion is created which tends to be much faster than the physical diffusion in the atmosphere. Therefore, any local gradients tend to be levelised too fast in an Eulerian model approach.

Semi-Lagrangian modelling tries to overcome the problem of numerical diffusion in the Eulerian modelling. Although Semi-Lagrangian models are based into a subdivision of the atmosphere in grid cells, the advection of particles representing the grid cell centre is done independently from this grid. Backward trajectories are calculated for each grid box during each time step t_{n+1} for the respective length of the time step. Therefore, the nearest grid box of the origin of the air parcel at t_n in a Lagrangian interpretation is known. Using spatial interpolation the species concentration at the origin of the air parcel gets known and is taken as the new value in the grid box at t_{n+1} . As long as back trajectories do not cross each other during a time step, this procedure is numerically much more stable. Unfortunately, the Semi-Lagrangian approach can be affected by a violation of the mass conservation principle due to the spatial interpolation in the backward field. Especially, long integration times in climate models result in in-acceptable results (Staniforth and Cote, 1991).

Lin and Rood (1996) proposed a **flux-form Semi-Lagrangian** approach. In this approach the particle fluxes through each of the grid box walls and therefore each spatial direction are treated separately. For each box wall a Semi-Lagrangian technique is applied as described above. This approach has the advantage of being mass conserving. MATCH uses an implementation of the so called **SPITFIRE** (Split Implementation of Transport using Flux Integral Representation) algorithm published by Rasch and Lawrence (1998).

3.4 Emission data bases

3.4.1 SO_x emission data base

Anthropogenic sulfur emissions are described in the Global Emissions Inventory Activity (GEIA) dataset (Benkowitz et al., 1996; <http://www.geiacenter.org>) with extensions made by Smith et al. (2001, fig. 3.2 and 3.3).

County-level sulfur dioxide emissions were used from the US Environmental Protection Agency (USEPA), the European Environment Agency (EEA) supplemented by IIASA, an inventory for the FSU-Region by Ryaboshapko et al. (1996) and Environment Canada. For Australia and New Zealand, emissions were taken from the 1985 GEIA 1B inventory (Scholtz et al., 1998). For the rest of Asia, Latin America, Africa and the Middle East, emissions were calculated from regional fuel consumption and fuel properties. Ship emissions are taken from bunker fuel numbers provided by IEA/OECD (1997). Industrial process emissions for developing regions were taken from the Emission Database for Global Atmospheric Research (EDGAR, Olivier et al., 1996), while the

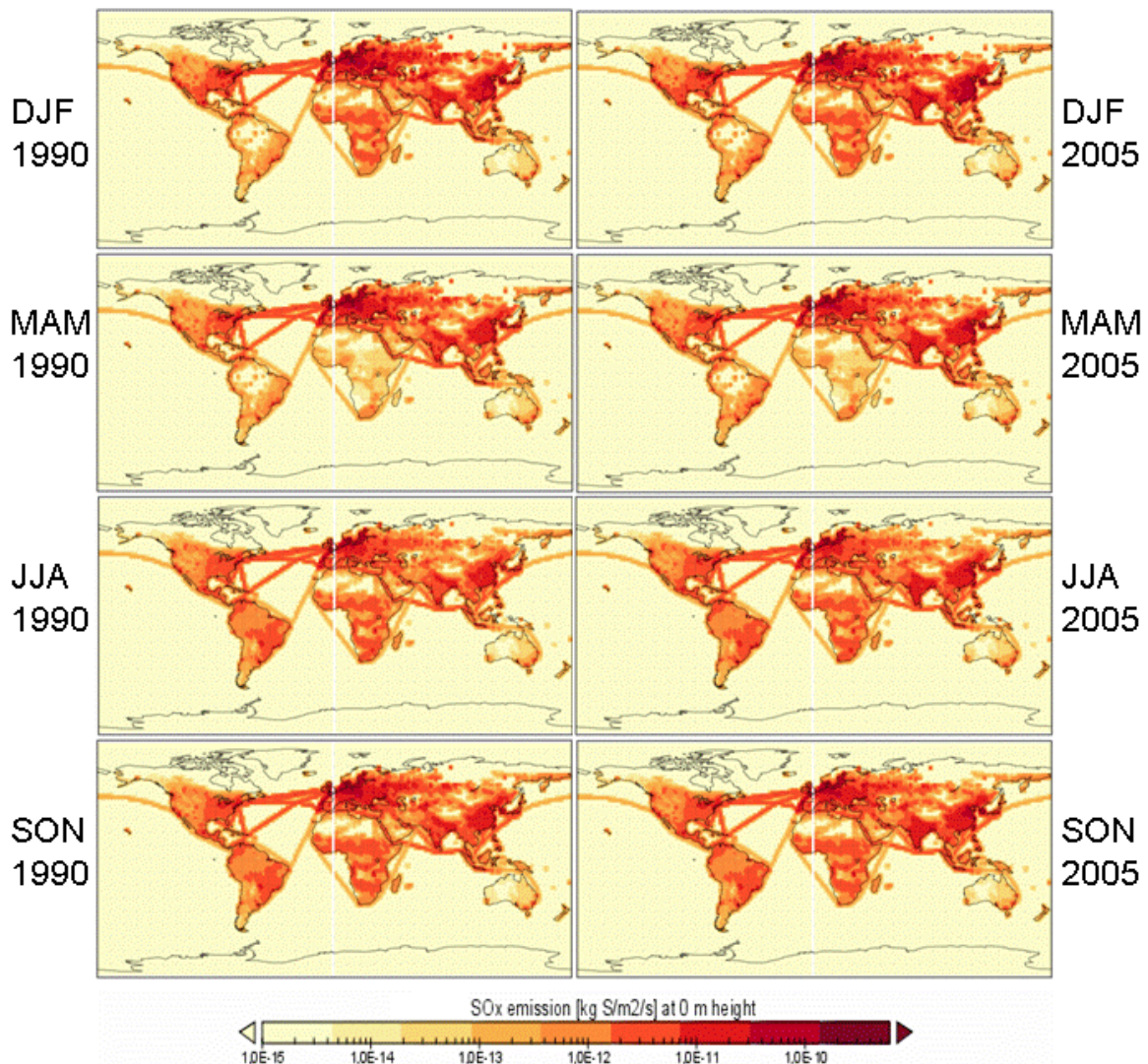


Fig. 3.2. GEIA/SMITH sulfur emission database [kg S/(m² s)] for winter, spring, summer and autumn 1990 (left) and 2005 (right) emission rates at 0 m height (surface).

EDGAR database was omitted for more developed regions with existing country-level inventories due to observed overestimations in the EDGAR database in those regions. For biomass burning emissions, the EDGAR estimates were used, while emissions from traditional biomass combustion were taken from the Streets and Waldhoff (1998) database.

Country-level based emission rates were spatially distributed using the EDGAR emissions inventory as spatial template within 11 world regions. A seasonal dependence was introduced reflecting the fossil fuel consumption as a function of weather conditions described as degree months with a monthly averaged temperature below 65°F. Biomass burning emissions seasonality was estimated using regional fire data compilations.

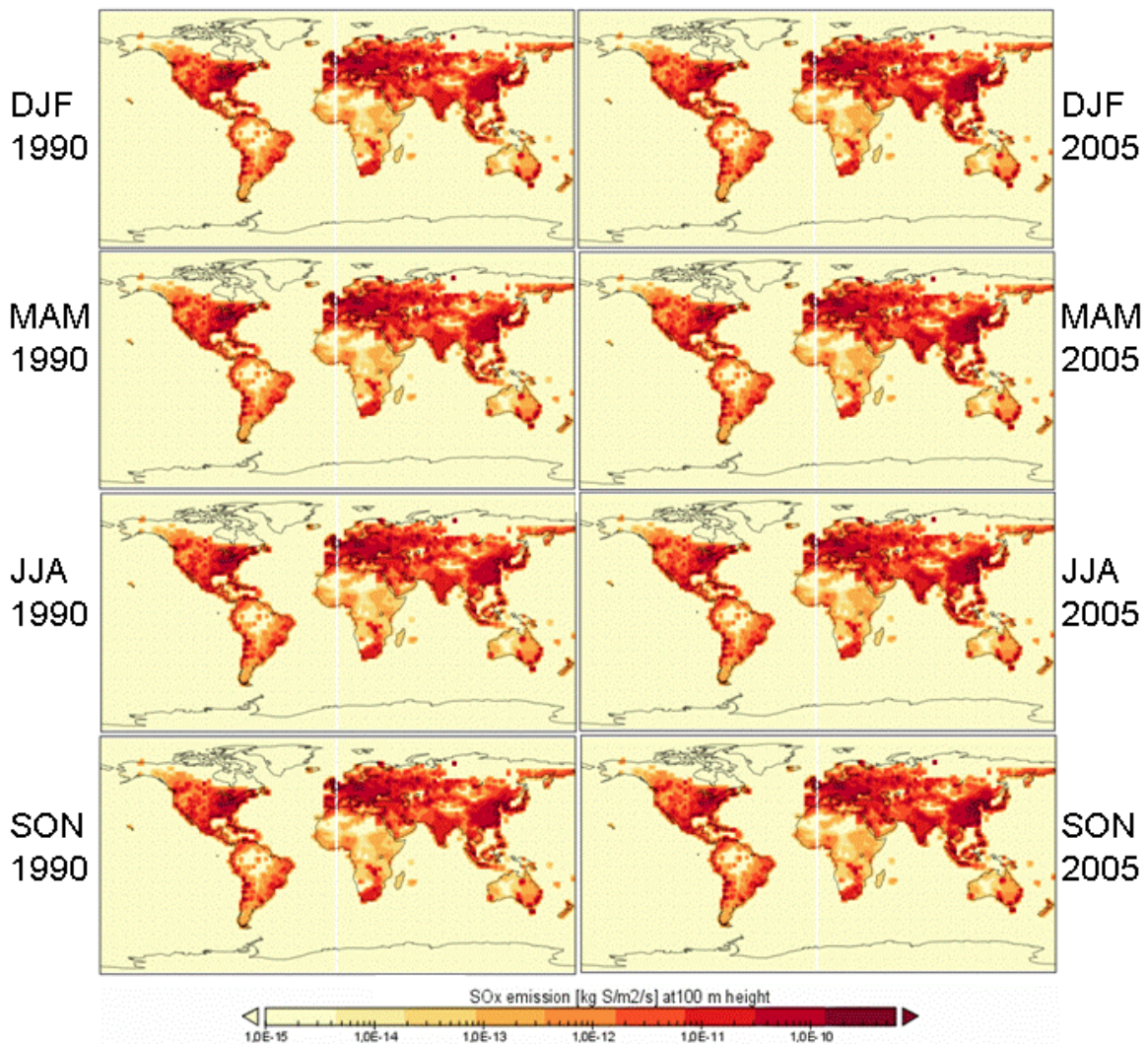


Fig. 3.3. GEIA/SMITH sulfur emission database [kg S/(m² s)] for winter, spring, summer and autumn 1990 (left) and 2005 (right) emission rates at 100 m height.

Emissions for SO₂ and SO₄ (SO_x) are provided on a global grid with a spatial resolution of 1°x1° for the reference year of 1990 and projected into the future years 2005, 2020, 2035, 2050, 2065, 2080, and 2095. Seasonal emissions are given for 15th of January, April, July, and October, respectively. Emissions at the surface (0m height) from low-temperature burning are distinguished from 100 m injection height sulfur as typical for factory or ship sources with high-

temperature combustion. Routines in soxwnd.f90 interpolate the emission database linearly towards the actual date.

Further description can be found in the CAM3.0 model description (<http://www.cesm.ucar.edu/models/atm-cam/docs/cam3.0/description/index.html>)

3.4.2 DMS emissions

Ocean dimethyl sulfide (DMS) is the dominant natural sulfur source in the atmosphere. DMS is oxidized to sulphuric and methanesulfonic acids which form new aerosol particles through condensation or coagulation. DMS transfer to the atmosphere is controlled by surface turbulence, seawater temperature and gas diffusivity. Oceanic DMS concentrations are described in a monthly climatology derived by Kettle et al. (1999, fig. 3.4).

This database was derived from approx. 15000 point measurements of DMS surface seawater concentrations obtained from 1972 to 1998 and mapped to a monthly 1 x 1° climatology of surface emissions.

3.4.3 Carbonaceous emissions

Carbon emission inventories are monthly climatologies based on Liousse et al. (1996, fig. 3.5 and 3.6) for biomass burning aerosols and Penner et al. (1993, fig. 3.8 and 3.9) for fossil fuel burning sources. Both climatologies provide sources for black and organic carbon.

Natural organic aerosols resulting from terpene emissions are included additionally. The production of natural organics (fig. 3.7) is assumed as 10% (Collins et al., 2001) of the total terpene emissions as described in Guenther et al. (1995).

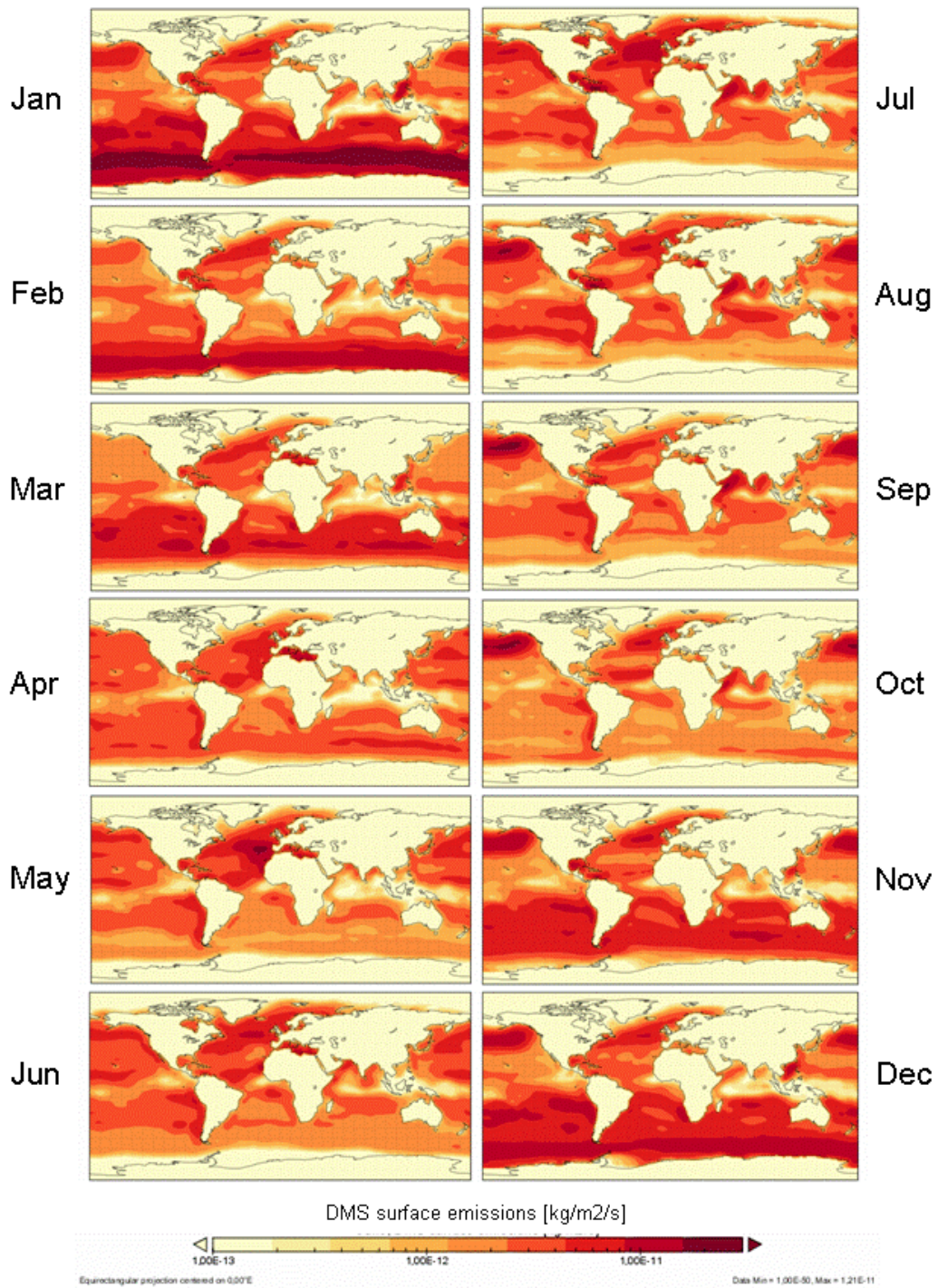


Fig. 3.4. Monthly mean DMS surface emissions (derived from the data base as described in Kettle et al. 1999)

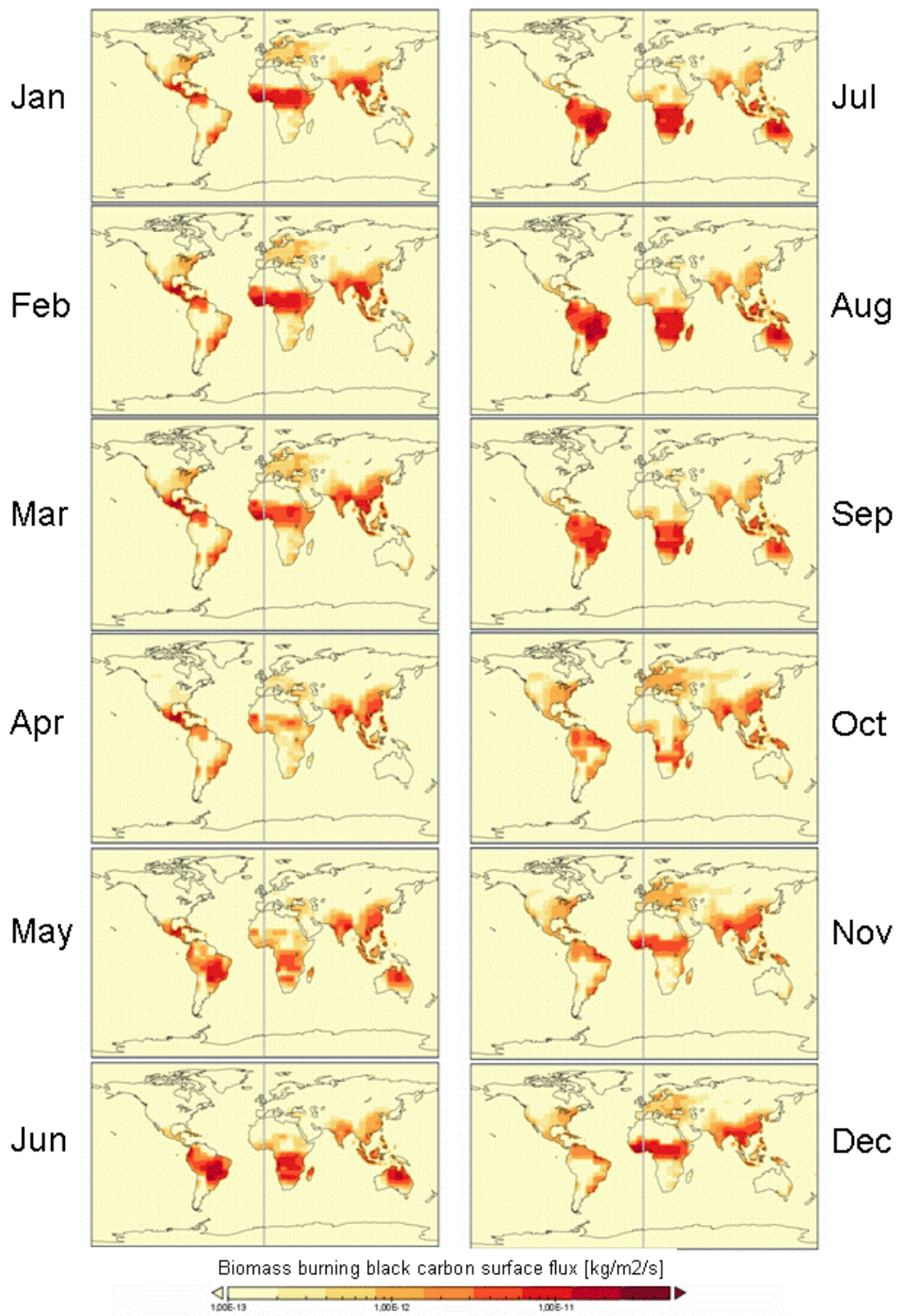


Fig. 3.5. Monthly mean biomass burning black carbon surface flux (derived from the data base as described in Liousse et al. 1996)

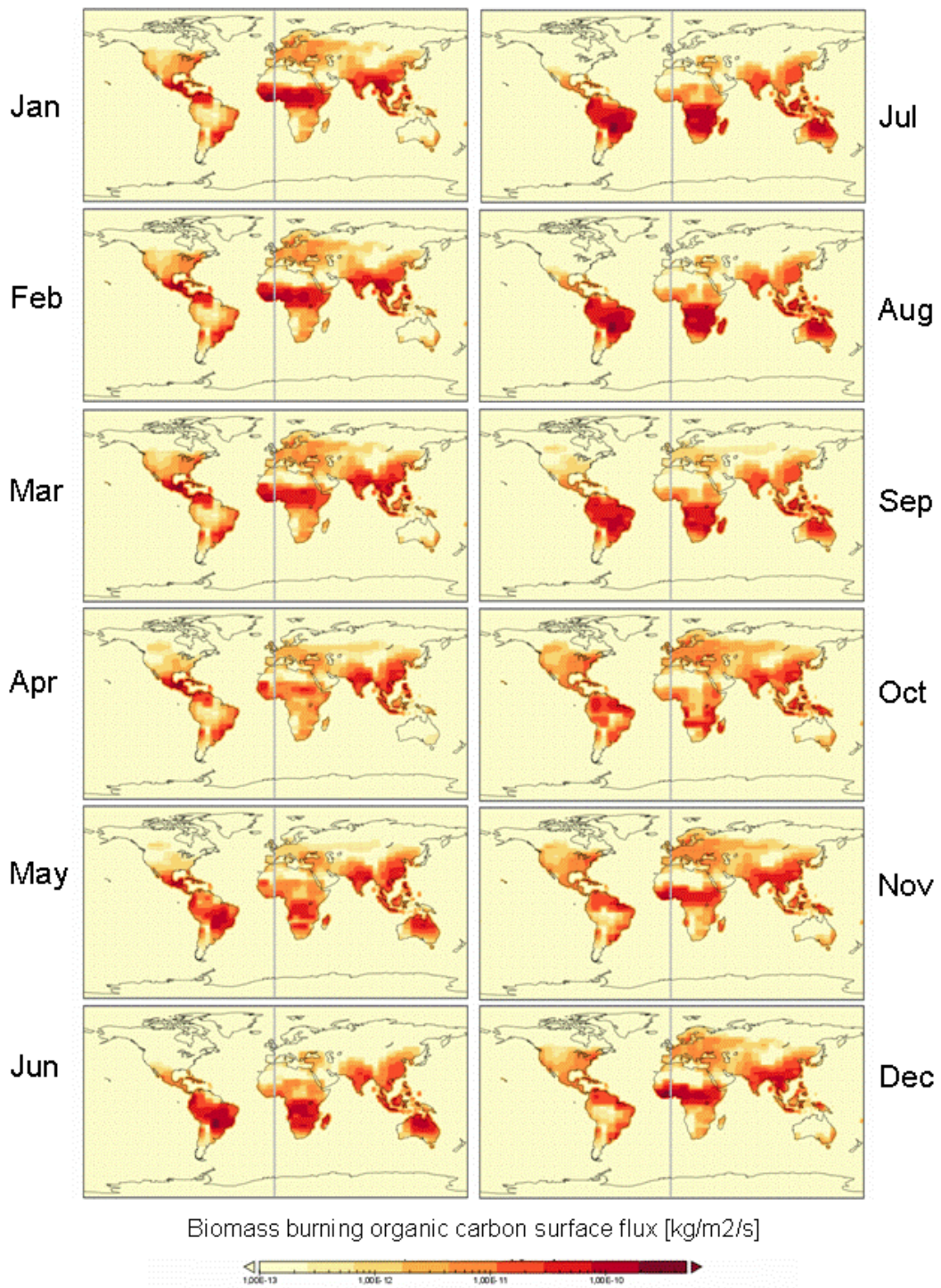


Fig. 3.6. Monthly mean biomass burning organic carbon surface flux (derived from the data base as described in Liousse et al. 1996)

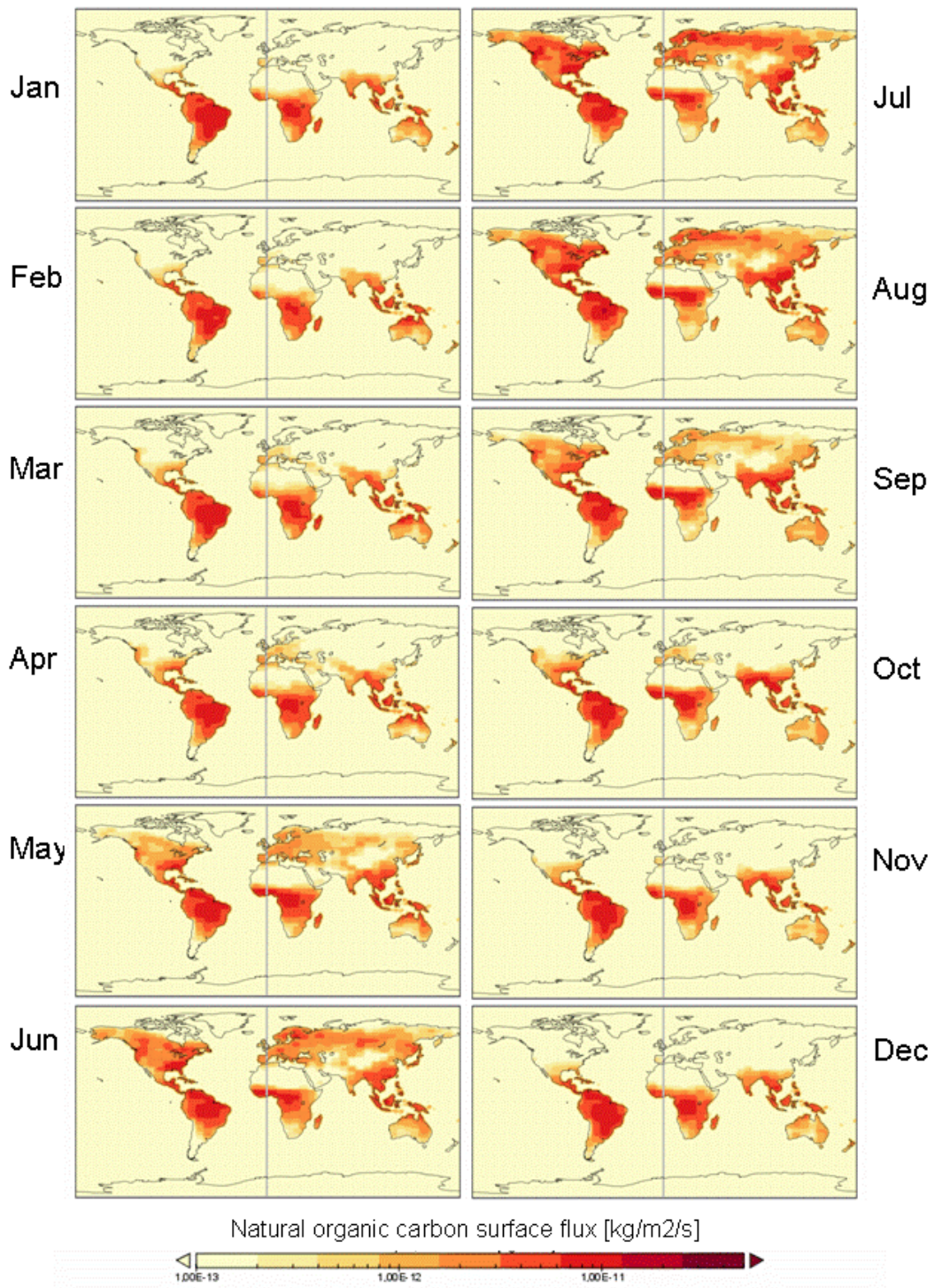


Fig. 3.7. Monthly mean natural organic carbon surface flux (assumed as 10% from terpene emissions after Guenther et al., 1995)

fossil fuel black carbon surface flux

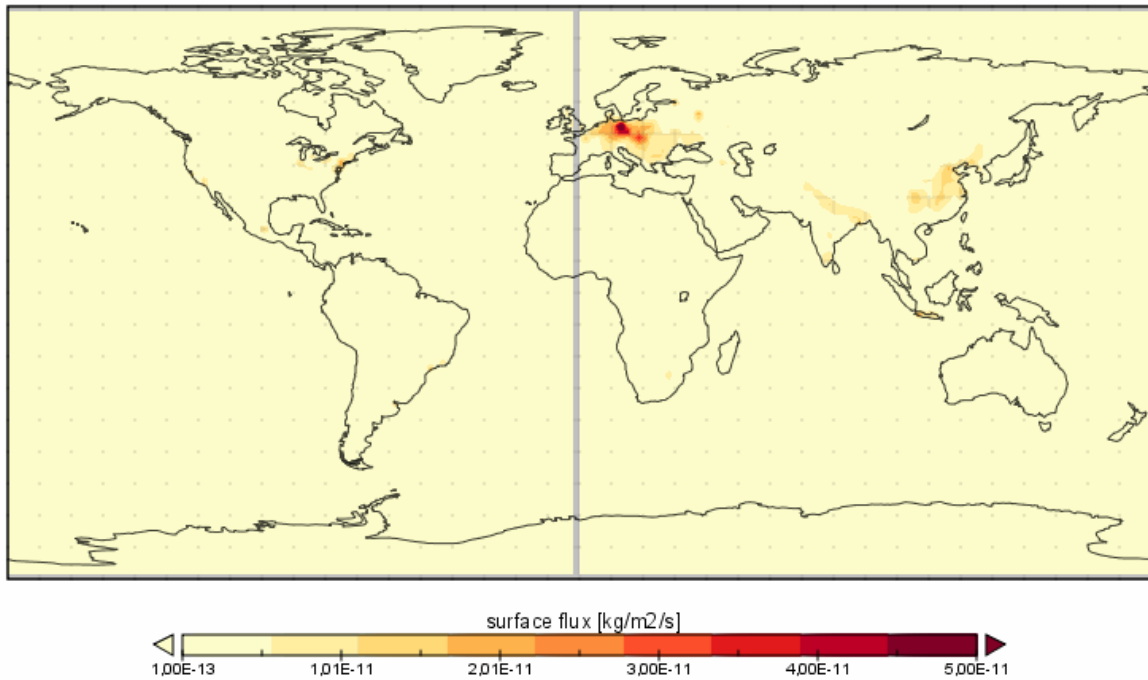


Fig. 3.8. Fossil fuel black carbon surface flux (derived from the data base as described in Penner et al., 1993)

fossil fuel organic carbon surface flux

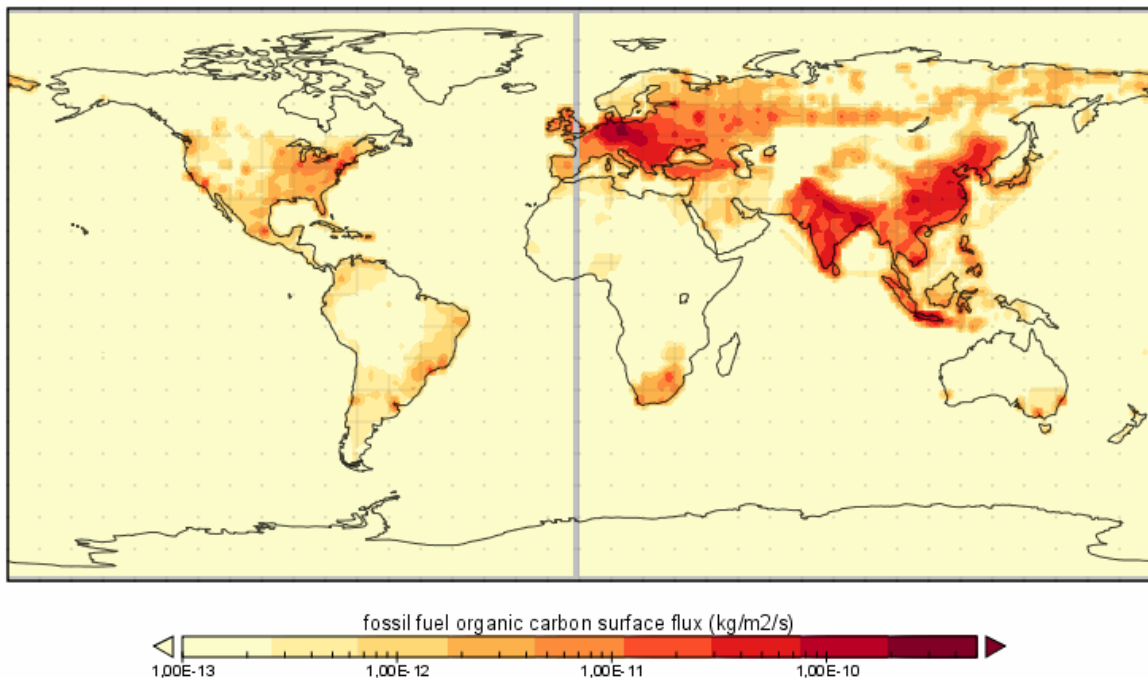


Fig. 3.9. Fossil fuel organic carbon surface flux (derived from the data base as described in Penner et al., 1993)

3.4.4 Sea salt

Vertical sea salt profiles are derived from 10 m wind speed after Blanchard and Woodcock (1980) in each time step. Sea salt is not transported. A prognostic sea salt scheme is foreseen for a next version of CAM (Community Atmosphere Model of NCAR) which will include a MATCH update.

Up to an altitude of 300 m the sea salt mass density $\rho_{sslt}(z)$ in units of $\mu\text{g}/\text{m}^3$ is calculated from

$$\rho_{sslt}(z) = 5 (6.3 \times 10^{-6} z)^{(0.21-0.39 \log_{10} u_{10})} \quad (\text{eq 3.1})$$

with z as the altitude above sea level in m and u_{10} the 10-m wind speed in m/s. Above 300 m the sea salt concentration is decreased exponentially with a 500 m scale height (Fillmore, 2005).

3.5 Dust emissions and model

The dust model DEAD (Mineral Dust Entrainment and Deposition, Zender et al., 2003) is implemented in the MATCH model.

Mineral dust mobilisation is initiated by strong winds blowing over bare ground and erodible particles. Medium range sand-sized particles above $60 \mu\text{m}$ particle diameter are lifted up, but also fall quickly down again to the ground. This behaviour is known as **saltation** (fig. 3.10). The momentum of the landing particles results in the loosening of small and fast moving particles which are known as sandblasting particles. These are typically clay-sized with a particle diameter below $2.5 \mu\text{m}$ or silt-sized with a particle diameter between 2.5 and $60 \mu\text{m}$. Dust particles are mixed into higher atmospheric layers by turbulent processes and transported in the atmospheric flow over larger distances.

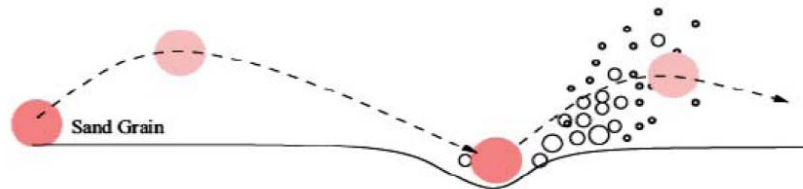


Fig. 3.10. Saltation process (after Shao, 2008)

The turbulent surface shear stress τ_0 at surface height 0 m describes the atmospheric force per area affecting the ground. The wind drag has to overcome gravitational and cohesive forces to start the saltation process. Therefore, a threshold wind friction velocity u_{*t} has to be reached first, before dust mobilisation starts.

Friction velocity u_* and shear stress τ at the ground are related to each other through the atmospheric density ρ

$$u_*^2(0) = \frac{\tau_0}{\rho} \quad (\text{eq 3.2})$$

The **threshold friction velocity u_{*t}** is described by Zender et al. (2003) as a function of particle density, the gravitational acceleration constant g , the particle diameter, the kinematic viscosity of the air and the air density ρ . The exact relationship was obtained by Marticorena and Bergametti (1995) based on wind tunnel experiments. On the one hand, the threshold friction velocity needs to increase with growing particle size to balance the gravitational force. On the other hand, for small particles additional cohesive forces at the ground gets larger and also increase the threshold friction velocity. Therefore, a minimum particle size is found between 60 and $75 \mu\text{m}$ (fig. 3.11).

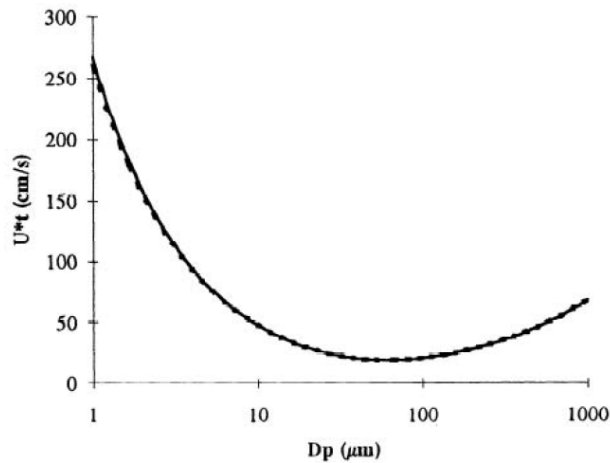


Fig. 3.11. Threshold friction velocity as a function of particle size (after Marticorena and Bergametti, 1995)

Further effects as drag partitioning, the Owen effect and the moisture inhibition effect are taken into account and increase u_{*t} :

Drag partitioning describes that other non-erodible obstacles like large stones, vegetation, or trees on the surface represent additional atmospheric momentum sinks which slow down the friction velocity without any resulting erosion effect. The aerodynamic roughness length z_0 inside the DEAD dust model is globally set to 100 μm as a typical value for erodible soils. Also, a smooth roughness length $z_{0s} = 33.3 \mu\text{m}$ accounting for the erodible particles itself is assumed as a global constant. An empirical parameterization using z_0 and z_{0s} describes the drag partitioning coefficient and therefore increases u_{*t} .

The Owen effect is a positive feedback effect as the saltation process itself increases the surface roughness length.

Near surface soil gravimetric water content (as taken from the meteorological driving fields) also increases u_{*t} as the specific weight of wet dust is increased and additional capillary forces occur.

The **horizontal saltating mass flux Q_s** is described as the product of an area mass deposition rate and a characteristic path length of the saltating particles and results in the following formulation

$$Q_s = \frac{c_s \rho u_*^3}{g} \left(1 - \frac{u_{*t}}{u_*}\right) \left(1 + \frac{u_{*t}}{u_*}\right)^2 \quad (\text{eq 3.3})$$

with $c_s = 2.61$ as a constant determined from wind tunnel experiments. Saltation occurs only if the threshold friction velocity is exceeded.

This horizontal mass flux of medium sized particles results in a **vertical mass flux F** of small dust particles described by a sandblasting mass efficiency α as proportionality constant.

Following Marticorena and Bergametti (1995) the constant α is described as an empirical function of the clay-sized particles in the underlying soil type.

Only bare soil is a potential dust emission source. A monthly leaf area index map is used to exclude areas with a sum of leaf and stem area index above 0.3 m^2/m^2 or those covered with snow.

An analysis of regional hot spots in dust emission by Gillette (1999) observed a coincidence between hot spots and topographic depressions. The hypothesis is that in historical times these

depressions acted as hydrological basins creating alluvial sediment areas. It is assumed, that these topographic low areas provide a sufficient amount of sediment particles which can act nowadays as erodible particles while other areas in the world have been lost their small particles already in earlier geological periods.

A **surface erodibility factor S** was derived comparing local altitudes and identifying regional minima in altitude within $10 \times 10^\circ$ boxes resulting in a map of historical hydrological basins in the Saharan and Sahel region (Ginoux et al., 2001, fig. 3.12).

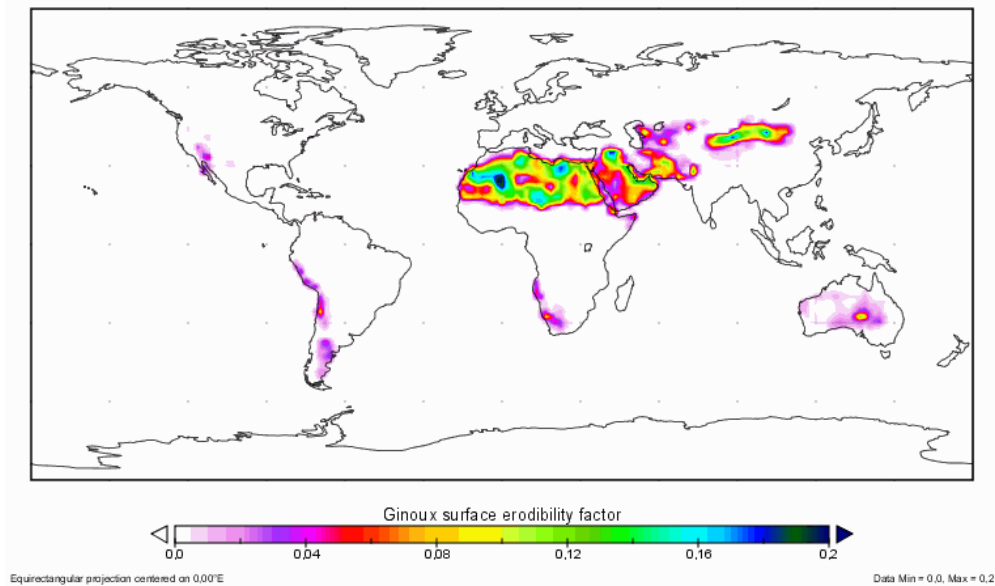


Fig. 3.12. Surface erodibility factor (Ginoux et al., 2001)

Aerosols are mixed into the lowest model sigma coordinate level.

Dry deposition of dust particles is modelled through gravitational settling and turbulent mix-out. The gravitational settling velocity results from a balancing of frictional and gravitational forces as a function of particle size and density. A turbulent particle deposition is modelled as a function of aerodynamic resistance of a particle.

Wet deposition is modelled as in-cloud and below-cloud scavenging. Particles in precipitating clouds are removed by nucleation scavenging, while particles beneath precipitating clouds are removed by collision scavenging. Stratiform and convective clouds are treated separately.

Dust particles are modelled in four size bins for effective radii between 0.01-1, 1-20, 10-20, 20-50 μm .

3.6 Stratospheric aerosols

MATCH v4.2 does not include stratospheric aerosols. Volcanic emissions from the Andres and Kasgnoc (1998) database have been tested by the MATCH development team. Nonetheless, this database has been removed from the MATCH standard installation. Therefore, it is recommended to continue using the optical depth database of stratospheric aerosols as derived by Sato et al. (1993) as done currently in the SOLEMI database.

3.7 Aerosol optical depth

Aerosol optical depth (AOD) is calculated separately for each aerosol type (Collins et al., 2001). AOD is calculated for an aerosol mixing ratio q of type i using the optical extinction coefficient for each species χ_i and using the gravitational acceleration g to account for the pressure coordinate system.

$$AOD = g^{-1} \int_0^{p_s} \sum_i \chi_i(p) q_i(p) dp \quad (\text{eq 3.4})$$

Optical extinction coefficients are described as a product of the dry value and a hygroscopic growth factor f_i , which is a function of relative humidity RH .

$$\chi_i = \chi_{i,dry} \times f_i(RH) \quad (\text{eq 3.5})$$

Hygroscopic growth factors f_i , for sulfate are taken from Kiehl et al. (2000). Additionally, the geometric mean radius and the standard deviation of the lognormal size distribution are modelled as a function of relative humidity.

For sea salt, a mean mass-weighted extinction of 2.5 m²/g at 70% relative humidity is assumed at the 550 nm wavelength. This is scaled to other relative humidity values accordingly.

Dust optical properties are calculated from Mie theory. The refractive index used is based on Patterson (1981). Each dust size bin is distributed according to a lognormal distribution. There is no hygroscopic growth assumed for dust particles. Optical extinction coefficients are pre-calculated (table 1, Collins et al. 2001):

Table 3.2: Physical and optical properties for the four dust size bins, from Collins et al., 2001

Size, μm	v_g^a , cm/s	v_t^b , cm/s	r_g^c , μm	$\ln \sigma_g^d$	χ_i^e , m ² /g
0.01–1	0.02	0.03	0.4	0.7884	1.303
1–10	1.42	0.50	2.0	0.7884	0.124
10–20	8.39	7.00	15.0	0.7884	0.040
20–50	38.87	25.00	25.0	0.7884	0.017

^aGravitational settling velocity.

^bTurbulent deposition velocity.

^cGeometric mean radius.

^dWidth of lognormal distribution.

^eOptical extinction at $\lambda = 630$ nm.

Extinction coefficients for carbonaceous aerosols is chosen as $\chi_i = 9$ m²/g for both hydrophilic and hydrophobic carbon. Optical extinction coefficients as given in the literature vary from 2.5 to 12 m²/g. The uncertainty in the extinction coefficient is much larger than a hygroscopic growth of hydrophilic carbon would be and therefore, no hygroscopic growth is modelled.

4 Available Datasets

4.1 NCAR/MATCH-MODIS

The NCAR/MATCH-MODIS data set was derived by Fillmore (2005) in order to derive climatological monthly means for a climate model. MODIS level 3 daily gridded AOD at 550 nm in 1 x 1 ° spatial resolution was assimilated in this model run using an optimal interpolation method. Monthly mean values in 1.9° spatial resolution are available from 1980 to 2005, while the un-

derlying daily values are available at both the NCAR and the DLR archive only from 2000 to 2005.

4.2 DLR/MATCH 2004

The DLR/MATCH dataset consists of hourly values for the period 1.1. to 31.12.2004 modelled with MATCH v4.2 (as described above) in a 1.9° spatial resolution. AOD is calculated for the 550 nm wavelength and there is no assimilation scheme applied.

4.3 AERONET validation data

AERONET (AErosol RObotic NETwork) provides ground-based sun photometer measurements (Holben et al. 1998). The NASA-operated AERONET program is operated to gather aerosol information and provide validation data for satellite retrievals of aerosol optical properties. Datasets are available at <http://aeronet.gsfc.nasa.gov> and contain AOD measurements at 16 different wavelengths at 1640, 1020, 870, 675, 667, 555, 551, 532, 531, 500, 490, 443, 440, 412, 380 and 340 nm as well as solar zenith angles, total water vapor column measurements and several variability coefficients used for automatic cloud screening procedures. The accuracy of AERONET AOD values is ± 0.01 for wavelengths up to 440 nm and ± 0.02 for shorter wavelengths (Holben et al. 1998). In this study, daily means of AERONET version 2, level 2 data are used.

5 Validation of Aerosol Optical Depth

5.1 NCAR/MATCH-MODIS

5.1.1 General validation

The validation of 12 UTC NCAR/MATCH-MODIS AOD values was performed versus daily mean measurements of the AERONET network. Overall a number of 10800 coincidences were analysed from 79 stations in Europe and Africa (fig. 5.1). The overall mean bias deviation is 0.06 with a root mean square deviation of 0.24 and a Pearson correlation coefficient $r = 0.62$.

Generally, a good agreement within 0.1 can be observed for a majority of all cases. Nevertheless, a remarkable scatter can be observed as well and is analysed in the further sections.

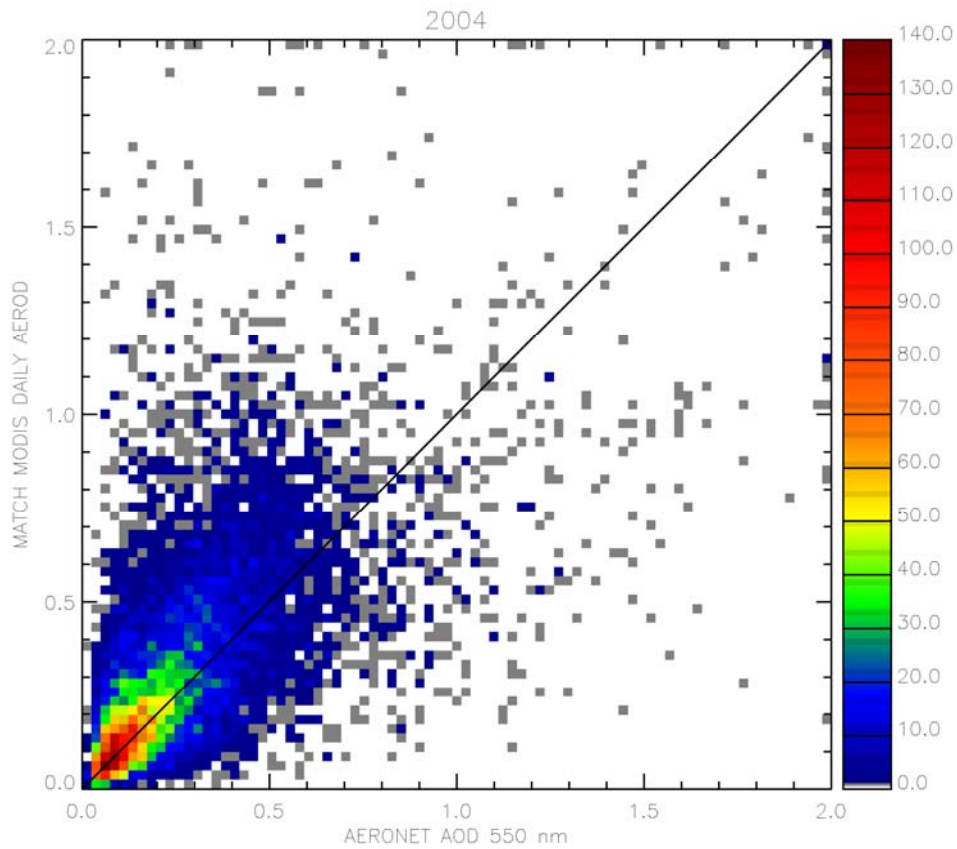


Fig. 5.1. Two-dimensional histogram of AOD from the NCAR/MATCH-MODIS data set vs. daily AOD means measured at the AERONET network in Europe and Africa for 2004. The colour bar indicates the number of occurrences in each bin of the AERONET and MATCH-MODIS AOD axes.

5.1.2 High sulfate AOD value problem

For Central European stations an overestimation of AOD is frequently observed with strong peaks of short duration and values up to 2.

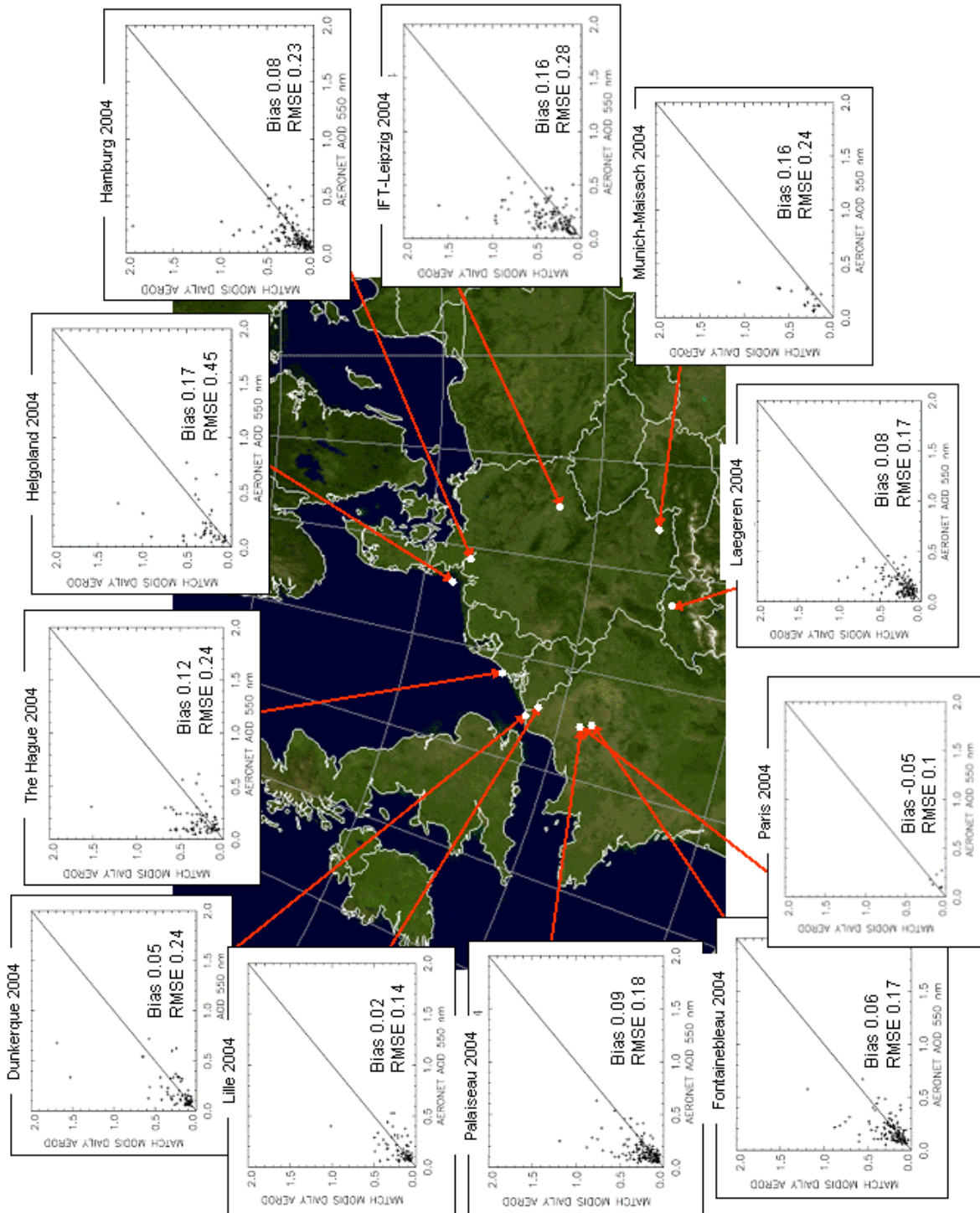


Fig. 5.2. Scatter plots for the NCAR/MATCH-MODIS dataset for all Central European AERONET validation stations together with mean bias deviation and root mean square deviation for 2004

Examples are e.g. the AERONET stations Dunkerque (MBD 0.05), The Hague (MBD 0.12), Helgoland (MBD 0.17), Hamburg (MBD 0.08), IFT-Leipzig (MBD 0.16), Munich (MBD 0.16), Laegeren (MBD 0.08), and Palaiseau (MBD 0.09). Fig. 5.2 gives an overview over all Central European

validation results for the test year 2004, while Fig 5.3 illustrates this problem for the case of the IFT-Leipzig station.

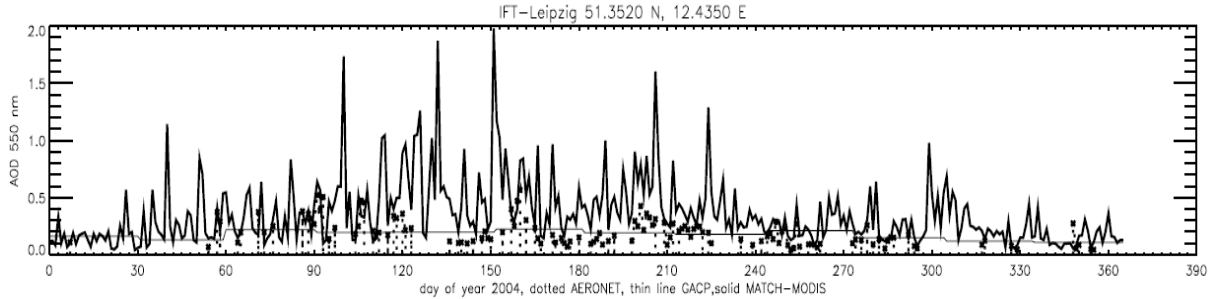


Fig. 5.3. AOD time series from the NCAR/MATCH-MODIS data set (bold line) vs. daily AOD means measured at the AERONET station IFT-Leipzig (dotted with crosses) for 2004. Additionally, the standard monthly GACP climatology is given as grey line.

As sea salt is a non-advected species, the sea salt concentration is not adjusted through the data assimilation procedure (Fillmore, 2005). Assimilation is done for an AOD τ^* which is the difference between observed or background AOD minus the background sea salt AOD. τ^* estimates the sum of sulfate, dust and carbonaceous aerosols in both the observations and the background field. As the satellite observations do not deliver a separate sea salt AOD, the modelled background value has to be taken as best estimate also in the observation space.

$$\begin{aligned}
 \tau_{obs}^* &= \tau_{obs} - \tau_{sslt} \\
 \tau_{x_b}^* &= \tau_{x_b} - \tau_{sslt} \\
 \tau_{ana} &= (\tau_{x_b} - \tau_{sslt}) \times \left(\frac{\tau_{obs} - \tau_{sslt}}{\tau_{x_b} - \tau_{sslt}} \right)
 \end{aligned}
 \tag{eq 5.1}$$

This is a numerical approach which takes the situation of a non-advected sea salt field into account. There are problems due to this inconsistency in the assimilation approach: In cases with $\tau_{obs} > \tau_{x_b}$ the assimilation factor is generally larger than 1. In cases with a modelled τ_{sslt} much larger than the (unknown) true value, the assimilation factor gets much larger than 1 and achieves unrealistically high values. This occurs only over the ocean due to the sea salt mobilisation and therefore, the sulfate AOD shows this overshooting effect most prominently. As sulfate is transported, the overestimated values stay in the dataset for the typical sulfate lifetime. As the true value of sea salt concentration is not known in the assimilation procedure, there is no opportunity to avoid this behaviour unless aerosol type resolved information is assimilated.

A typical example of this behaviour is given in fig. 5.4: The SO₄ optical depth field shows a linear structure in the Northern Atlantic. While the assimilated MODIS values show no similar gradient along the latitudinal circle, the SO₄ field is increased in those areas with large sea salt optical depth.

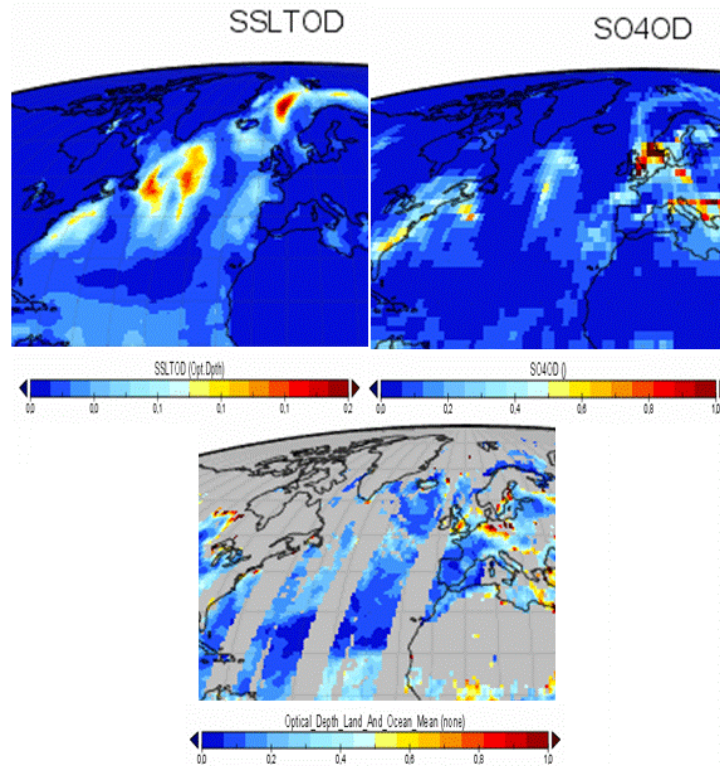


Fig. 5.4. Example of the sulfate/sea salt assimilation problem on 26th April 2004 (MATCH sea salt AOD, upper left; MATCH SO₄ AOD, upper right; MODIS LV3 gridded AOD, lower image)

5.1.3 Mediterranean Region

The Mediterranean region is of special interest to the solar energy community. On the Iberian Peninsula, a low MBD of 0.02 is found in El Arenosillo and Evora, Cabo da Roca shows a MBD of 0.04 and Palencia of 0.09. The RMSD remains low with 0.11 in Cabo da Roca and El Arenosillo, 0.12 in Evora and increases for Palencia with 0.2 (Fig. 5.5).

Strong overestimation with AOD values of 1.5 or 2 in the NCAR/MATCH-MODIS dataset can be found in Lampedusa, Sede Boker, Nes Ziona, Forth_Crete, Lecce University and Venice, while Toulouse ($r = 0.59$), Avignon ($r = 0.55$), IMS-METU-ERDEMLI ($r = 0.63$) and Blida ($r = 0.72$) show a rather good correlation. Venice is generally affected by a large scatter both towards under- and overestimations. Lecce, Forth Crete, Nes Ziona, Sede Boker and Lampedusa are dominated by larger overestimations.

Only the station Cairo University shows an underestimation (MBD = -0.1) which is probably due to its location in the large city of Cairo where AOD is probably driven by local emissions.

Another relevant point for solar irradiance modelling is the frequency of dust events. Dubovik (2002) suggests identifying dust outbreak cases by the criteria

$$\text{AOD}_{1020 \text{ nm}} > 0.3 \text{ and } \alpha_{440_870} < 0.6 \quad (\text{eq 5.2})$$

Therefore, a dust case in the following analysis is defined as a daily mean AERONET measurement fulfilling these criteria (Fig. 5.6). Applying the criteria to daily means is even a stricter filter as the whole day needs to be affected significantly by dust. Cases with strong horizontal gradients at the edge of a dust outbreak area are probably not detected.

The stations in Southern France and Italy observe between 2 and 5 dust cases and 8 cases are found in Palencia in Northern Spain. For the South of the Iberian Peninsula 10 cases are observed in Cabo da Roca and Evora, while 20 cases occur in El Arenosillo. Blida is affected by strong dust occurrence on 34 days, Sede Boker shows 21 cases, Nes Ziona 17 and Crete 15 cases.

5.1.4 Overestimation in dust AOD

Another problem observed are large peaks in the dust AOD not observed in coincident AERONET measurements. The selection of data points is done by applying the criterion published by Dubovik et al., 2002, section 5.1.3) to AERONET measurements (Fig. 5.6).

This analysis shows that mainly Nes Ziona, Sede Boker and Forth Crete are affected by overestimations in dust cases. Lampedusa shows 6 dust cases but without major over- or underestimation. All other stations are affected by dust cases as well, but show no remarkable overestimations.

The overestimations in Nes Ziona, Sede Boker and Forth Crete are a result of a few strong emissions which are transported from Southwest Saharan regions over long distances towards the East Mediterranean Sea. Forth Crete is affected by two events, while Nes Ziona and Sede Boker are affected by three events. These long-range transport events are spatially large and therefore, result in deviations between MATCH-MODIS and AERONET over several days. It is not clear if wrong spatial emission regions, a too strong emission at correct locations or an in-effective dry deposition scheme results in this overestimation. This is subject to further MATCH development work.

It was checked if a time shift within the day between AERONET measurements and MATCH modelling occurs in these large scale events. A validation using daily mean AERONET measurements could pretend such deviations. Nevertheless, no such indication was found.

Additionally, a similar validation was performed for the Arabian Peninsula. Again, fig. 5.7 provides the scatter plot of NCAR/MATCH-MODIS 12 UTC AOD values against daily mean AERONET AOD measurements at 550 nm, while fig. 5.8 provides the scatter plots for those cases detected as dust events with the Dubovik criterion.

The overestimation of NCAR/MATCH-MODIS can be seen in nearly all stations on the Arabian Peninsula with exception of Sir Bu Nuair, Dhadnah and Saih Salam close to the Strait of Hormuz. Strong examples of overestimation specifically in the dust cases can be observed at the AERONET stations Jabal Hafeet, SMART_POL, Al Khaznah, Hamim, Mezaira, Al Qlaa and Mussafa. These stations are located close to the border between the United Arab Emirates and Oman. Mostly, dust events affecting these stations and causing these overestimations in 2004 are dominated by emission sources in Oman and the South of Saudi-Arabia. Contrary to the Israeli stations, the overestimations at these stations are not caused by long-range transported dust events, but by rather nearby local emissions. As these events are typically transported to the South-East, it cannot be derived from this validation study, if the long-range transported cases are overestimated as well or not. Due to missing AERONET stations in the Arabian Sea, this cannot be evaluated.

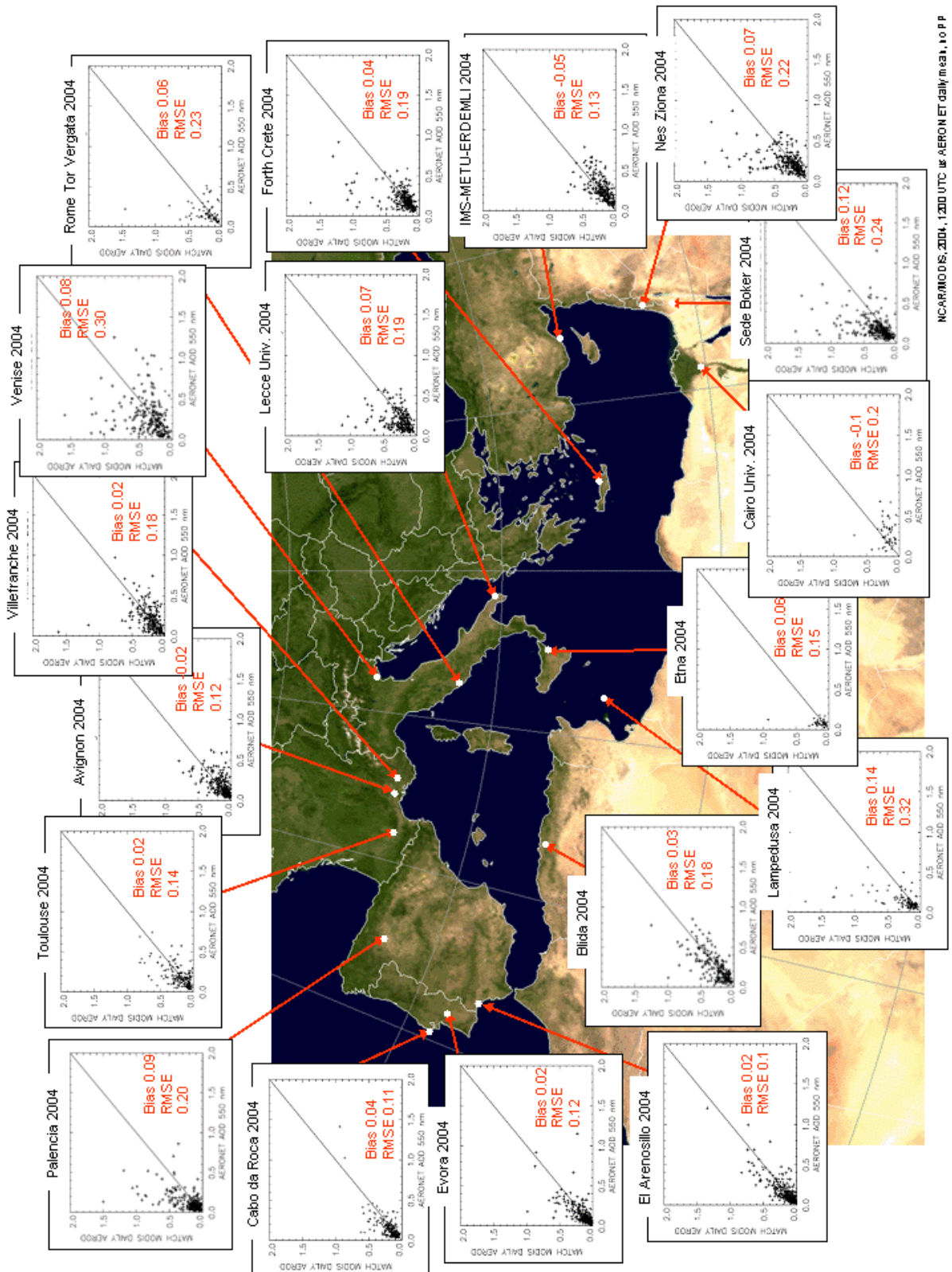


Fig. 5.5. Scatter plots for the NCAR/MATCH-MODIS dataset for all AERONET validation stations around the Mediterranean Sea together with mean bias deviation and root mean square deviation for 2004

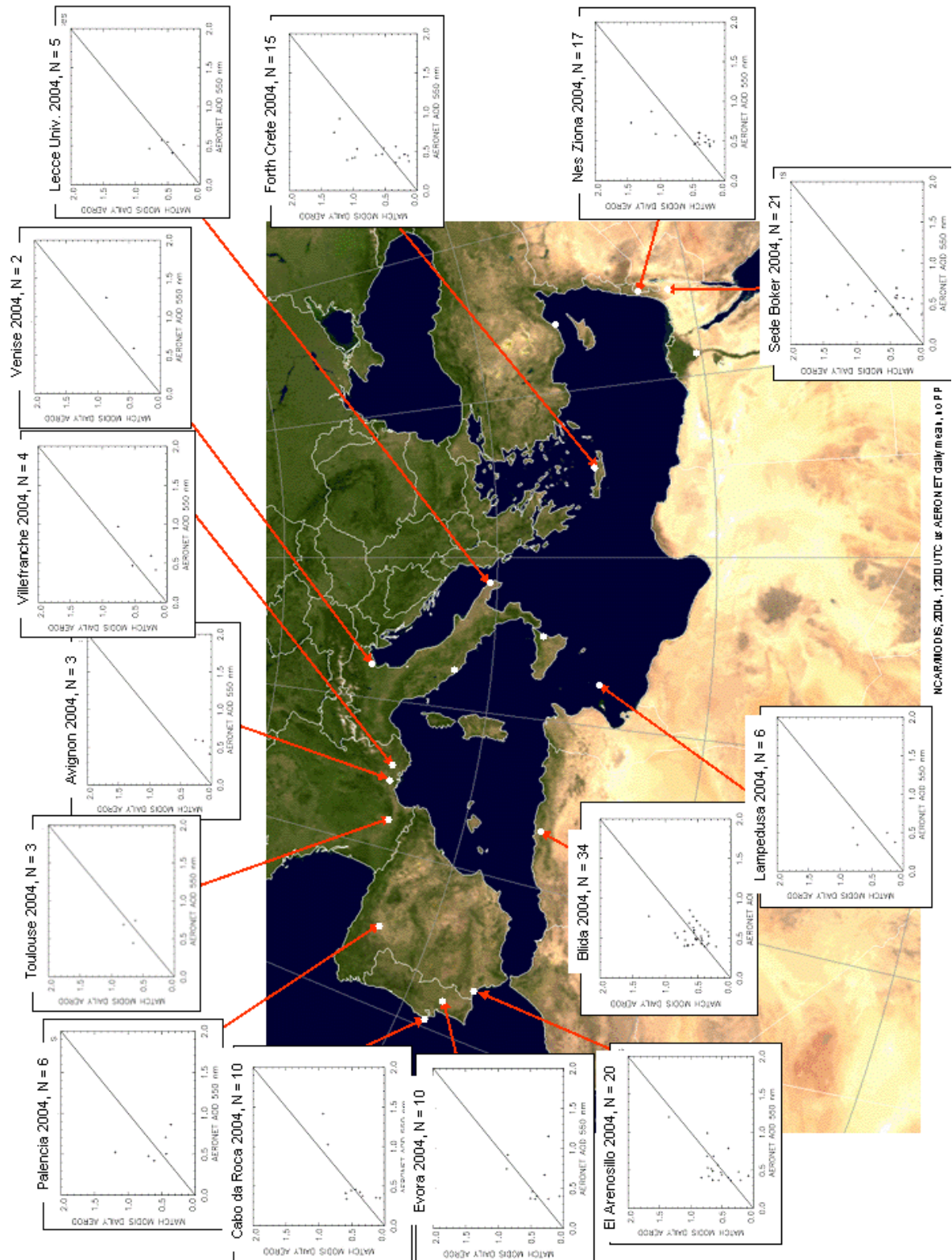


Fig. 5.6. Scatter plots for the NCAR/MATCH-MODIS dataset for all AERONET validation stations around the Mediterranean Sea for 2004, only dust cases as selected with the 'Dubovik criterion'

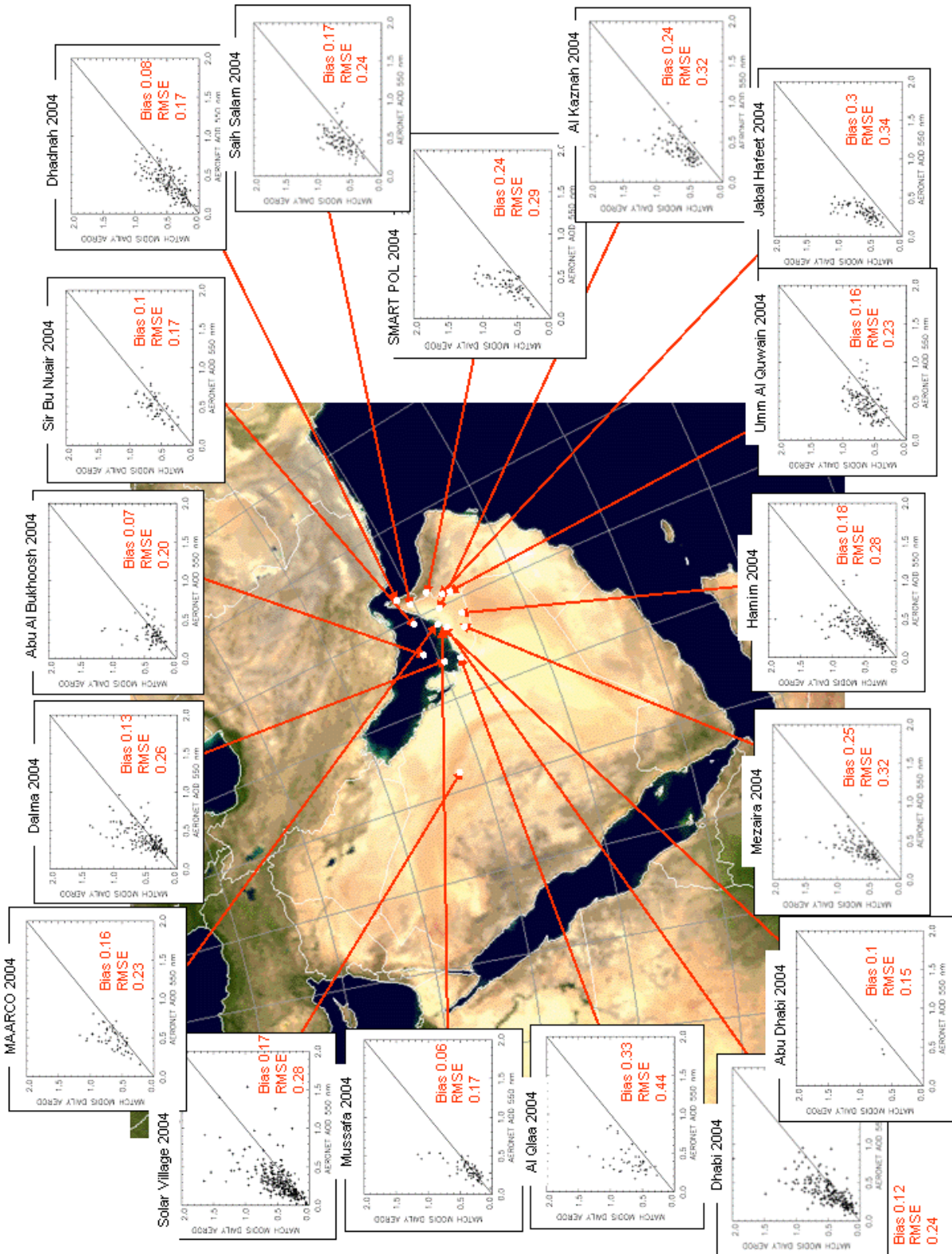


Fig. 5.7. Scatter plots for the NCAR/MATCH-MODIS dataset for all AERONET validation stations at the Arabian Peninsula together with mean bias deviation and root mean square deviation for 2004

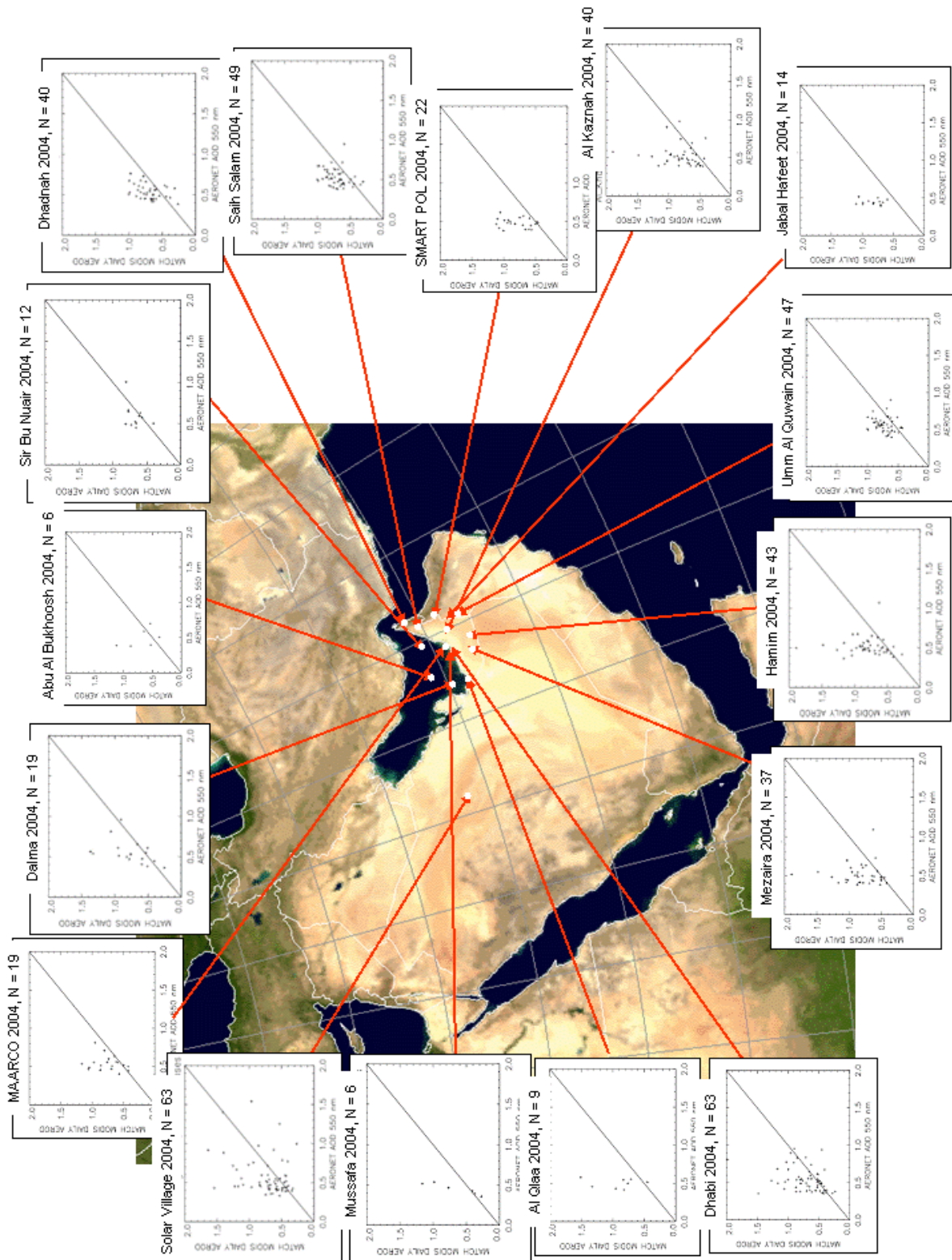


Fig. 5.8. Scatter plots for the NCAR/MATCH-MODIS dataset for all AERONET validation stations at the Arabian Peninsula for 2004, only dust cases as selected with the ‘Dubovik criterion’

It has to be noted that at some stations only a few major events are dominating such an overestimation. It is not clear, if this is a general effect for this region occurring in every year – this could be concluded only from a validation study covering many more years.

Fig. 5.9 shows a typical example of an overestimating station in this region. The dust events are rather well met in time, but overestimated in most cases, partly even strongly. This leads to the vertically tilted scatter plot typical for this region.

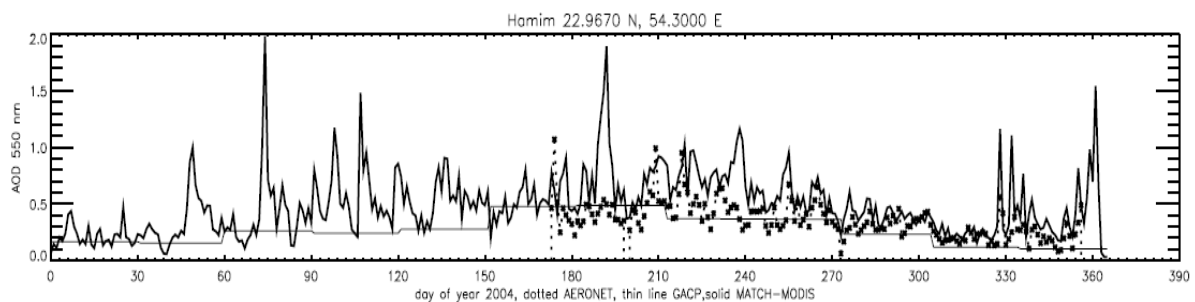


Fig. 5.9. AOD time series from the NCAR/MATCH-MODIS data set (bold line) vs. daily AOD means measured at the AERONET station Hamim, Abu Dhabi (dotted with crosses) for 2004. Additionally, the standard monthly GACP climatology is given as grey line.

5.1.5 Africa

AERONET stations in Africa are located mainly south of the Sahara in a region affected by dust outbreaks but also by biomass burning as another important aerosol source.

The bias observed at all African stations is generally lower than on the Arabian Peninsula (fig. 5.10). The scatter is typically larger, but a dedicated overestimating branch cannot be seen in the scatter plots. This holds also for the dust cases selected by the Dubovik criterion as described in section 5.1.3 (fig. 5.11). This remarkable and general difference between the African and the European stations on the one hand and the Arabian stations on the other hand indicates, that dust overestimations seem to be a regional issue for the Arabian Peninsula and the Middle East. This may point towards the erodibility databases as the most relevant factor for improvement instead of a general mis-modelling e.g. of the dry deposition or the dust mobilisation. On the other hand it is not clear without any deeper analysis if those air masses reaching the AERONET stations south of the Sahara have been altered by wet deposition which may overlay a possible mis-modelling in the dry deposition scheme.

Remarkable are the stations Djougou and Ilorin showing a general underestimation with a MBD = -0.17 at Djougou and -0.2 at Ilorin. According to the AERONET site description the dust plumes observed in Ilorin typically originate from the Bodele Depression in the Chad Basin, a well known strong emission source. This may indicate an underestimation of the surface erodibility of this region in MATCH.

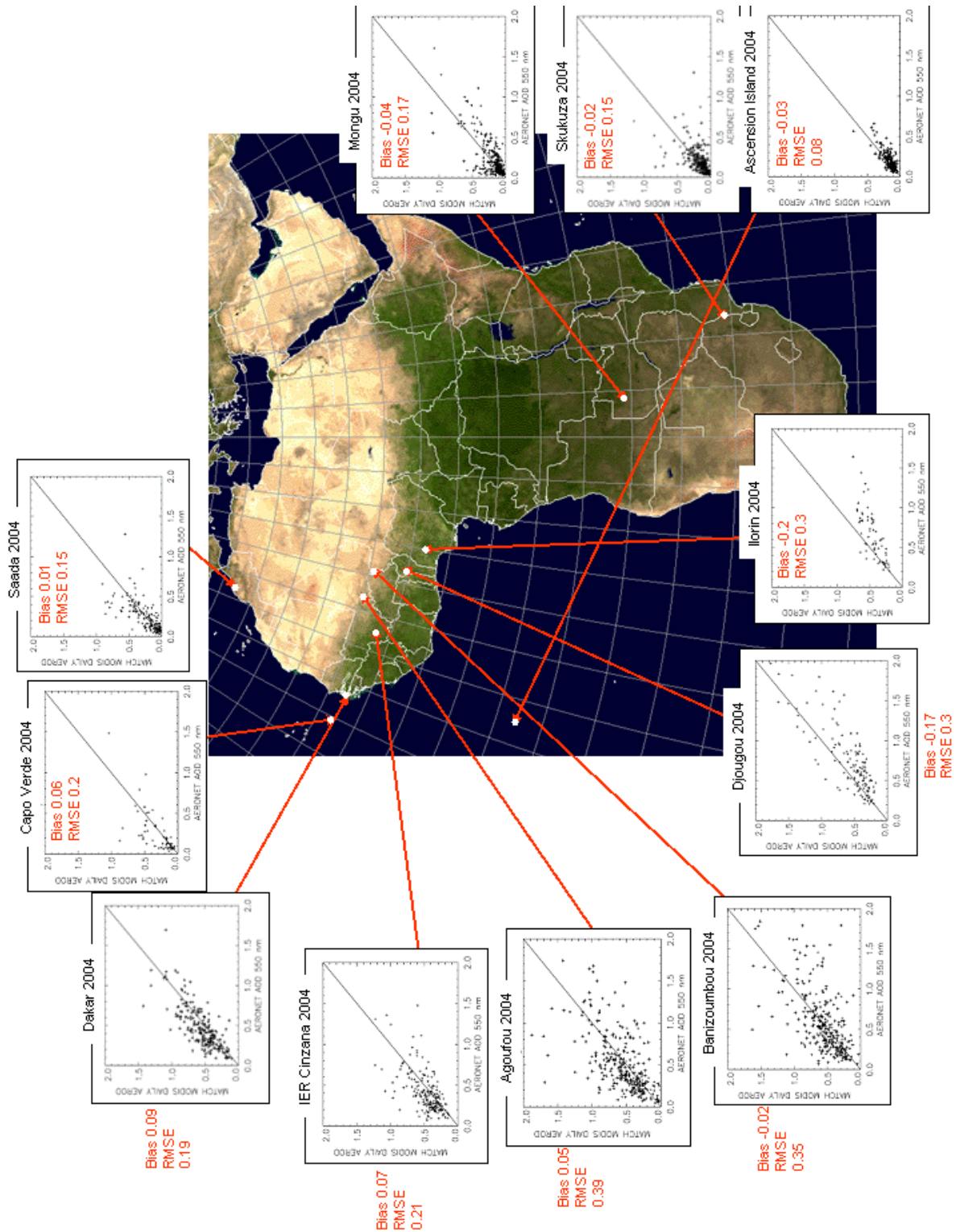


Fig. 5.10. Scatter plots for the NCAR/MATCH-MODIS dataset for all African AERONET validation stations together with mean bias deviation and root mean square deviation for 2004

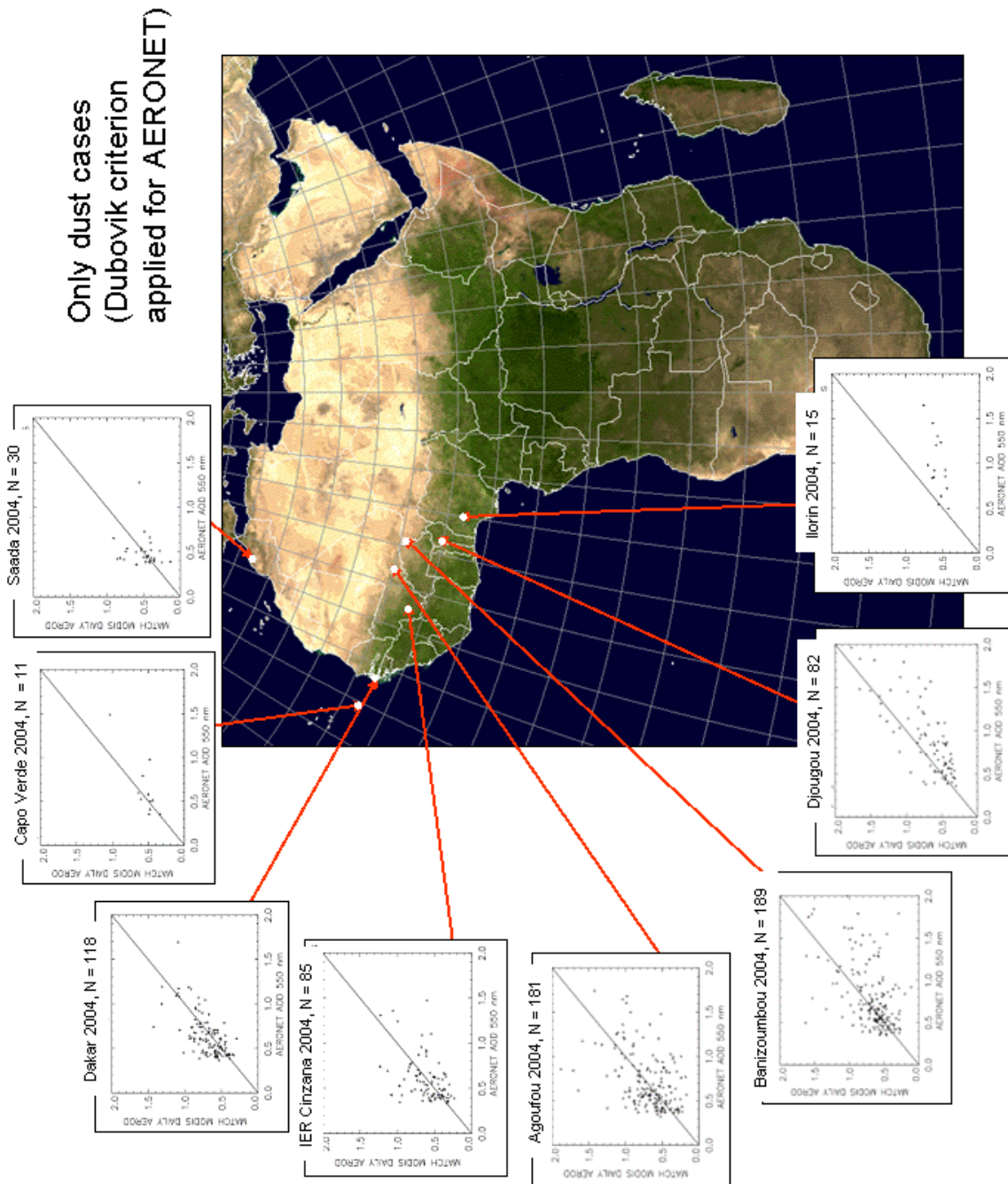


Fig. 5.11. Scatter plots for the NCAR/MATCH-MODIS dataset for all African AERONET validation stations for 2004, only dust cases as selected with the 'Dubovik criterion'

5.1.6 Asia

A similar validation of the NCAR/MATCH-MODIS data set against the Asian AERONET stations is shown in fig. 5.12 for the total AOD at 550 nm. A separate analysis of dust cases based on the Dubovik criterion results in the occurrence of 34 dust cases at the station of Kanpur, India, while all other stations seem to be not affected by dust as detected in the Dubovik criterion.

The AERONET stations in Beijing, Osaka, Shirahama, Gwangju, Taipei, Chen-Kung Univ., Chulalongkorn and Kanpur are located in large urban areas. There are probably dominated by local emission regimes and show a large scatter. But also other stations like Gosan, Bac Giang, and

Anmyon show a large scatter and some stations have even an underestimation of a MBD = -0.1 in Pimai or -0.32 in XiangHe. As Asia is not in the current focus of the SESK project, a further analysis is not performed.

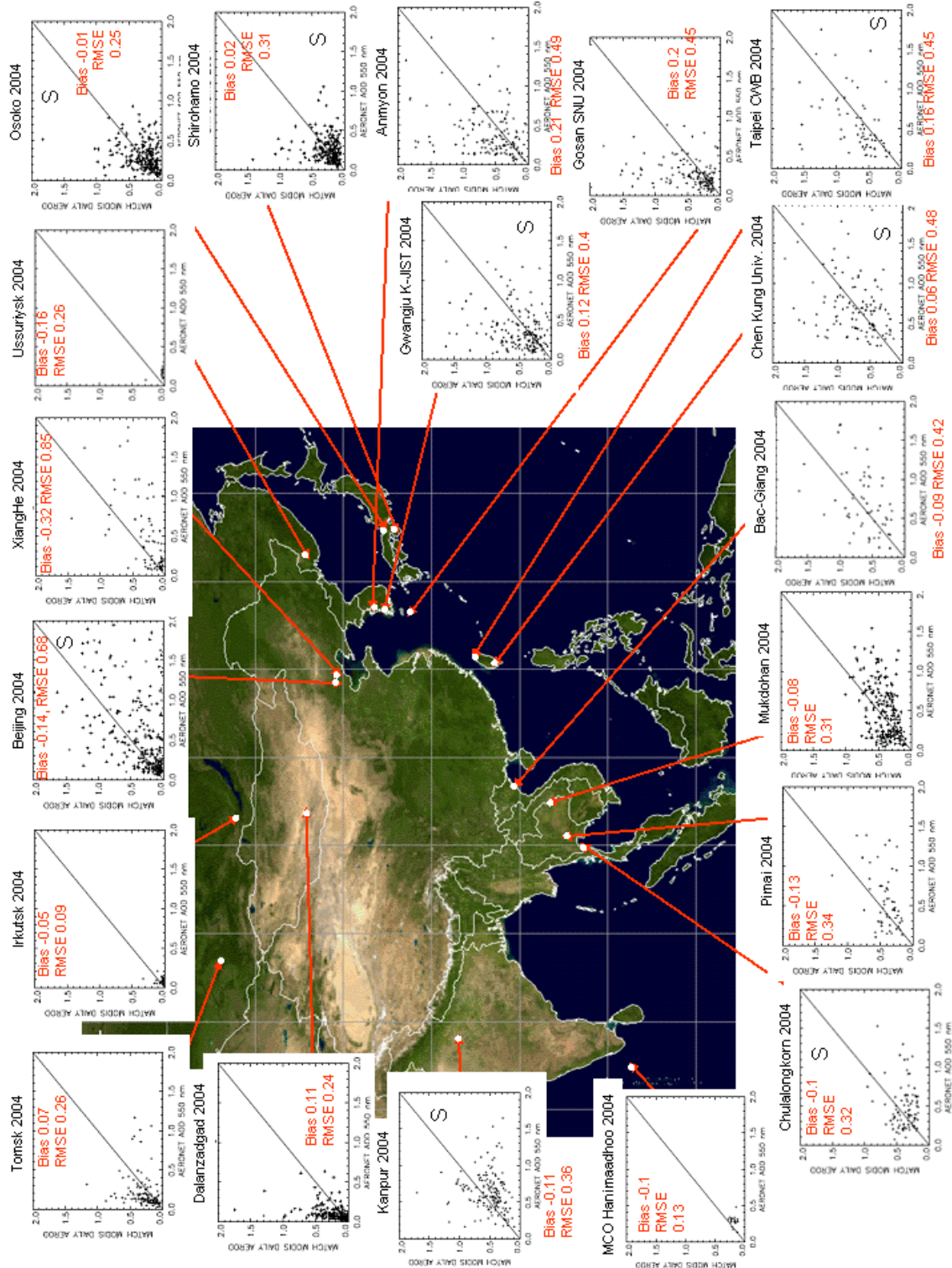


Fig. 5.12. Scatter plots for the NCAR/MATCH-MODIS dataset for all Asian AERONET validation stations together with mean bias deviation and root mean square deviation for 2004

5.1.7 Post processing

As discussed in section 5.1.2 and 5.1.4 an overestimation of AOD is frequently caused by strong peaks either in the sulfate or the dust aerosol component. The NCAR/MATCH-MODIS data set consists of a rather long period from 2000 to 2005 and is based on data assimilation using the MODIS instrument AOD measurements. It is a remarkable effort of providing MODIS measurements and performing an assimilation run. Therefore, it is worth as an intermediate step to exclude such strong peaks in the existing data set using an empirically derived post processing. Later on, a new reprocessing of MATCH including an assimilation scheme is foreseen, but this needs some further development work first. In the meanwhile, the following post processing for the existing data set is suggested:

NCAR/MATCH-MODIS values are marked as **suspicious dust events** if either a strong temporal gradient occurs

$$\text{AOD}_{\text{dust},i+1} - \text{AOD}_{\text{dust},i} > 0.7 \text{ with } i = i^{\text{th}} \text{ day in the time series} \quad (\text{eq 5.3})$$

or the AOD value is large and also dominated strongly by dust

$$\text{AOD}_{\text{dust},i} / \text{AOD}_{\text{total},i} > 0.95 \text{ and } \text{AOD}_{\text{total},i} > 1.0 \quad (\text{eq 5.4})$$

As typically large scale dust events last longer than one day, all days following a detected dust peak on a day j with

$$\text{AOD}_{\text{dust},j+n} - \text{AOD}_{\text{dust},j} > 0.3 \quad (\text{eq 5.5})$$

with $n = 1, 2, 3, \dots$ as long as criterion of eq. 5.5 is met

are also marked as suspicious dust events.

NCAR/MATCH-MODIS values are marked as **suspicious sulfate events** if

$$\text{AOD}_{\text{SO}_4,i+1} - \text{AOD}_{\text{SO}_4,i} > 0.4 \text{ with } i = i^{\text{th}} \text{ day in the time series} \quad (\text{eq 5.6})$$

The sulfate peaks are typically shorter in time than dust events, but it was observed that they may last longer than one day. Therefore, the day following a detected sulfate peak with

$$\text{AOD}_{\text{SO}_4,j+2} - \text{AOD}_{\text{SO}_4,j} > 0.5 \quad (\text{eq 5.7})$$

is also marked as suspicious sulfate cases.

For all suspicious cases the flagged values are eliminated from the time series and replaced by a linear interpolation between the last and the first 'good' data point around the gap. Additionally, a low pass filter with a length of 3 days is applied to smooth the time series.

The post processing is empirically developed using NCAR/MATCH-MODIS time series of the full year 2003 at all AERONET stations in the MSG field of view (Europe, Middle East, and Africa, not in Asia). It improves validation results for 2003 by reducing the RMSD from 0.21 to 0.17 with a constant bias of 0.02 and an improved correlation coefficient of 0.63 instead of 0.57.

For 2004 with 10800 coincidences as a test case for the post processing the MBD is reduced from 0.06 to 0.04, the RMSD is reduced from 0.24 to 0.2 and the correlation coefficient is 0.67 instead of 0.62. Tab. 5.1, 5.2, and 5.3 show the changes for all AERONET stations used in this comparison. Similar improvements can be observed also for 2005 with a MBD reduction from 0.01 to 0.0, a RMSD reduction from 0.25 to 0.22 and a correlation coefficient increase from 0.56 to 0.65.

In the Central European region a general reduction of the MBD can be observed at all stations together with a clearly visible RMSD reduction. The number of coincidences is sufficient for all stations with the exception of Paris where only 7 coincidences exist in 2004.

In the Mediterranean, a clear improvement by the post processing can be observed in Blida, Forth Crete, Lampedusa, Lecce, Nes Ziona, Palencia, Rome, Sede Boker, Toulouse, Venise, and Villefranche. The other stations are not improved. For Avignon, Cabo da Roca, Cairo University, and IMS METU ERDEMLI this is caused mainly by the non-availability of AERONET measurements in those cases eliminated by the post processing. Therefore, an impact of the post processing at these stations exists, but cannot be quantified. For Evora and El Arenosillo it has to be noted, that a strong and short peak of AOD is observed in the AERONET measurement, but filtered out by the post processing.

On the Arabian Peninsula, a significant positive impact of the post processing can be observed only at Abu Al Bukhoosh (RMSD 0.20 to 0.17), Dalma (MBD 0.13 to 0.12, RMSD 0.26 to 0.22), Hamim (MBD 0.18 to 0.17, RMSD 0.28 to 0.25), Mussafa (MBD 0.06 to 0.04, RMSD 0.17 to 0.12), and Solar Village (MBD 0.17 to 0.13, RMSD 0.28 to 0.23). For most stations, there is no coincidence with AERONET measurements in those cases with eliminated peaks by the post processing. Therefore, the impact of the post processing cannot be quantified.

The same can be observed in Africa. Only the station Agoufou has coincident AERONET measurements in those cases changed by the post processing scheme. Its MBD is reduced from 0.05 to 0.01 and the RMSD from 0.39 to 0.33.

The impact of the post processing scheme for the Asian stations is given in Tab. 5.3. Stations like Anmyon, Dalanzadgad, Gosan SNU, Gwangju K-JIST, Shirohama, Taipei and Tomsk show both an improved MBD and RMSD. Nearly no impact of the post processing scheme can be observed in Chulalongkorn, Irkutsk, MCO Hanimaadhoo, Mukdahan, and Ussuriysk. Again, these are stations with cases eliminated in the post processing scheme, but without a possibility to validate those cases due to missing AERONET coincidences in time. For Bac Giang, Beijing, Chen Kung University, Kanpur, Osaka, and XiangHe an increased underestimation (larger negative MBD) can be observed while the overall RMSD is still improved by the post processing scheme. At these stations a high variability in the AOD with many short-term peaks are observed also in AERONET, but overestimated in the MATCH sulfate component. The post processing corrects these peaks too strongly in its temporal interpolation scheme and therefore, results in an underestimation. For Pimai, the same effect can be seen in the time series of MATCH vs. AERONET, but only in this case also the RMSD is increased through the post processing scheme.

Tab. 5.1: Validation results NCAR/MATCH-MODIS AOD 550 nm, 12 UTC vs. AERONET daily means with and without an empirical post processing (PP) for the period 1.1. – 31.12.2004, mean bias deviation (MBD) and root mean square deviation (RMSD) is given for AERONET stations in Central Europea

MBD	MBD with PP	RMSD	RMSD with PP	no. of values	station
0.05	0.02	0.24	0.12	65	Dunkerque
0.06	0.05	0.17	0.14	106	Fontainebleau
0.08	0.07	0.23	0.14	115	Hamburg
0.17	0.07	0.45	0.19	40	Helgoland
0.16	0.14	0.28	0.19	129	IFT Leipzig
0.08	0.05	0.17	0.12	125	Laegeren
0.02	0.02	0.14	0.10	71	Lille
0.16	0.12	0.24	0.15	18	Munich Maisach
0.09	0.08	0.18	0.14	139	Palaiseau
-0.05	-0.05	0.1	0.09	7	Paris
0.12	0.08	0.24	0.16	73	The Hague

Tab. 5.2: Validation results NCAR/MATCH-MODIS AOD 550 nm, 12 UTC vs. AERONET daily means with and without an empirical post processing (PP) for the period 1.1. – 31.12.2004, mean bias deviation (MBD) and root mean square deviation (RMSD) is given for AERONET stations in the Mediterranean region

MBD	MBD with PP	RMSD	RMSD with PP	no. of values	station
-0.02	-0.02	0.12	0.11	264	Avignon
0.03	0.0	0.18	0.13	220	Blida
0.04	0.04	0.11	0.11	193	Cabo da Roca
-0.1	-0.1	0.2	0.19	52	Cairo
0.02	0.01	0.1	0.11	302	El Arenosillo
0.02	0.02	0.12	0.11	266	Evora
0.06	0.07	0.15	0.15	40	Etna
0.04	0.03	0.19	0.12	272	Forth Crete
-0.05	-0.05	0.13	0.11	235	IMS METU ERDEMLI
0.14	0.08	0.32	0.29	111	Lampedusa
0.07	0.06	0.19	0.15	219	Lecce University
0.07	0.04	0.22	0.13	299	Nes Ziona
0.09	0.05	0.20	0.12	258	Palencia
0.06	0.06	0.23	0.18	66	Rome Tor Vergata
0.12	0.09	0.24	0.16	310	Sede Boker
0.02	0.02	0.14	0.11	176	Toulouse
0.08	0.02	0.30	0.21	230	Venise
0.02	0.01	0.18	0.14	235	Villefranche

Tab. 5.3: Validation results NCAR/MATCH-MODIS AOD 550 nm, 12 UTC vs. AERONET daily means with and without an empirical post processing (PP) for the period 1.1. – 31.12.2004, mean bias deviation (MBD) and root mean square deviation (RMSD) is given for AERONET stations in the Asian region

MBD	MBD with PP	RMSD	RMSD with PP	no. of values	station
0.21	-0.03	0.49	0.32	143	Anmyon
-0.09	-0.14	0.42	0.40	59	Bac Giang
-0.14	-0.31	0.68	0.63	271	Beijing (urban)
0.06	-0.16	0.48	0.45	120	Cheng-Kung Univ. (urban)
-0.1	-0.11	0.32	0.32	94	Chulalongkorn (urban)
0.11	0.1	0.24	0.18	240	Dalanzadgad
0.2	0.01	0.45	0.19	140	Gosan SNU
0.12	-0.01	0.4	0.32	185	Gwanju K-IST (urban)
-0.05	-0.05	0.09	0.08	35	Irkutsk
-0.11	-0.12	0.36	0.34	161	Kanpur (urban)
-0.1	-0.1	0.13	0.12	20	MCO Hanimaadhoo
-0.08	-0.08	0.31	0.3	216	Mukdahan
-0.01	-0.06	0.25	0.18	219	Osaka (urban)
-0.13	-0.17	0.34	0.37	60	Pimai
0.02	-0.02	0.31	0.16	240	Shirohama (urban)
0.16	-0.02	0.45	0.34	65	Taipei CWB (urban)
0.07	0.05	0.26	0.21	119	Tomsk
-0.16	-0.15	0.26	0.25	13	Ussuriysk
-0.32	-0.39	0.85	0.76	69	XiangHe

5.1.8 Comparison with GACP climatology

Currently, the SOLEMI database for long-term global and direct irradiance time series is based on the GACP (NASA/GISS) data set (Tegen et al., 1997). Based on chemical transport modelling optical thickness is provided as monthly means for sea salt, soil dust, sulfate, carbonaceous aerosols and black carbon. Its spatial resolution is $4 \times 5^\circ$ on a global scale. The monthly means are meant as representative datasets applicable for all calendar years.

Obviously, this temporal and spatial resolution is rather coarse. Using MATCH with a daily or even hourly temporal resolution and with a spatial resolution of 0.7, 1.4 or 1.9 degrees holds the potential to improve this situation. Therefore, a comparison between validation results against AERONET measurements is performed for the NCAR/MATCH-MODIS data set and the GACP data set.

Fig. 5.13, 5.14, and 5.15 show in alphabetical station order MBD, RMSD and the correlation coefficient for both the NCAR/MATCH-MODIS data set and the GACP data set derived for all AERONET stations. The GACP data set shows large underestimations up to -0.5 in the mean bias deviation. The NCAR/MATCH-MODIS data set shows MBD between -0.1 and 0.1 for most stations, but tends to overestimate at several stations. Overall, the MBD exceeds the [-0.1, 0.1] range for 24 stations out of a total of 77 stations in the GACP data set, while only 15 stations show this effect in the NCAR/MATCH-MODIS data set. For 41 out of 77 stations the RMSD of the NCAR/MATCH-MODIS data set is lower than the RMSD shown by the GACP data set vali-

dated vs. AERONET measurements. The correlation coefficient of the NCAR/MATCH-MODIS data set is significantly higher for most stations. Correlation coefficients above 0.7 are reached frequently. This shows clearly the improvement obtained by using daily modelling of the actual calendar year instead of a monthly climatology taken as constant for each calendar year.

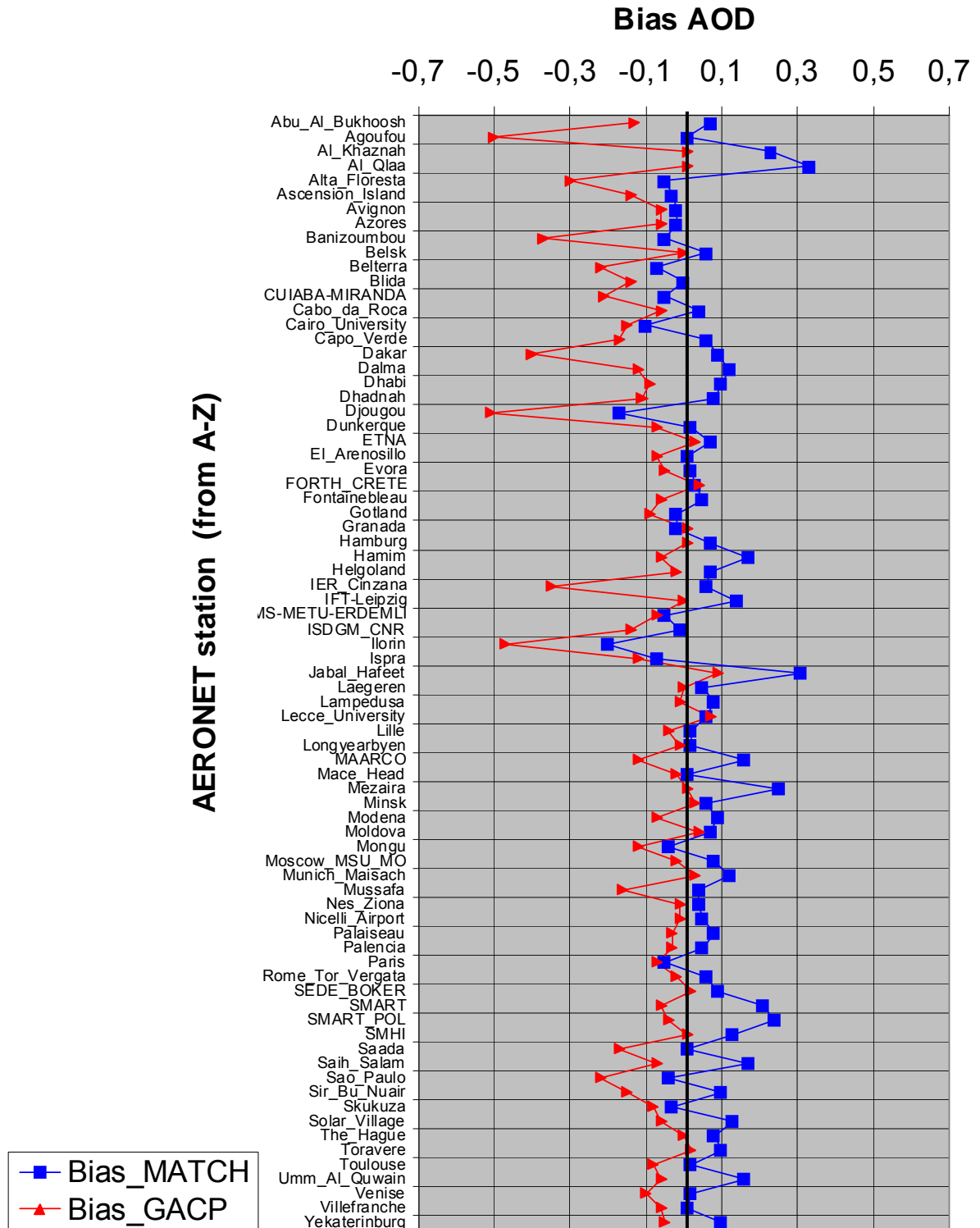


Fig. 5.13. Bias for the NCAR/MATCH-MODIS and GACP aerosol dataset for all AERONET stations within the MSG field of view for 2004

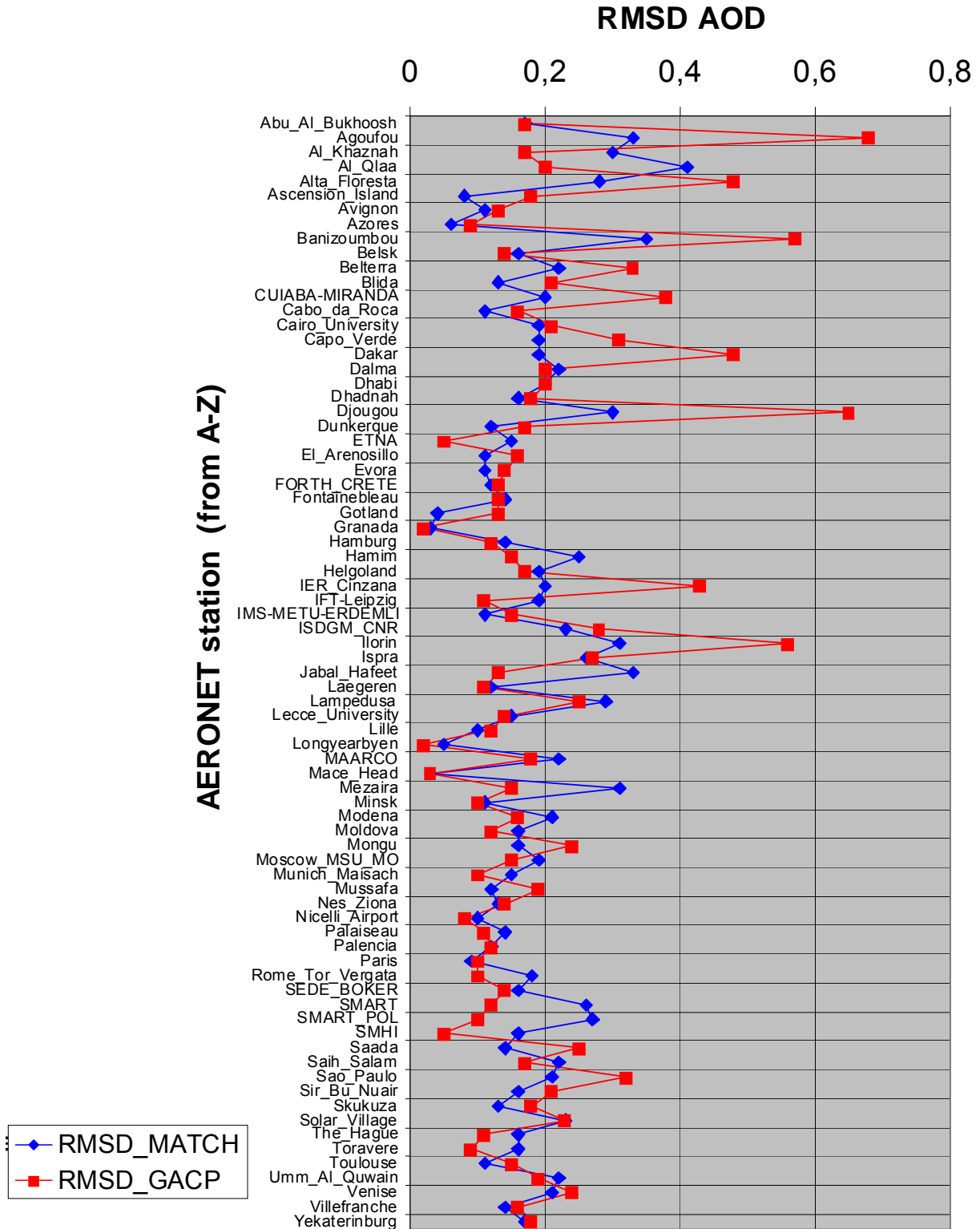


Fig. 5.14. RMSD for the NCAR/MATCH-MODIS and GACP aerosol dataset for all AERONET stations within the MSG field of view for 2004

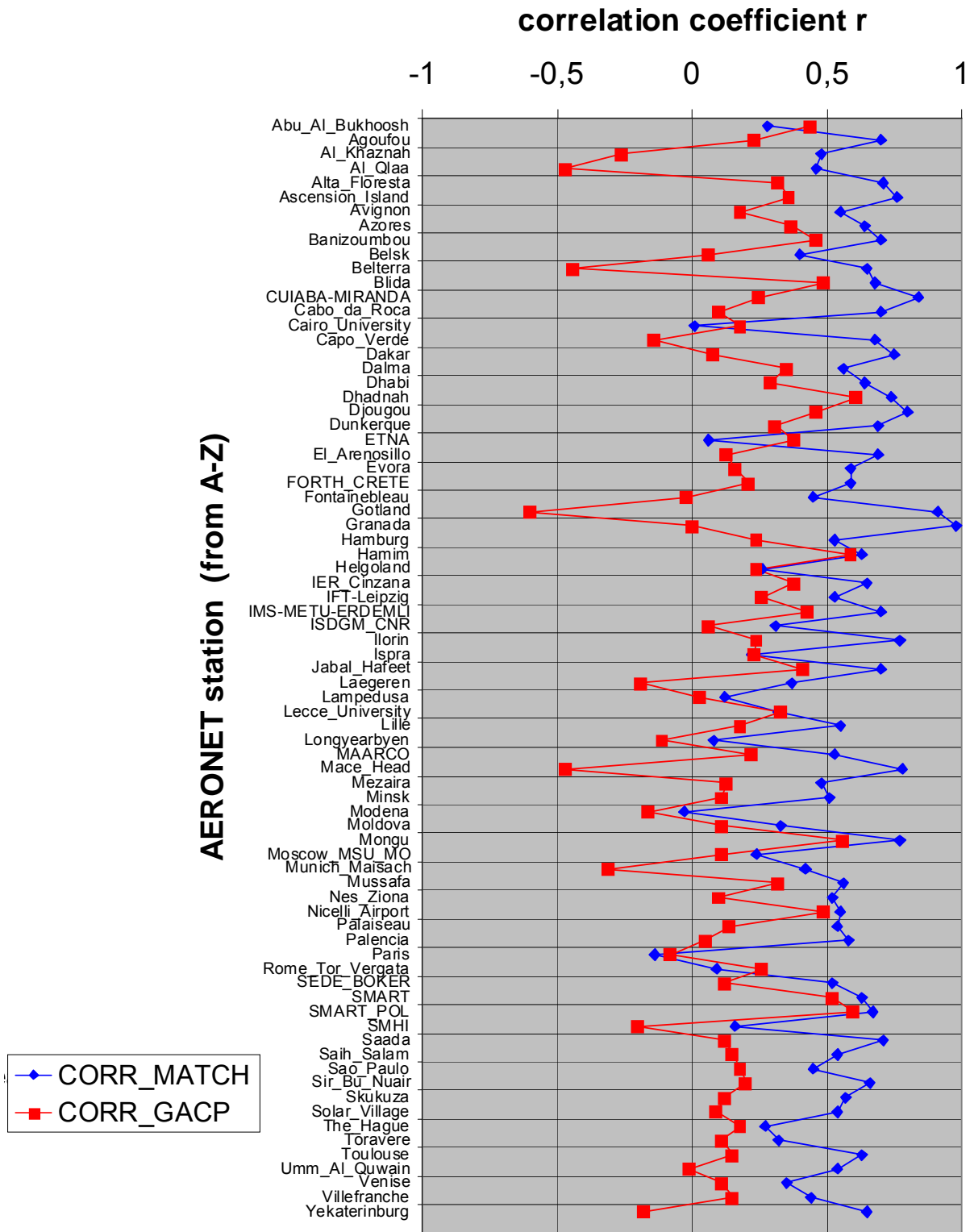


Fig. 5.15. Correlation coefficients for the NCAR/MATCH-MODIS and GACP aerosol dataset for all AERONET stations within the MSG field of view for 2004

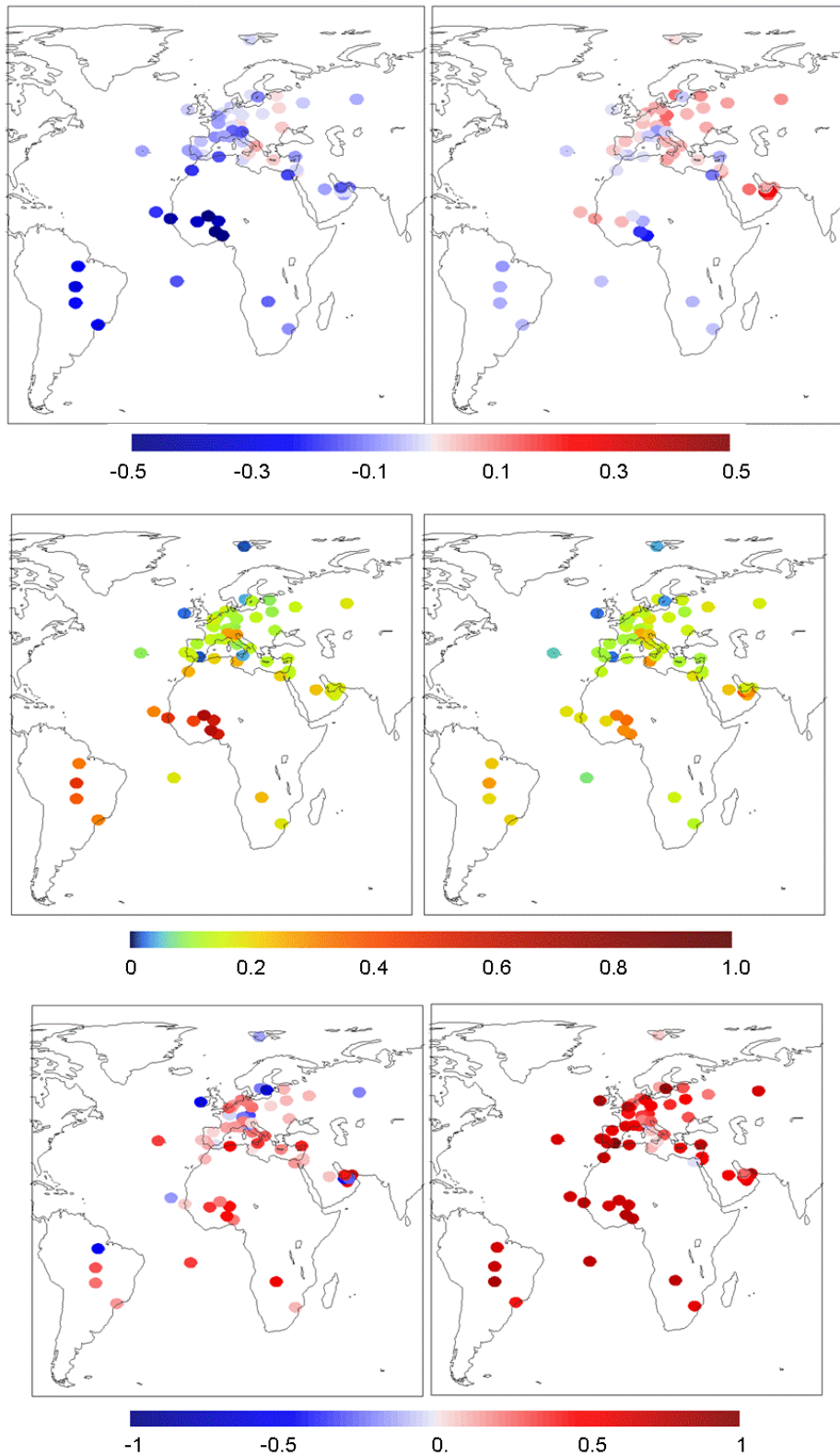


Fig. 5.16. MBD (top), RMSD (middle) and correlation coefficients (bottom) for the GACP (left) and NCAR/MATCH-MODIS (right) aerosol dataset for all AERONET stations within the MSG field of view for 2004

5.2 DLR/MATCH 2004

5.2.1 Assimilation impact

First of all, an impact analysis is performed to clarify about the assimilation impact of the MODIS AOD assimilation in the NCAR/MATCH-MODIS dataset. Therefore, the DLR/MATCH dataset was calculated for 2004. This dataset provides hourly information, but for this comparison, only 12 UTC values are used in order to keep the comparability with the NCAR/MATCH-MODIS data set which also consists of 12 UTC values only.

Tab. 5.4 shows smaller MBD, smaller RMSD and larger correlation coefficients (marked in blue) for the 'no assim' case at nearly all stations in the Central, North and Eastern European subset. This corresponds to the high sulfate AOD problem described in section 5.1.2 which is a numerical artefact produced by the assimilation scheme as used for the NCAR/MATCH-MODIS data set. Removing the assimilation scheme results in an improved validation in this region.

The situation in the Mediterranean subset is less clear (tab. 5.4). Several stations show better validation results in the 'no assim' case, while other stations show improved results through the assimilation scheme. Those stations affected frequently by dust outbreaks show an improved RMSD as a result of the assimilation scheme.

For the African stations, the assimilated MODIS AOD results in improved values for MBD, RMSD and correlation coefficient for most stations (tab. 5.5). Here, a positive assimilation impact is clearly visible.

On the Arabian Peninsula (tab 5.7), the MBD values are smaller in the 'no assim' case for the majority of cases. But looking at the RMSD and the correlation coefficient, a positive impact of the data assimilation scheme can clearly be seen.

In Asia, most stations show significantly smaller MBD as an impact of the assimilation (tab 5.8). This holds especially for the large urban conglomerations in the second group in the table. Nevertheless, the RMSD and the correlation coefficient reveals better results in the 'no assim' case for many stations. Therefore, the impact of MODIS data assimilation in Asia can't be clearly described as positive or negative.

Overall, it can be stated that the problem of high sulfate values vanishes as expected if the assimilation scheme is turned off. On the other hand a positive impact of the assimilation can be seen in those regions far from the west wind zone which transport the extreme sulfate values from the Atlantic Ocean towards Europe. Especially, modelling in Africa and the Arabian Peninsula shows benefits from the MODIS AOD assimilation. Therefore, a future implementation of a MODIS or probably METOP AOD assimilation scheme is recommended.

Tab. 5.4: Validation results NCAR/MATCH-MODIS AOD 550 nm, 12 UTC vs. AERONET daily means ('with assim' case) and DLR/MATCH AOD 550nm, 12 UTC vs. AERONET daily means ('no assim' case) for the period 1.1. – 31.12.2004 in the Central, North and Eastern European region, improvements (blue) and declined values (red)

MBD with assim	MBD no assim	RMSD with assim	RMSD no assim	r with assim	r no assim	No.	station
Central, North and Eastern Europe							
0,05	-0,04	0,24	0,14	0,59	0,68	65	Dunkerque
0,06	-0,04	0,17	0,14	0,49	0,45	106	Fontainebleau
0,08	-0,02	0,23	0,11	0,38	0,56	115	Hamburg
0,17	-0,05	0,45	0,17	0,26	0,46	40	Helgoland
0,16	0,06	0,28	0,19	0,4	0,5	129	IFT-Leipzig
0,08	0	0,17	0,1	0,49	0,64	125	Laegeren
0,02	-0,04	0,14	0,12	0,49	0,51	71	Lille
0,16	-0,02	0,24	0,09	0,68	0,45	18	Munich_Maisach
0,09	-0,01	0,18	0,11	0,51	0,59	139	Palaiseau
-0,05	-0,07	0,1	0,09	0,08	0,54	7	Paris
0,12	-0,02	0,24	0,14	0,24	0,38	73	The_Hague
0,19	0,05	0,41	0,23	0,23	0,51	150	Belsk
-0,08	-0,15	0,22	0,29	0,61	0,02	81	Belterra
-0,05	-0,06	0,07	0,07	0,81	0,91	8	Gotland
0,01	-0,02	0,04	0,04	0,09	0,04	30	Longyearbyen
0	0	0,03	0,05	0,59	0,11	5	Mace_Head
0,15	0,02	0,29	0,12	0,34	0,57	88	Minsk
0,11	0,08	0,23	0,21	0,44	0,47	190	Moldova
0,1	-0,01	0,24	0,17	0,23	0,43	165	Moscow_MSU_MO
0,22	0,08	0,39	0,17	0,49	0,53	25	SMHI
0,12	0,01	0,22	0,14	0,31	0,41	139	Toravere

Tab. 5.5: Validation results NCAR/MATCH-MODIS AOD 550 nm, 12 UTC vs. AERONET daily means ('with assim' case) and DLR/MATCH AOD 550nm, 12 UTC vs. AERONET daily means ('no assim' case) for the period 1.1. – 31.12.2004 in the Mediterranean region, improvements (blue) and declined values (red)

MBD with assim	MBD no assim	RMSD with assim	RMSD no assim	r with assim	r no assim	No.	station
Mediterranean subset							
-0,02	-0,06	0,12	0,12	0,55	0,65	264	Avignon

0,03	0,03	0,18	0,23	0,72	0,73	220	Blida
0,04	0,01	0,11	0,12	0,72	0,74	193	Cabo_da_Roca
-0,1	-0,12	0,2	0,23	0,04	-0,09	52	Cairo_University
0,02	0,02	0,1	0,14	0,8	0,79	302	El_Arenosillo
0,06	0,02	0,15	0,07	0,16	0,14	40	ETNA
0,02	0	0,12	0,12	0,65	0,7	266	Evora
0,04	0,09	0,19	0,29	0,47	0,62	272	FORTH_CRETE
-0,02	-0,03	0,03	0,04	0,99	0,87	3	Granada
0,03	-0,05	0,3	0,3	0,15	0,04	209	ISDGM_CNR
-0,05	-0,09	0,13	0,18	0,63	0,48	235	IMS-METU-ERDEMLI
-0,07	-0,14	0,27	0,27	0,25	0,34	200	Ispra
0,14	0,14	0,32	0,41	0,63	0,46	111	Lampedusa
0,07	0,05	0,19	0,21	0,28	0,49	219	Lecce_University
0,15	0,02	0,3	0,19	0,03	0,18	70	Modena
0,07	0,03	0,22	0,3	0,44	0,45	299	Nes_Ziona
0,06	0,04	0,12	0,13	0,56	0,23	10	Nicelli_Airport
0,09	0,01	0,2	0,11	0,52	0,6	258	Palencia
0,06	-0,01	0,23	0,24	0,15	0,05	66	Rome_Tor_Vergata
0,12	0,08	0,24	0,28	0,41	0,55	310	SEDE_BOKER
0,02	-0,02	0,14	0,14	0,59	0,64	176	Toulouse
0,08	-0,01	0,3	0,28	0,22	0,1	230	Venise
0,02	-0,02	0,18	0,17	0,37	0,37	235	Villefranche

Tab. 5.6: Validation results NCAR/MATCH-MODIS AOD 550 nm, 12 UTC vs. AERONET daily means ('with assim' case) and DLR/MATCH AOD 550nm, 12 UTC vs. AERONET daily means ('no assim' case) for the period 1.1. – 31.12.2004 in the African region, improvements (blue) and declined values (red)

MBD with assim	MBD no assim	RMSD with assim	RMSD no assim	r with assim	r no assim	No.	Station
African subset							
0,05	0,03	0,39	0,42	0,61	0,58	316	Agoufou
-0,02	-0,06	0,35	0,4	0,67	0,58	325	Banizoumbou
0,06	0,15	0,2	0,24	0,69	0,79	59	Capo_Verde
0,09	0,14	0,19	0,28	0,76	0,64	219	Dakar
-0,17	-0,25	0,3	0,39	0,8	0,71	136	Djoujou
0,07	0,01	0,21	0,21	0,62	0,66	195	IER_Cinzana
-0,2	-0,33	0,3	0,44	0,76	0,44	66	Ilorin

-0,04	-0,11	0,17	0,23	0,74	0,59	238	Mongu
0,01	0,09	0,15	0,27	0,69	0,64	158	Saada
-0,02	-0,09	0,15	0,17	0,5	0,48	279	Skukuza

Tab. 5.7: Validation results NCAR/MATCH-MODIS AOD 550 nm, 12 UTC vs. AERONET daily means ('with assim' case) and DLR/MATCH AOD 550nm, 12 UTC vs. AERONET daily means ('no assim' case) for the period 1.1. – 31.12.2004 in the Arabian Peninsula region, improvements (blue) and declined values (red)

MBD with assim	MBD no assim	RMSD with assim	RMSD no assim	r with assim	r no assim	No.	station
Arabian subset							
0,07	-0,02	0,2	0,29	0,27	0,23	83	Abu_Al_Bukhoosh
0,1	-0,15	0,15	0,2	0,85	0,67	4	Abu_Dhabi
0,24	0,21	0,32	0,37	0,48	0,26	100	Al_Khaznah
0,33	0,38	0,44	0,59	0,45	0,48	44	Al_Qlaa
0,13	0,15	0,26	0,54	0,59	0,42	161	Dalma
0,12	0,2	0,24	0,37	0,67	0,53	203	Dhabi
0,08	-0,02	0,17	0,23	0,71	0,47	161	Dhadnah
0,18	0,14	0,28	0,35	0,61	0,44	183	Hamim
0,3	0,21	0,34	0,32	0,65	0,49	83	Jabal_Hafeet
0,16	0,07	0,23	0,28	0,56	0,38	56	MAARCO
0,25	0,18	0,32	0,35	0,47	0,33	124	Mezaira
0,06	0,08	0,17	0,33	0,7	0,45	75	Mussafa
0,21	0,11	0,27	0,28	0,62	0,46	55	SMART
0,24	0,13	0,29	0,28	0,63	0,53	58	SMART_POL
0,17	0,05	0,24	0,24	0,48	0,4	111	Saih_Salam
0,1	-0,02	0,17	0,24	0,62	0,46	60	Sir_Bu_Nuair
0,17	0,18	0,28	0,33	0,65	0,63	284	Solar_Village
0,16	0,06	0,23	0,25	0,48	0,29	135	Umm_Al_Quwain

Tab. 5.8: Validation results NCAR/MATCH-MODIS AOD 550 nm, 12 UTC vs. AERONET daily means ('with assim' case) and DLR/MATCH AOD 550nm, 12 UTC vs. AERONET daily means ('no assim' case) for the period 1.1. – 31.12.2004 in the Asian region, improvements (blue) and declined values (red)

MBD with assim	MBD no assim	RMSD with assim	RMSD no assim	r with assim	r no assim	No.	station
Asian subset							
0,21	-0,12	0,49	0,3	0,3	0,45	143	Anmyon
-0,09	-0,37	0,42	0,54	0,37	0,25	59	Bac_Giang
0,11	0,04	0,24	0,27	0,4	0,24	240	Dalanzadgad
0,2	-0,05	0,45	0,19	0,41	0,43	140	Gosan_SNU
-0,05	-0,07	0,09	0,08	0,02	0,1	35	Irkutsk
-0,1	-0,1	0,13	0,13	0,08	0,39	20	MCO-Hanimaadh.
-0,08	-0,24	0,31	0,39	0,46	0,42	216	Mukdahan
-0,13	-0,31	0,34	0,46	0,4	0,26	60	Pimai
0,07	-0,05	0,26	0,2	0,25	0,46	119	Tomsk
-0,16	-0,19	0,26	0,26	-0,25	-0,24	13	Ussuriysk
-0,32	-0,54	0,85	0,85	0,3	0,66	87	XiangHe
0,05	-0,03	0,11	0,07	0,33	0,36	69	Yakutsk
-0,14	-0,41	0,68	0,68	0,41	0,49	271	Beijing
0,06	-0,26	0,48	0,47	0,35	0,2	120	Chen-Kung_Univ
-0,1	-0,24	0,32	0,38	0,17	-0,06	94	Chulalongkorn
0,12	-0,15	0,4	0,36	0,36	0,37	185	Gwangju_K-JIST
-0,11	-0,27	0,36	0,44	0,17	0	161	Kanpur
-0,01	-0,13	0,25	0,21	0,27	0,38	219	Osaka
0,02	-0,1	0,31	0,21	0,19	0,26	240	Shirahama
0,16	-0,16	0,45	0,37	0,41	0,43	65	Taipei_CWB

5.2.2 Post processing

The post processing as described in section 5.1.7 was developed for the NCAR/MATCH-MODIS dataset especially. It takes the observed limitations as described in section 5.1.2 and 5.1.4 into account. Separate tests for detecting sulfate and dust peaks are applied.

Having shown in section 5.2.1 that the sulfate peaks in Central Europe are not observed anymore in a MATCH run without the assimilation, it raises the question whether the post processing needs to be applied at all or modified accordingly.

Therefore, a validation of DLR/MATCH daily means (derived from hourly values) and AERONET daily mean values is performed with and without post-processing.

The post-processing for high sulfate peaks is not applied anymore in the Central European region. This corresponds to the assimilation impact analysis showing that the sulfate peaks in Central Europe seem to be an artefact of the assimilation scheme. On the contrary, in Asia the sulfate correction tends to remove sulfate peaks seen also in the AERONET ground measurement. Therefore, it is recommended to apply no sulfate peak post-processing anymore.

Regarding the post processing on dust peaks, the situation is two-sided. A positive impact can be observed in the Arabian Peninsula region as well as in Mediterranean stations as Blida, Forth Crete, Lampedusa, Lecce, Lille, Nes Ziona, Rome, and Sede Boker with a reduced RMSD. These are mainly those regions showing a systematic overestimation of dust in the NCAR/MATCH-MODIS validation (section 5.1). On the other hand, in Africa sometimes well modelled dust peaks are removed by the post processing (e.g. in Agoufou, Banizoumbou, Dakar, Djougou). Also, El Arenosillo shows a better modelling without this filter. These are mainly the same regions showing good validation results in section 5.1.5. As the main focus for solar energy applications is currently in the Mediterranean and Arabian Peninsula region, it is recommended to keep the dust post processing until the dust mobilisation is improved in DLR/MATCH and these regional dependencies are clarified.

5.2.3 Hourly variability

Soluble aerosols as sulfate, sea-salt and organic carbon are a subject of hygroscopic growth which is modelled as a function of relative humidity during the calculation of aerosol optical depths. All meteorological input values are instantaneous values at a specified time every 6 hours. They are interpolated linearly towards the actual time step. Intra-day variations are also a result of horizontal mass concentration gradients, dry and wet deposition.

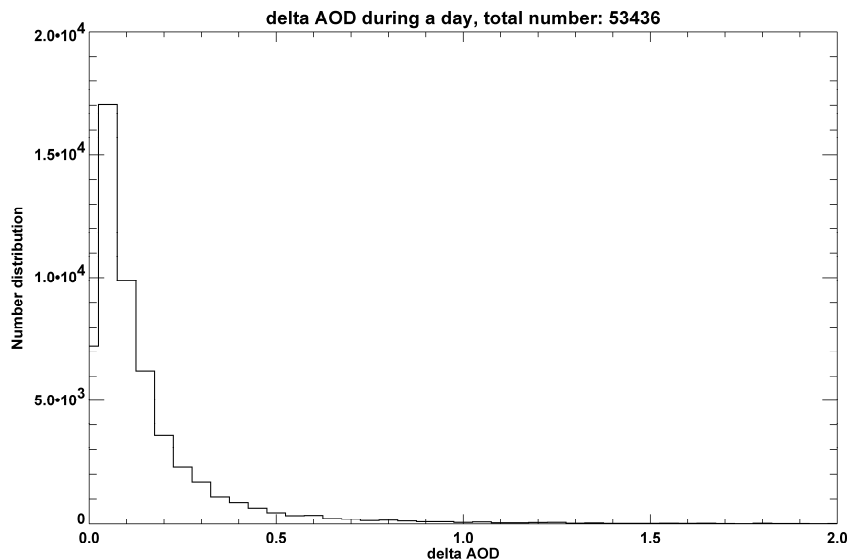


Fig. 5.17. Intra-day variability of DLR/MATCH for 2004 calculated as difference between minimum and maximum AOD value of each day.

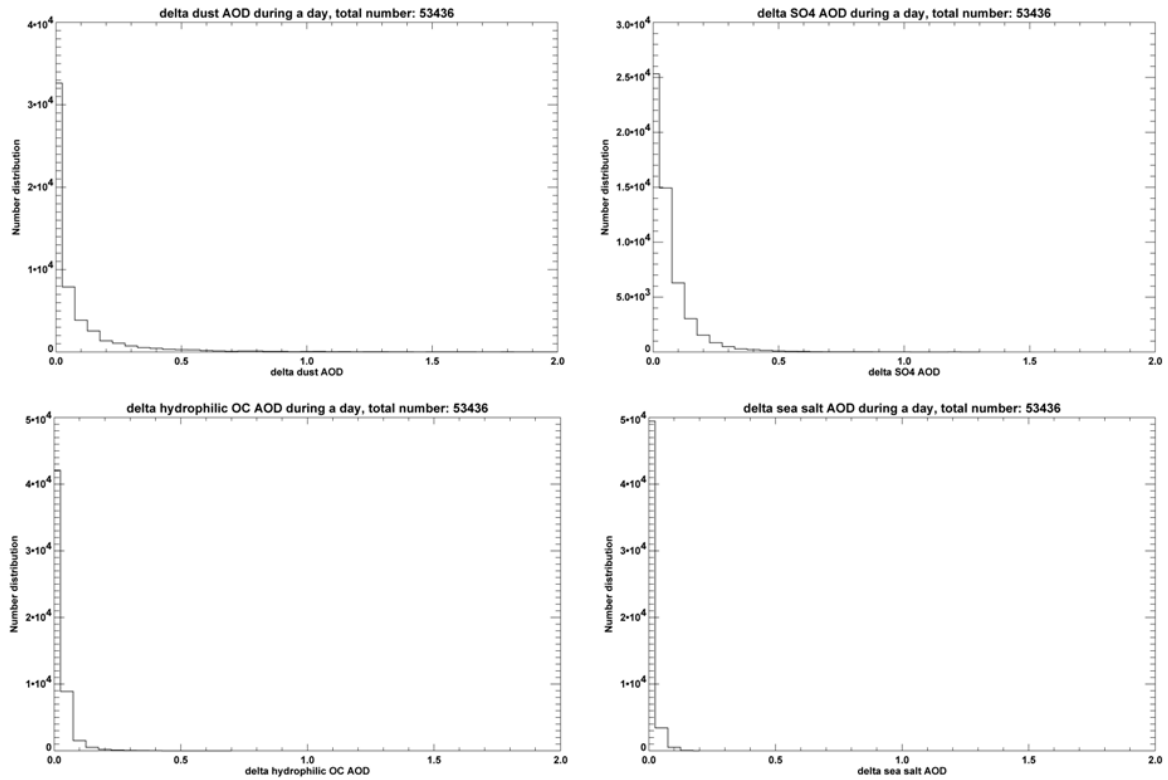


Fig. 5.18. Intra-day variability of DLR/MATCH for 2004 separated into contributions from dust, sulfate, hydrophilic organic carbon and sea salt.

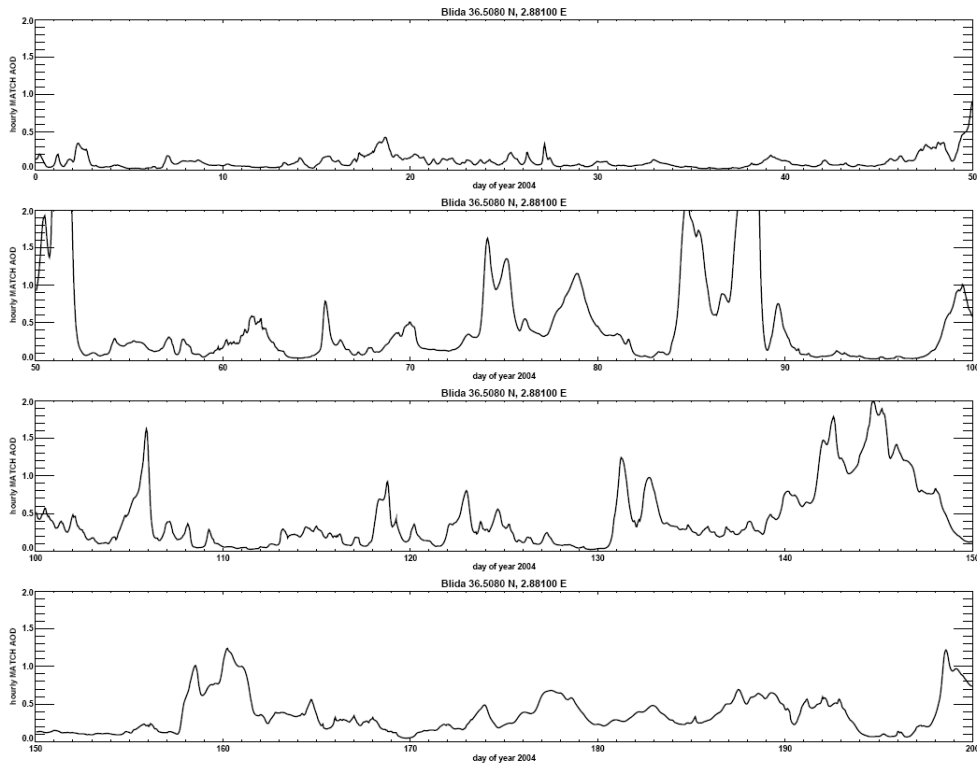


Fig. 5.19. A typical example of an hourly resolved DLR/MATCH time series for the AERONET station Blida.

Taking the rather coarse input data temporal resolution into account, it needs to be evaluated how much intra-day variability occurs in the MATCH modelling. Fig. 5.17 shows the intra-day variability calculated as difference between each minimum and maximum AOD value occurring each day. Fig. 5.18 shows that this intra-day variability can be attributed mainly to the horizontal gradients of dust concentrations (as dust is not subject of a hygroscopic growth in the model) and to the hygroscopic substances sulfate (dominant contribution), hydrophilic organic carbon and sea salt. An example of hourly resolved MATCH data is given in fig. 5.19.

5.3 DLR/MATCH 2004 Regional Validation

All further validation studies in this section are based on daily mean AERONET measurements. Hourly resolved DLR/MATCH output is averaged between 0 and 23 UTC. A future comparison using hourly DLR/MATCH model output versus AERONET individual measurements is foreseen, but not part of this study.

The validation of daily mean DLR/MATCH AOD values after the post processing procedure as described in 5.2.2 was performed versus daily mean measurements of the AERONET network for the year 2004. Overall a number of 10800 coincidences were analysed from 78 stations in Europe and Africa.

Generally, a good agreement within 0.1 can be observed for a majority of all cases. Nevertheless, a remarkable scatter can be observed as well. Fig. 5.20 shows the validation of all data without post-processing on the left side, while the right side shows the dataset after post-processing. Without post-processing the overall mean bias deviation is 0.01 with a root mean square deviation of 0.25 and a Pearson correlation coefficient $r = 0.57$. After post-processing the overall mean bias deviation is 0.01 with a root mean square deviation of 0.23 and a Pearson correlation coefficient $r = 0.55$. In the overall statistics the effect of the post-processing affecting extreme outliers disappears nearly. This is reasonable, as those occur only in a small number compared to the overall number of coincidences and only at some stations. Only the scatter plot reveals that a significant number of strong DLR/MATCH overestimations are excluded in the post processing scheme.

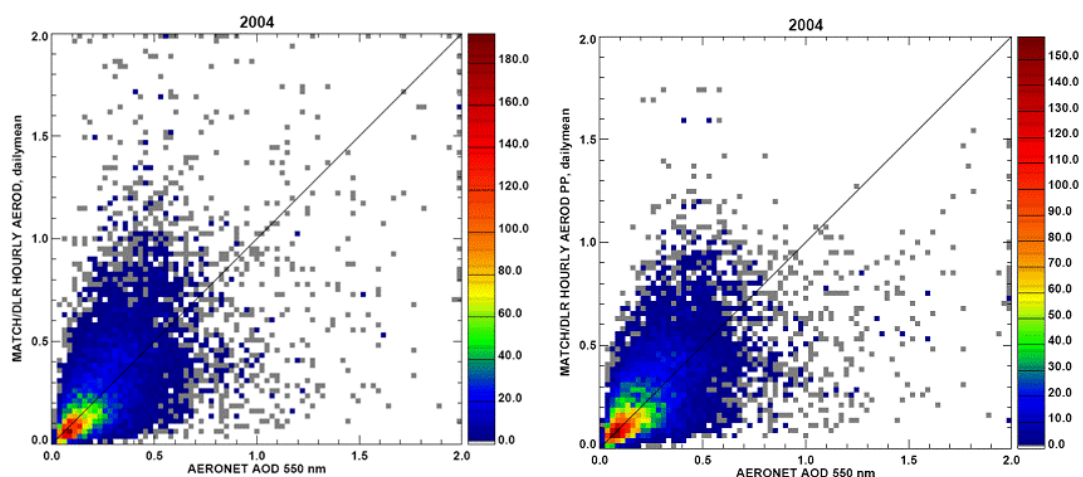


Fig. 5.20. Two-dimensional histograms of AOD from the DLR/MATCH data set vs. daily AOD means measured at the AERONET network in Europe and Africa for 2004. All data is shown on the left side, while the right side shows the dataset after post-processing. The colour bar indicates the number of occurrences in each bin of the AERONET and MATCH-MODIS AOD axes.

A remarkable difference in the number of occurring underestimations of MATCH can be seen between the NCAR/MATCH-MODIS overall scatter plot (section 5.1.1) and the DLR/MATCH run

without data assimilation. In the left plot of Fig. 5.20 (without post processing) an overall underestimation can be observed also in the range of 0 to 0.3 illustrating the positive impact of the data assimilation. The post processing (right plot) reduces the bias also in this data range, but tends to create also additional underestimations in the range above 1.0 in AERONET measurements. This is probably due to the interpolation of excluded values in the post-processing which seems to underestimate.

A dependency on station height can not be observed in any of the statistical measures.

In the following sections a station-wise validation sorted in different regions is given. All further validation results show the DLR/MATCH data set with post-processing.

5.3.1 Central Europe

Fig. 5.21 gives an overview over all Central European validation results for the test year 2004. The MBD is always below 0.1, reaching values below ± 0.03 in Dunkerque, Fontainebleau, Hamburg, Helgoland, Laegeren, Lille, Palaiseau and The Hague. The RMSD lasts from 0.08 in Munich-Maisach to 0.19 in Helgoland. Compared to the NCAR/MATCH-MODIS dataset the MBD is generally reduced with exception of Paris where the MBD is -0.07 instead of -0.05 in the NCAR dataset. For Lille, Fontainebleau, and Dunkerque the MBD shows a small underestimation but smaller than -0.03 instead of a slight overestimation up to 0.06 in the NCAR dataset. The RMSD is strongly reduced from a range among 0.1 to 0.45 in the NCAR dataset to a range from 0.08 to 0.19. Comparing the scatter plots reveals that the large overestimations of up to an AOD of 2 disappeared completely in the DLR/MATCH dataset. This shows again the impact of the sulfur assimilation problem as discussed in section 5.1.2. Therefore, it is recommended to use the DLR/MATCH dataset in Europe.

5.3.2 Mediterranean Region

The Mediterranean region is shown in fig. 5.22. On the Iberian Peninsula, a low MBD of 0.03 for Cabo da Roca, 0.02 for Palencia and El Arenosillo and 0.01 for Evora is found. The RMSD remains low between 0.1 and 0.13.

Strong overestimations with AOD values up to 1.8 can be seen only in Lampedusa (MBD 0.1) and Forth Crete (MBD 0.05), while similar overestimations seen in the NCAR/MATCH-MODIS dataset at Sede Boker, Nes Ziona, Lecce University and Venise are not found anymore in the DLR/MATCH dataset. Venise shows a strong underestimation of AOD values above 0.5 even if the MBD remains low at 0.01. Also, Cairo University shows a distinct underestimation for AOD above 0.4 resulting in a MBD of -0.1, while IMS-METU-Erdemli also shows an MBD of -0.08 resulting from underestimations in all data ranges. All other stations show a scatter both towards under- and overestimations together with a MBD below ± 0.06 .

Compared to the NCAR/MATCH-MODIS dataset the MBD is reduced at all stations with exception of Avignon, Forth Crete and IMS-METU-Erdemli which show a slight increase by 0.02 or 0.03 in MBD. Also the RMSD is reduced at most stations with exception of slight increases in RMSD in Blida (0.2 instead of 0.18), El Arenosillo (0.13 instead of 0.1), Forth Crete (0.2 instead of 0.19), IMS-METU-Erdemli (0.16 instead of 0.13), and Lampedusa (0.39 instead of 0.32). In El Arenosillo two events are underestimated by DLR/MATCH compared to the NCAR/MATCH-MODIS run where the data assimilation seems to be able to introduce additional information about these events.

Additionally, the modelling of dust events is analysed by using the Dubovik criterion (Dubovik et al., 2002, see section 5.1.3) for AERONET measurements to detect dust cases (fig. 5.23). The stations in Southern France and Italy observe between 2 and 5 dust cases and 6 cases are found

in Palencia in Northern Spain. For the South of the Iberian Peninsula 10 cases are observed in Cabo da Roca and Evora, while 20 cases occur in El Arenosillo. Blida is affected by strong dust occurrence on 34 days, Lampedusa has 6 cases, Sede Boker shows 21 cases, Nes Ziona 17 and Crete 15 cases.

Compared to the NCAR/MATCH-MODIS dataset the overestimation of dust cases in Nes Ziona, Palencia and Sede Boker are reduced, while Forth Crete shows overestimations due to long-range transports as well. On the other hand, dust events are underestimated in some cases in Blida, Cabo da Roca, El Arenosillo, Lampedusa, Venise, and Villefranche in this model run without data assimilation of MODIS measurements. It has to be noted that the number of these cases is rather small (1-2 at each station).

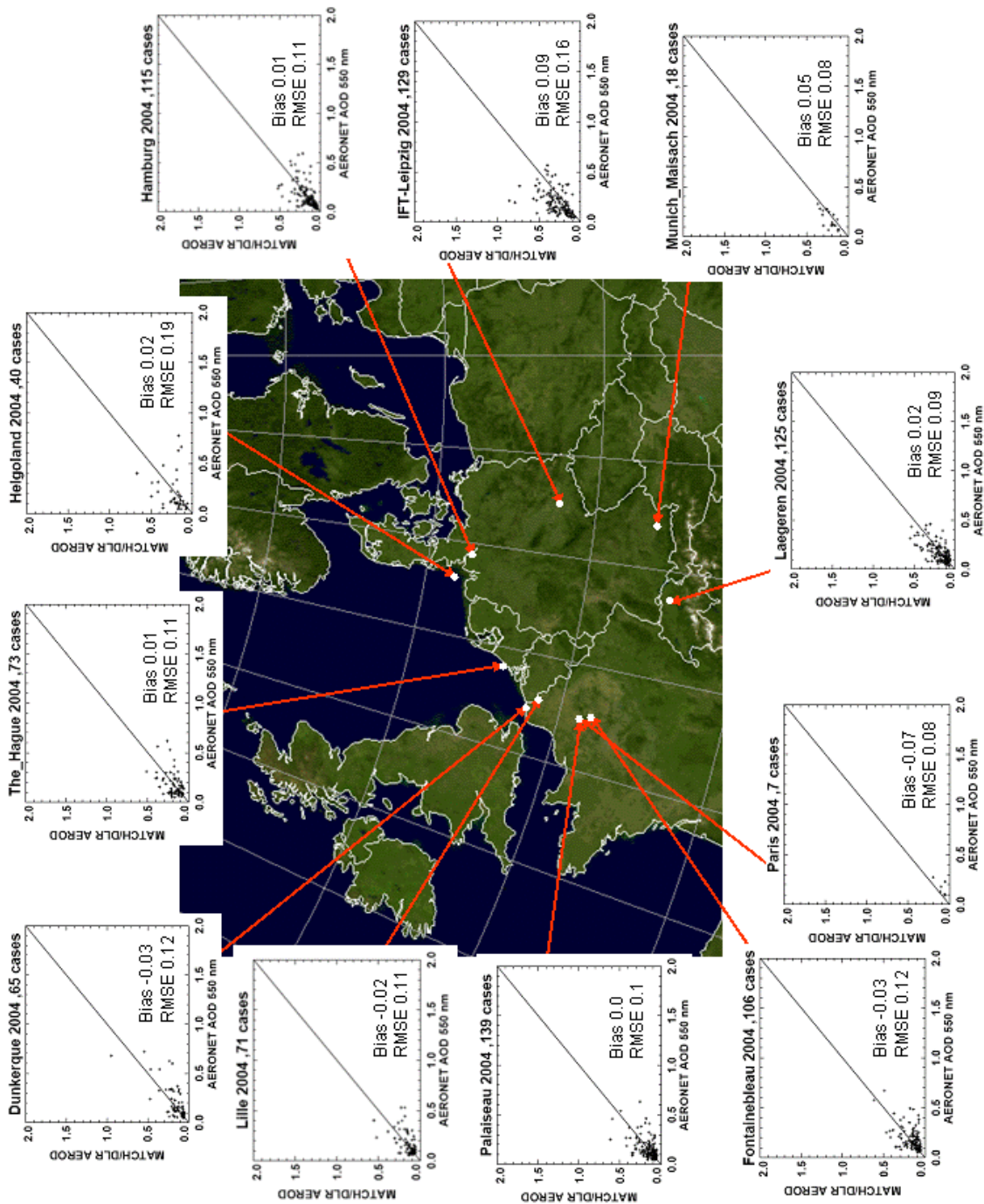


Fig. 5.21. Scatter plots for the NCAR/MATCH-MODIS dataset for all Central European AERONET validation stations together with mean bias deviation and root mean square deviation for 2004

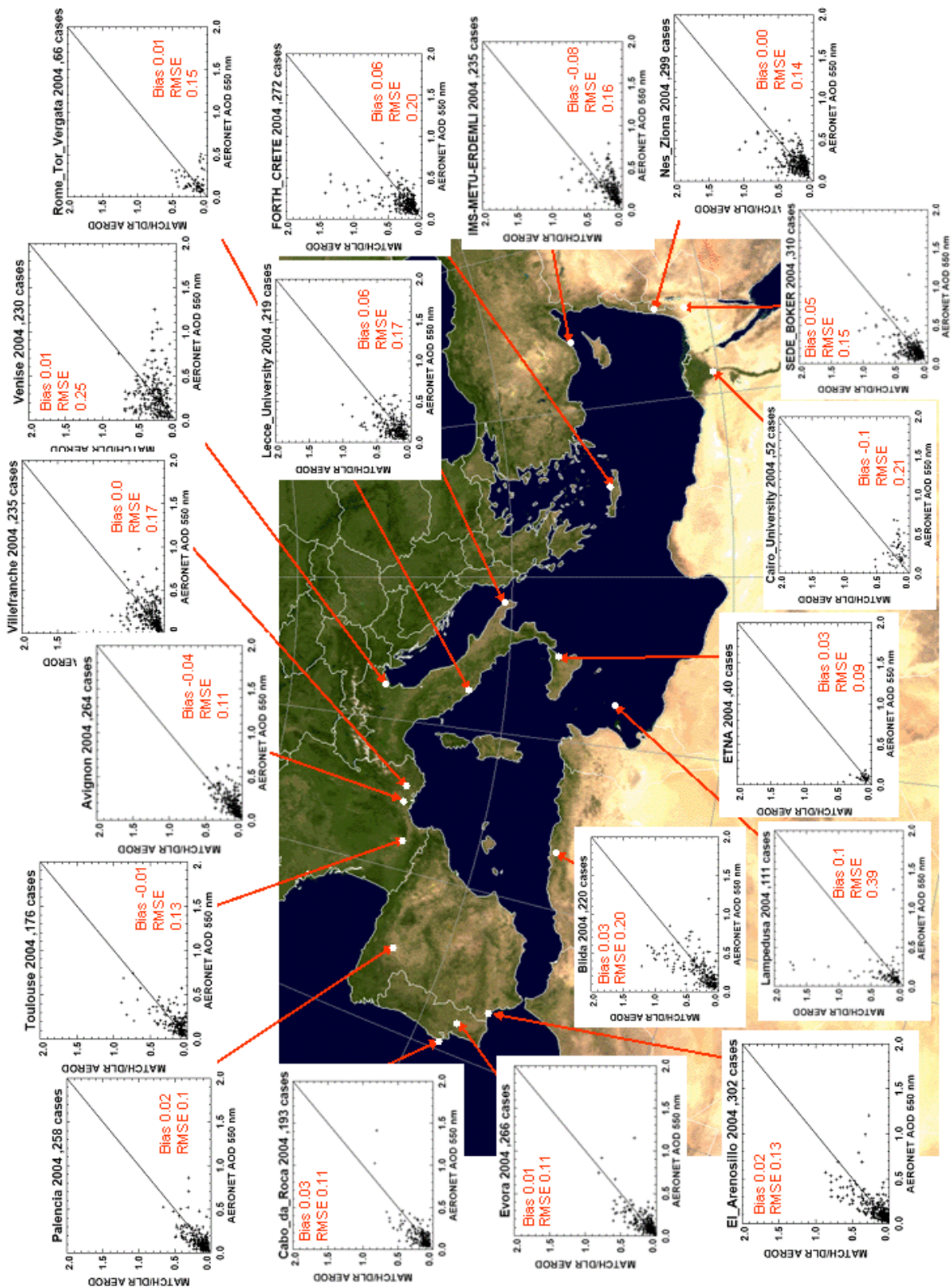


Fig. 5.22. Scatter plots for the NCAR/MATCH-MODIS dataset for all AERONET validation stations around the Mediterranean Sea together with mean bias deviation and root mean square deviation for 2004

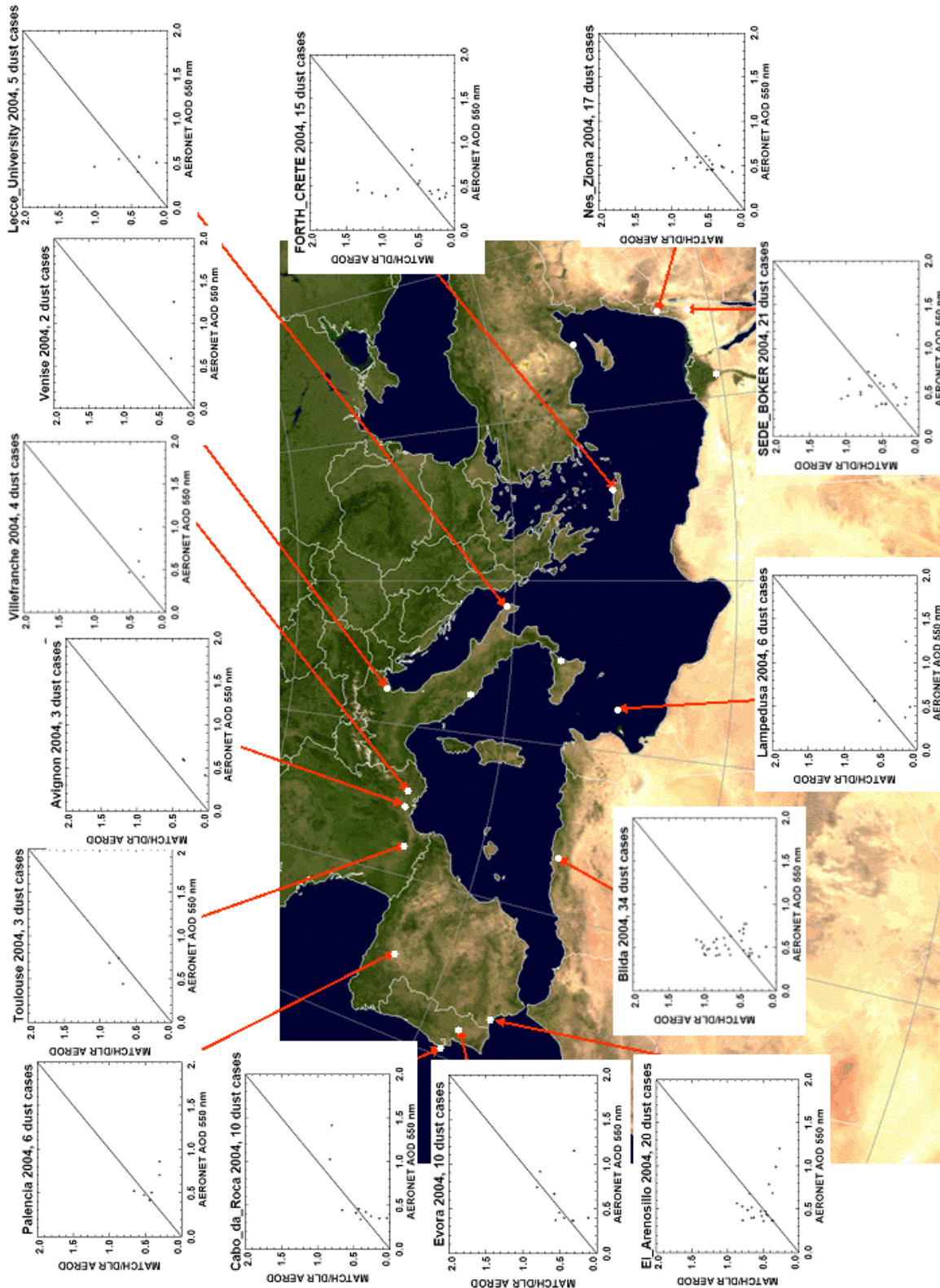


Fig. 5.23. Scatter plots for the NCAR/MATCH-MODIS dataset for all AERONET validation stations around the Mediterranean Sea for 2004, only dust cases as selected with the 'Dubovik criterion'

5.3.3 Arabian Peninsula

A similar validation was performed for the Arabian Peninsula (fig. 5.24). A general overestimation with MBD above 0.1 is found at Al Khaznah, Al Qlaa, Dhabi, Hamim, Jabal Hafeet, Mezaira, and SMART_POL (United Arab Emirates) and Solar Village (8 out of 17 stations), while Abu Dhabi has a MBD of -0.09. All other stations e.g. in the Strait of Hormuz (Abu Al Bukhoosh, Dalma, Dhadnah, Maarco, Mussafa, Saih Salam, Sir Bu Nuair, and Umm Al Quwain) show a MBD between -0.02 and 0.06. The RMSD is high with values between 0.16 and 0.34 at all stations – no dedicated regional dependence is found.

The strongly overestimating stations are mostly located close to the border between the United Arab Emirates and Oman. Mostly, dust events affecting these stations and causing these overestimations in 2004 are dominated by emission sources in Oman and the South of Saudi-Arabia. Contrary to Forth Crete and Lampedusa, the overestimations at these stations are not caused by long-range transported dust events, but by rather nearby local emissions. As these events are typically transported to the South-East, it cannot be derived from this validation study, if the long-range transported cases are overestimated as well or not. Due to missing AERONET stations in the Arabian Sea, this cannot be evaluated.

Compared to the NCAR/MATCH-MODIS data set, the MBD is significantly reduced in the DLR/MATCH data set with exception of the Station Dhabi (slightly increased MBD 0.15 instead of 0.12). On the other hand, the RMSD at several stations in the United Arab Emirates (Abu Al Bukhoosh, Al Khaznah, Dhadnah, Jabal Hafeet, Maarco, Mussafa, and Sir Bu Nuair) is larger than in the NCAR/MATCH-MODIS dataset. Therefore, a general comment on the advantage of data assimilation of MODIS measurements in this region dominated by deserts and with a lower accuracy of MODIS AOD values can not be made. The general form of the scatter plot remains similar in both data set validations.

Solar Village and Dalma show a larger number of high AERONET values classified as dust events in fig. 5.25, which are not seen in the DLR/MATCH run. At Umm Al Quwain several events with high AERONET AOD are not seen in DLR/MATCH, but these underestimations are not caused by dust cases. For all other stations a dedicated underestimation of AOD can not be found.

It is not clear if wrong spatial emission regions, a too strong emission at correct locations or an in-effective dry deposition scheme results in this wide overestimation and general scatter in this region. This is subject to further MATCH development work.

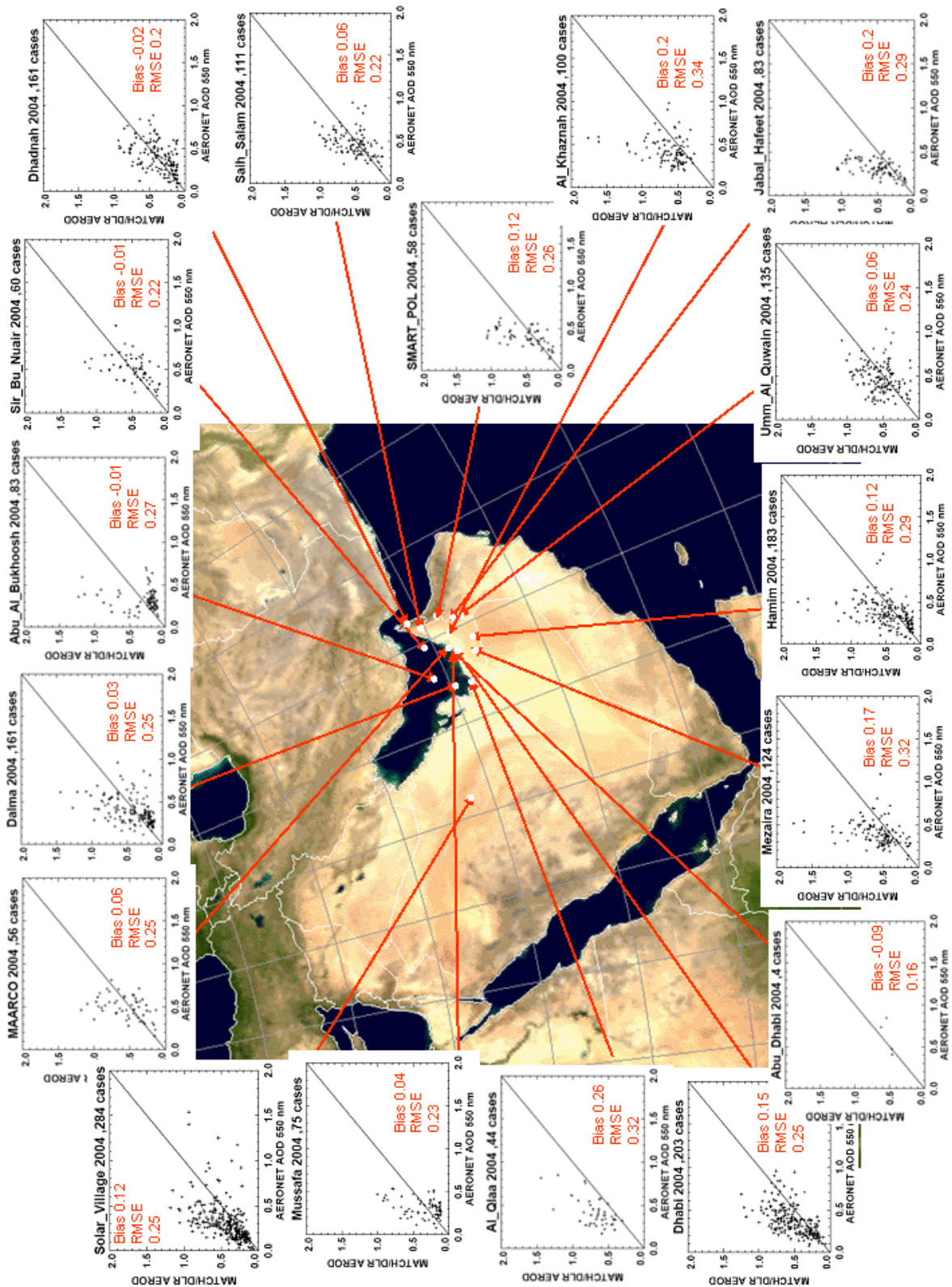
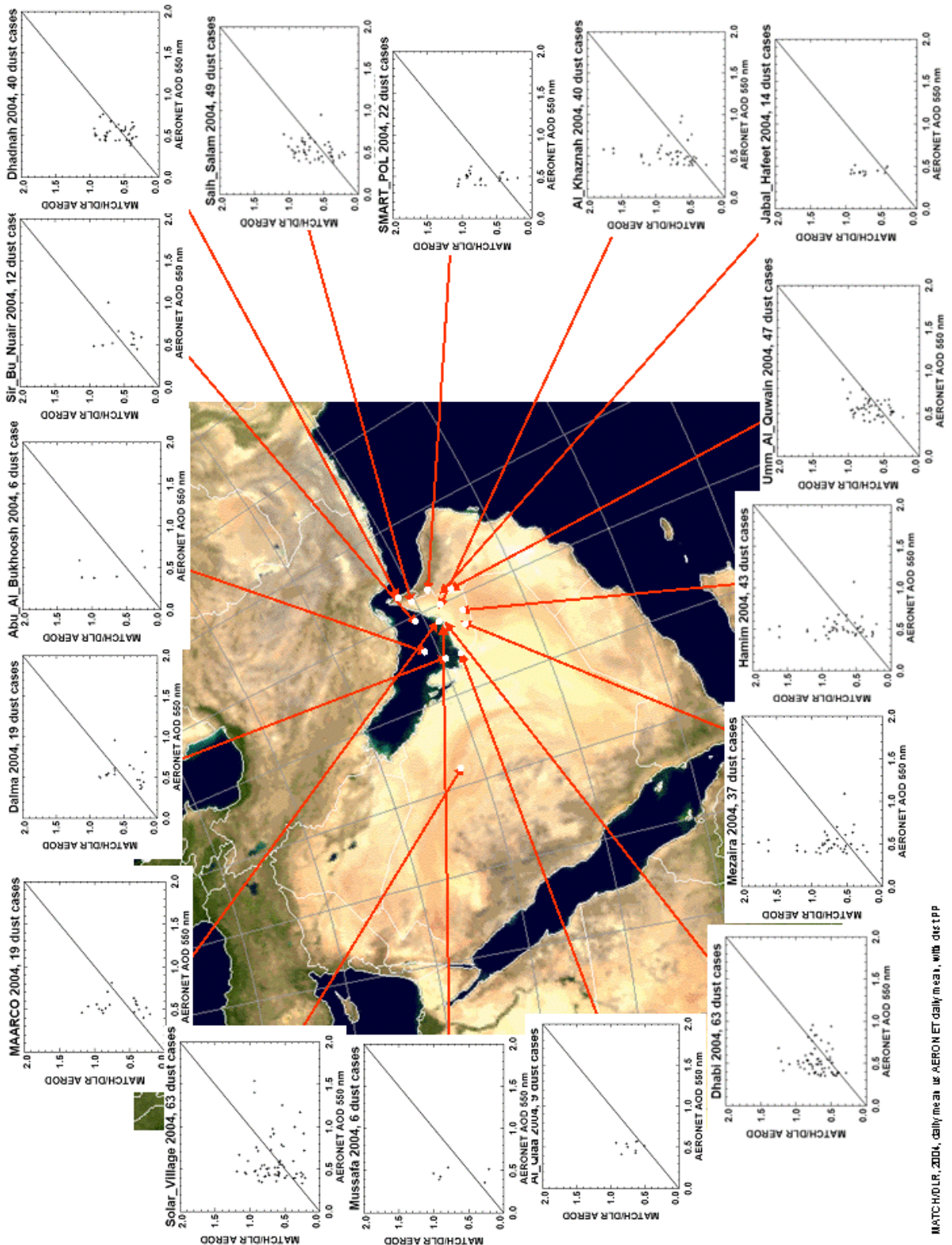


Fig. 5.24. Scatter plots for the NCAR/MATCH-MODIS dataset for all AERONET validation stations at the Arabian Peninsula together with mean bias deviation and root mean square deviation for 2004



MATCHDLR_2004, daily mean at 10 AERONET daily mean, with dts tpp

Fig. 5.25. Scatter plots for the NCAR/MATCH-MODIS dataset for all AERONET validation stations around the Mediterranean Sea for 2004, only dust cases as selected with the 'Dubovik criterion'

5.3.4 Africa

AERONET stations in Africa are located mainly south of the Sahara in a region affected by dust outbreaks but also by biomass burning as another important aerosol source. A dedicated over-estimating branch as on the Arabian Peninsula cannot be seen in the scatter plots. This holds also for the dust cases selected by the Dubovik criterion (fig. 5.26). This remarkable and general difference between the African and the European stations on the one hand and the Arabian stations on the other hand indicates, that dust overestimations seem to be a regional issue for the Arabian Peninsula and the Middle East also in the DLR/MATCH run. As said in section xx.xx this may point towards the erodibility databases as the most relevant factor for improvement instead of a general mis-modelling e.g. of the dry deposition or the dust mobilisation. On the other hand it is not clear without any deeper analysis if those air masses reaching the AERONET stations south of the Sahara have been altered by wet deposition which may overlay a possible mis-modelling in the dry deposition scheme. Remarkable are again the stations Djougou and Ilorin showing a general underestimation with a MBD = -0.29 at Djougou and -0.32 at Ilorin. According to the AERONET site description the dust plumes observed in Ilorin typically originate from the Bodele Depression in the Chad Basin, a well known strong emission source. This further strengthens the hypothesis of an underestimation of the surface erodibility of this region in MATCH.

Compared to the NCAR/MATCH-MODIS dataset, the MBD in the DLR/MATCH run is higher at the West African coast in Capo Verde (0.14 instead of 0.06), Dakar (0.12 instead of 0.09), and Saada (0.06 instead of 0.01), while the underestimation is increased around the Gulf of Guinea in Banizoumbou (-0.1 instead of -0.02), Djougou (-0.29 instead of -0.17), Ilorin (-0.32 instead of -0.2), and Ascension Island (-0.07 instead of -0.03). A similar observation is made for Mongu (-0.11 instead of -0.04) and Skukuza (-0.08 instead of -0.02). Only for IER Cinzana the MBD is improved from 0.07 to 0.0 and Agoufou shows a change from 0.05 to -0.06. The same effect can be found in the RMSD, where especially Djougou and Ilorin both increase from 0.3 to 0.43. With the exception of Saada and Capo Verde the DLR/MATCH run underestimates AERONET AOD cases above 0.5 strongly and the scatter plots show a remarkable 'saturation-like' type. It can be concluded, that the MODIS data assimilation improved results in Africa remarkably.

The separate analysis of dust cases shows, that especially in the Sahel region (Agoufou, Banizoumbou, Djougou and Ilorin) dust cases are underestimated in DLR/MATCH. The underestimation in Mongu and Skukuza can not be seen in the dust analysis, which supports the hypothesis, that biomass burning as a variable source causes this underestimation. In the NCAR/MATCH-MODIS run, the MODIS measurements clearly seem to have a positive impact in this region.

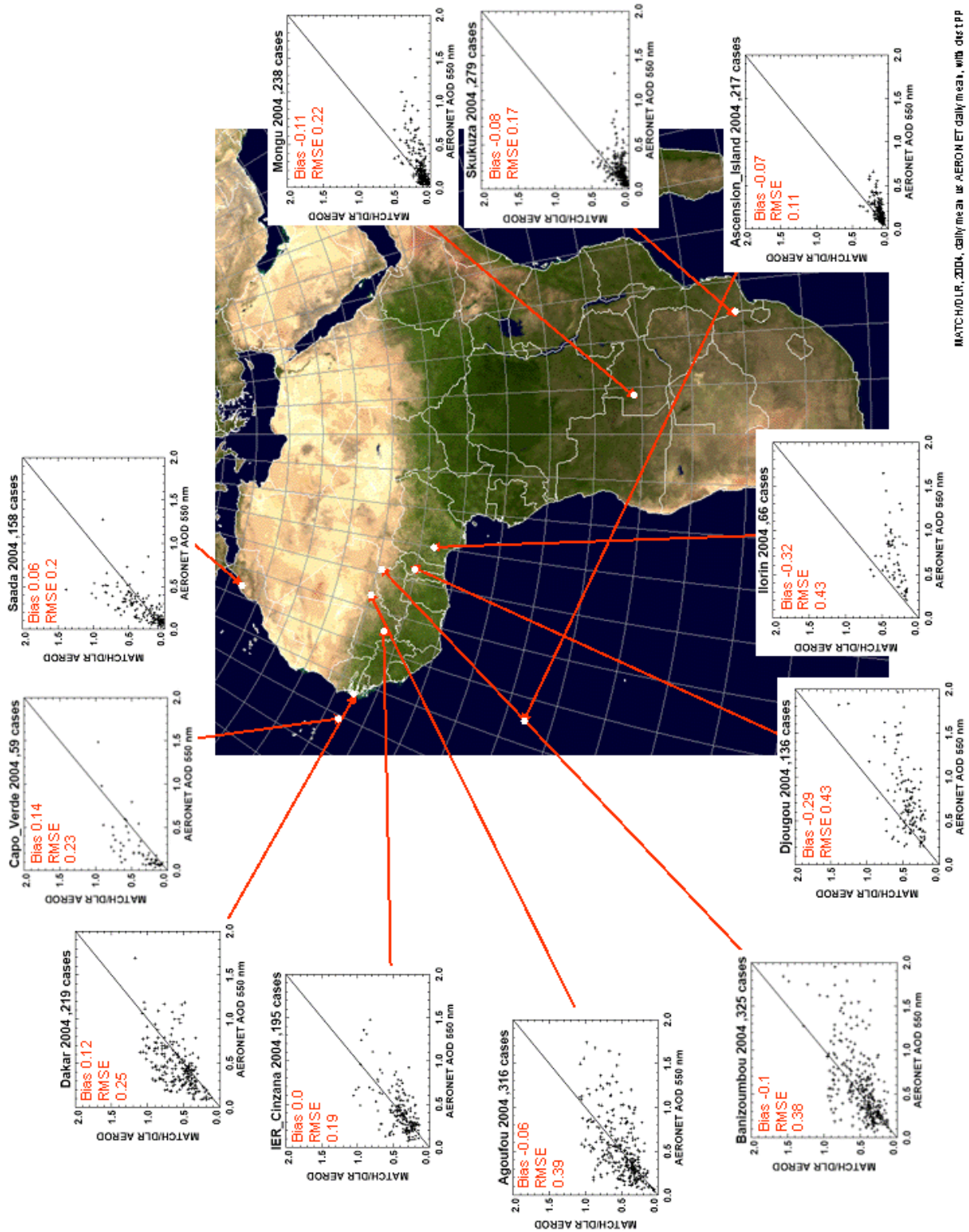


Fig. 5.26. Scatter plots for the NCAR/MATCH-MODIS dataset for all African AERONET validation stations together with mean bias deviation and root mean square deviation for 2004

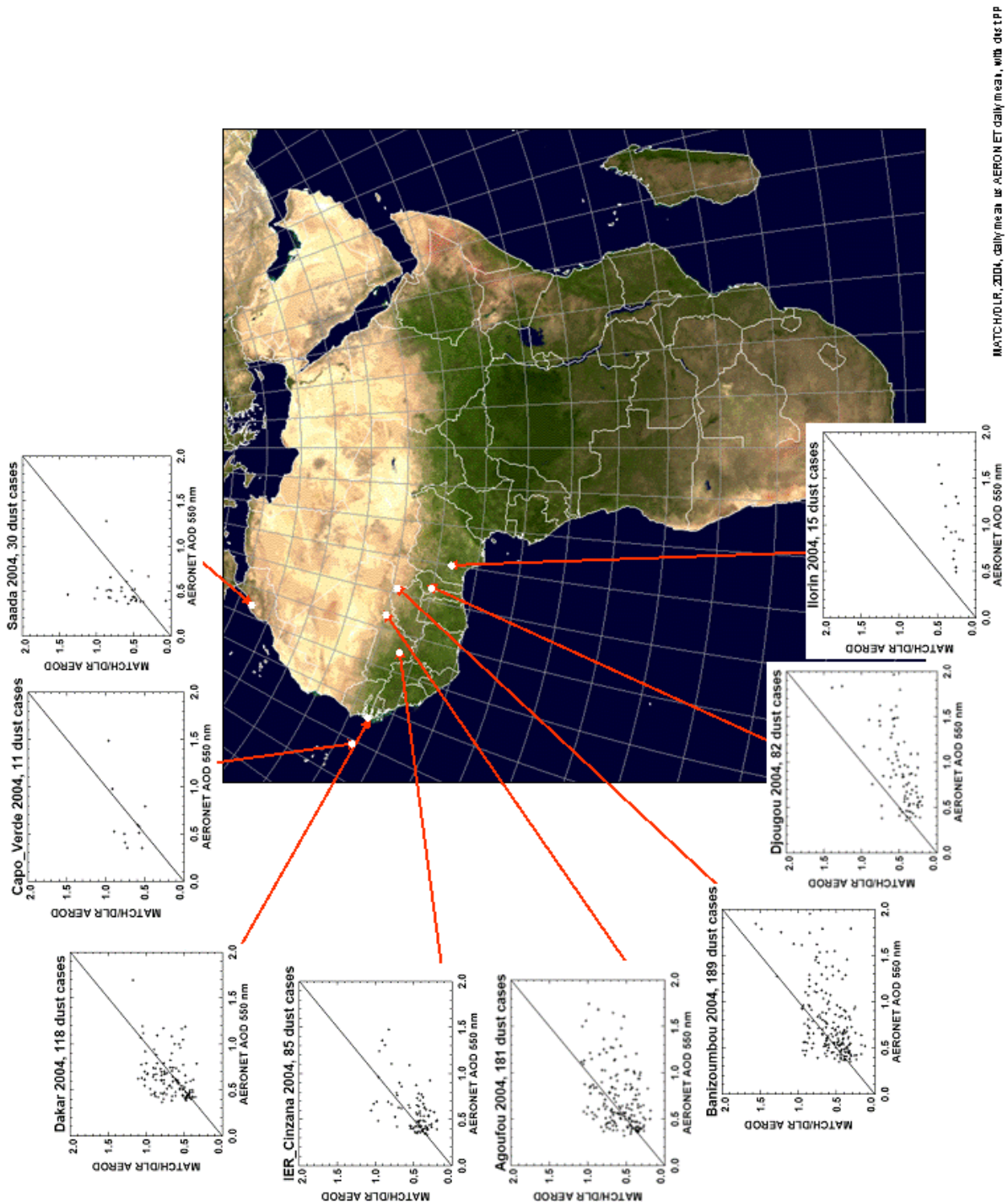


Fig. 5.27. Scatter plots for the NCAR/MATCH-MODIS dataset for all African AERONET validation stations for 2004, only dust cases as selected with the 'Dubovik criterion'

5.3.5 Asia

A similar validation of the DLR/MATCH data set against the Asian AERONET stations is shown in Fig. 5.28 for the total AOD at 550 nm. A separate analysis of dust cases based on the Dubovik criterion results is shown in fig. 5.29.

The AERONET stations in Beijing, Osaka, Shirahama, Gwangju, Taipei, Chen-Kung Univ., Chulalongkorn and Kanpur are located in large urban areas. There are probably dominated by local emission regimes and show a strong underestimation for AOD above 0.8.

Stations as Anmyon, Bac Giang, Beijing, Chen-Kung University, Chulalongkorn, Gwangju K-JIST, Kanpur, Mukdahan, Osaka, Pimai, Shirahama, Taipei CWB, and XiangHe which show in the DLR/MATCH dataset a strong underestimation for AOD above 0.8, have a strong scatter but a better correlation coefficient in the NCAR/MATCH-MODIS validation. This shows a positive impact of the MODIS data assimilation also in Asia. For Osaka and Shirahama (Japan) an improved RMSD (0.2 instead of 0.25 and 0.18 instead of 0.31) can be observed in the DLR/MATCH validation. Generally, the extreme overestimations observed in the NCAR dataset disappear in the DLR dataset and all values are damped to smaller values. On the other hand nearly all values above 0.8 can not be modelled in DLR/MATCH. Therefore the MBD is typically worse, while the RMSD is smaller. It can be interpreted, that the large overestimations in NCAR/MATCH-MODIS are caused by the sulfur problem as observed in Europe and therefore also improved in the 'no assimilation' DLR/MATCH run. On the other hand, the emission databases in MATCH seem to underestimate in Asia, which is corrected by the MODIS assimilation in the NCAR/MATCH-MODIS run.

The separate analysis of dust cases (fig. 5.29) reveal, that the underestimations are not caused by dust events, but by other aerosol components. Generally, the dust cases in Kanpur, India, are well met, while the other stations show only a small number of cases, which are generally underestimated. For Beijing, a partition in well met cases and underestimated dust cases can be observed.

As Asia is not in the current focus of the SESK project, a further analysis is not performed.

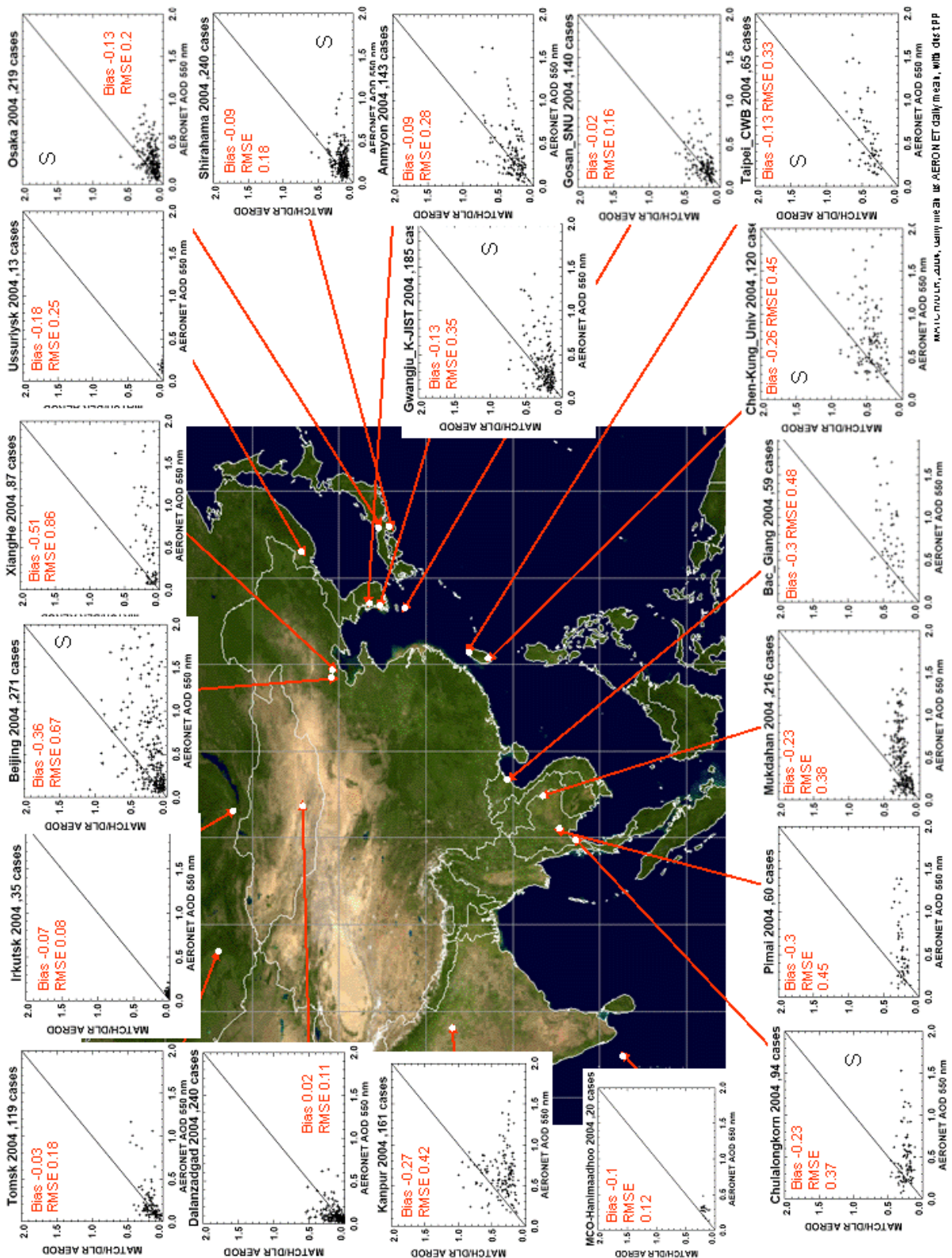


Fig. 5.28. Scatter plots for the NCAR/MATCH-MODIS dataset for all Asian AERONET validation stations together with mean bias deviation and root mean square deviation for 2004

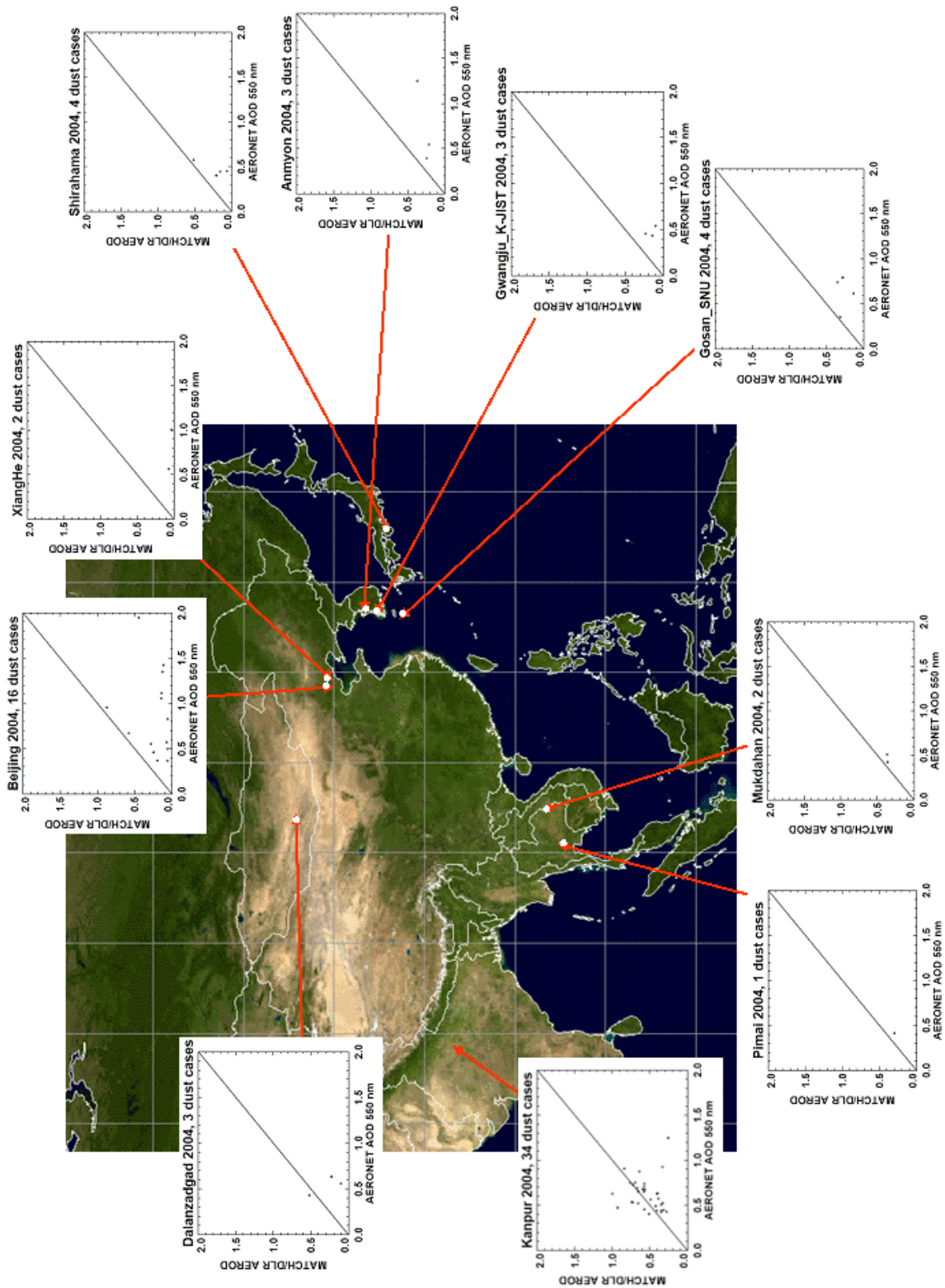


Fig. 5.29. Scatter plots for the NCAR/MATCH-MODIS dataset for all Asian AERONET validation stations for 2004, only dust cases as selected with the 'Dubovik criterion'

6 References

- Barth, M.C., P.J. Rasch, J. T. Kiehl, C.M. Benkovitz, S.E. Schwartz (2000): Sulfur chemistry in the National Center of Atmospheric Research Community climate Model: Description, evaluation, features and sensitivity to aqueous chemistry, *J. Geophys. Res.*, 105, 1387-1415
- Blanchard, D.C., A.H. Woodcock (1980): Production, concentration, and vertical distribution of the sea salt aerosol, *Ann. New York Acad. Sci.*, 338, 330-347
- Bonan, G.B. (1996): A land surface model (LSM version 1.0) for ecological, hydrological, and atmospheric studies: Technical description and user's guide, Tech. Rep. NCAR/TN-417+STR, National Center for Atmospheric Research, Boulder, Colorado, USA, Jan 1996
- Collins, W.D., P.J. Rasch, B.E. Eaton, B.V. Khattatov, J.-F. Lamarque (2001): Simulating aerosols using a chemical transport model with assimilation of satellite aerosol retrievals: Methodology for INDOEX, *Journ. Geophys. Res.*, Vol 106, No D7, 7313-7336
- Cooke, W.F., C. Liousse, H. Cachier, J. Feichter (1999): Construction of a 10 x 10 fossil fuel emission dataset for carbonaceous aerosol and implementation and radiative impact in the ECHAM-4 model, *J. Geophys. Res.*, 104, 22137-22162, 1999
- Dubovik, O., Holben, B., Eck, T. F., Smirnov, A., Kaufmann, Y. J., King, M. D., Tanré, D., and Slutsker, I. (2002). Variability of Absorption and Optical Properties of Key Aerosol Types Observed in Worldwide Locations. *Journal of the Atmospheric Sciences*, 59:590 – 608.
- Fillmore, D.W. (2005): Anthropogenic Aerosols and the Scattering and Absorption of Solar Radiation – Estimates of the Climatic Impacts through a Synthesis of Models and Satellite Observations, PhD Thesis, University of Colorado, USA
- Gillette, D.A. (1999): A qualitative geophysical explanation for hot spot dust emitting source regions, *Contributions to Atmospheric Physics*, 72 NO, 1, 67-77
- Ginoux, P., M. Chin, I. Tegen, J. M. Prospero, B. holben, O. Dubovik, S.-J. Lin (2001): Sources and distributions of dust aerosols simulated with the GOCART model, *Journal of Geophysical Research*, 106, No D17, 20255-20273
- Guenther, A., et al. (1995): A global model of natural volatile organic compound emissions, *Journ. Geophys. Res.*, 100, 8873-8892
- Gueymard, C.A. (2003): Direct solar transmittance and irradiance predictions with broadband models. Part II: validation with high-quality measurements. *Solar Energy* 74 (5), 381–395.
- Hack, J. J. (1994): Parameterization of moist convection in the National Center for Atmospheric Research Community Climate Model (CCM2), *J. Geophys. Res.*, 99, 5551–5568
- Herman, J.R., P.K. Bhartia, O. Torres, C. Hsu, C. Seftor, E. Celarier (1997): Global distributions of UV-absorbing aerosols from Nimbus 7/TOMS data, *Journ. Geophys. Res.*, 103, 6043-6058
- Hess, M., P. Koepke, and I. Schult (1998): Optical Properties of Aerosols and clouds: The software package OPAC, *Bull. Am. Met. Soc.*, 79, 831-844
- IEA, International Energy Agency/Organization for Economic Cooperation and Development (1997): Energy Statistics and Balances, IEA, Paris, diskette service, cited in Smith et al., 2001
- Iversen, J.D, B.R. White (1982): Saltation threshold on Earth, Mars, and Venus, *Sedimentology*, 29, 111-119
- Kalnay, E., M. Kanamitsu, R. Kistler, W. Collins, D. Deaven, L. Gandin, M. Iredell, S. Saha, G. White, J. Woollen, Y. Zhu, M. Chelliah, W. Ebisuzaki, W. Higgins, J. Janowiak, K.C. Mo, C.

-
- Ropelewski, J, Wang, A. Leetmaa, R. MReynolds, R. Jenne, D. Joseph (1996): The NCEP/NCAR 40-year reanalysis project, *Bull. Americ. Met. Society*, Vol 77, No 3, 437-471
- Kanamitsu, M. (1989): Description of the NMC global data assimilation and forecast system. *Wea. Forecasting*, 4, 334-342
- Kanamitsu, M., J.C. Alpert, K.A. Campana, P.M. Caplan, D.G. Deaven, M. Iredell, B. Katz, H.-L. Pan, J. Sela, G.H. White (1991): Recent changes implemented into the global forecast system at NMC, *Wea. Forecasting*, 6, 425-435
- Kettle, A.J., and 33 co-authors (1999): A global database of sea surface dimethylsulfide(DMS) measurements and a procedure to predict sea surface DMS as a function of latitude, longitude and month, *Global Biogeochem. Cycles*, 13, 399-444
- Kiehl, J.T., J.J. Hack, G.B. Bonan, B.B. Boville, D.L. Williamson, P.J. Rasch (1998): The National Center for Atmospheric Research Community Climate Model: CCM3, *Journ. Clim.*, 11, 1131-1149
- Kiehl, J.T., T.L. Schneider, P.J. Rasch, M.C. Barth, J. Wong (2000): Radiative forcing due to sulfate aerosols from simulations with the National Center for Atmospheric Research Community Climate Model, Version 3, *Journ. Geophys. Res.*, 105, 1441-1457
- Kinne, S., M. Schulz, C. Textor et al. (2005): An AeroCom Initial Assessment – Optical Properties in Aerosol Component Modules of Global Models. *Atm. Chem. Phys. Disc.*, **5**, 8285-8330.
- Lin, S.-J., R. B. Rood (1996): Multidimensional Flux-Form Semi-Lagrangian Transport Schemes, *Monthly Weather Review* 124, 2046-2070
- Liousse, C.J., J.E. Penner, C. Chunag, J.J. Walton, H. Eddleman, H. Cachier (1996): A global three-dimensional model study of carbonaceous aerosols, *J. Geophys. Res.*, 101, 19411-19432
- Marticorena, B., G. Bergametti (1995): Modeling the atmospheric dust cycle: 1. Design of a soil-derived dust emission scheme, *Journal of Geophysical Research*, 100, 16415-16430
- Olivier, J.G.J., A.F. Bouwman, C.W.M. Van der Maas, J.J.M. Berdowski, C. Veldt, J.P.J. Bloos, A.J.H. Visschedijk, P.Y.J. Zandveld, J.L. Haverlag (1996): Description of EDGAR Version 2.0, RIVM, Bilthoven, RIVM report nr. 771060 002/TNO MEP report nr. R96/119
- Patterson, E.M. (1981): Optical properties of the crustal aerosol: Relation to chemical and physical characteristics, *Journ. Geophys. Res.*, 86, 3236-3246
- Penner, J.E., J. Eddleman, T. Novakov (1993): Towards the development of a global inventory for black carbon emissions, *Atmos. Environ.*, 27, 1277-1295
- Rasch, P.J., N.M. Mahowald, B.E. Eaton (1997): Representations of transport, convection, and the hydrologic cycle in chemical transport models: Implications for the modeling of short-lived and soluble species, *Journ. Geophys. Res.*, 102, 28127-28138
- Rasch, P.J., M. Lawrence (1998): Recent development in transport methods at NCAR, Technical report, National Center for Atmospheric Research and Max Planck Institut für Chemie
- Rasch, P.J., J.E. Kristjansson (1998): A comparison of the CCM3 model climate using diagnosed and predicted condensate parameterizations, *Journ. Clim.*, 11, 1587-1614
- Rasch, P.J., M.C. Barth, J.T. Kiehl, S.E. Schwartz, C.M. Benkovitz (2000): A description of the global sulfur cycle and its controlling processes in the National Center for Atmospheric Research Community climate Model, Version 3, *Journ. Geophys. Res.*, 105, 1367-1385

- Rhyaboshpako, A.G. , P.A. Brukhanov, S.A. Gromov, Y.V. Proshina, O.G. Aginogenova (1996): Anthropogenic emissions of oxidized sulfur and nitrogen into the atmosphere of the Former Soviet Union in 1985 and 1990. Department of Meteorology, Stockholm University, Report CM-89.
- Sato, M., J.E. Hansen, M.P. McCormick, and J.B. Pollack (1993): Stratospheric aerosol optical depths, 1850-1990. *J. Geophys. Res.*, 98, 22987-22994, doi:10.1029/93JD02553.
- Schmidt, G. A., R. Ruedy, J.E. Hansen et al. (2006): Present-day Atmospheric Simulations Using GISS ModelE: Comparison to In Situ, Satellite, and Reanalysis Data. *J. Clim.*, 19, 153–192.
- Scholtz, M.T., Y.F. Li, C.M. Benkovitz, K.a. Davidson, E.C. Voldner (1998): A 1x1° global Sox and NOx 2-level seasonal emissions inventory resolved into emission sectors and point and area sources, unpublished manuscript, cited in Smith et al., 2001
- Shao, Y. (2008): 3rd International Workshop on Mineral Dust, 15 - 17 September, 2008, Leipzig, Germany. In Oral presentation: Progress and Challenges
- in Dust Emission Theory and Scheme. Smith, S.J., H. Pitcher, T.M.L. Wigley (2001): Global and regional anthropogenic sulfur dioxide emissions, *Glob. Biogeochem. Cycles*, 29, 99-119
- Staniforth, A., J. Côté (1991) Semi-Lagrangian Integration Schemes for Atmospheric Models—A Review, *Monthly Weather Review*, vol. 119, no. 9, 2206–2223
- Streets, D.G., S. Waldhoff (1998): Biofuel use in Asia and acidifying emissions, *Energy*, 23, 1029-1042.
- Tegen, I., I. Fung (1994): Modeling of mineral dust in the atmosphere: Sources, transport, and optical thickness, *Journ. Geophys. Res.*, 99, 22897-22914
- Tegen, I., P. Hollring, I. Chin, D. D. Fung, J. Penner (1997): Contribution of different aerosol species to the global aerosol extinction optical thickness: Estimates from model results, *Journ. Geophys. Res.*, 102, 23895-23915
- Ramanathan, V., M. Agrawal, H. Akimoto, M. Aufhammer, S. Devotta, L. Emberson, S.I. Hasnain, M. Iyengararasan, A. Jayaraman, M. Lawrance, T. Nakajima, T. Oki, H. Rodhe, M. Ruchirawat, S.K. Tan, J. Vincent, J.Y. Wang, D. Yang, Y.H. Zhang, H. Autrup, L. Barregard, P. Bonasoni, M. Brauer, B. Brunekreef, G. Carmichael, C.E. Chung, J. Dahe, Y. Feng, S. Fuzzi, T. Gordon, A.K. Gosain, N. Htun, J. Kim, S. Mourato, L. Naeher, P. Navasumrit, B. Ostro, T. Panwar, M.R. Rahman, M.V. Ramana, M. Rupakheti, D. Settachan, A. K. Singh, G. St. Helen, P. V. Tan, P.H. Viet, J. Yinlong, S.C. Yoon, W.-C. Chang, X. Wang, J. Zelikoff and A. Zhu (2008), Atmospheric Brown Clouds: Regional Assessment Report with Focus on Asia. Published by the United Nations Environment Programme, Nairobi, Kenya.
- Wittmann, M.; Breitkreuz, H.; Schroedter-Homscheidt, M.; Eck, M. (2008): Case Studies on the Use of Solar Irradiance Forecast for Optimized Operation Strategies of Solar Thermal Power Plants. *IEEE Journal of Selected Topics in Applied Earth Observations and Remote Sensing*, 1 (1), S. 18 - 27, ISSN 1939-1404, DOI: 10.1109/JSTARS.2008.2001152
- Zender, C.S. , H. Bian, D. Newman (2003): Mineral Dust Entrainment and Deposition (DEAD) model: Description and 1990s dust climatology, *Journal of Geophysical Research*, 108, D14, 4416-4434
- Zhang, G. J. and McFarlane, N. A. (1995): Sensitivity of climate simulations to the parameterization of cumulus convection in the Canadian Climate Centre general circulation model, *Atmos.-Ocean*, 33, 407–446

7 Abbreviations

AERONET	Aerosol Robotic Network
AOD	Aerosol Optical Depth
CAM	Community Atmosphere Model
DEAD	Mineral Dust Entrainment and Deposition model
DFD	Deutsches Fernerkundungsdatenzentrum
DLR	Deutsches Zentrum für Luft- und Raumfahrt
DMS	Dimethyl Sulfide
ECMWF	European Center for Medium Weather Forecast
EUMETSAT	European Organisation for the Exploitation of Meteorological Satellites
GACP	Global Aerosol Climatology Project
GAIA	Global Emissions Inventory Activity
LAI	Leaf Area Index
MATCH	Model of Atmospheric Transport and Chemistry
MBD	mean bias deviation
METEOSAT	meteorological satellites
METOP	meteorological operational satellite
MODIS	Moderate Resolution Imaging Spectroradiometer
MSG	Meteosat Second Generation satellite
NASA	National Aeronautics and Space Administration's
NOAA	National Oceanic and Atmospheric Administration
OPAC	Optical Properties of Aerosols and Clouds
PP	Post processing
RMSD	Root Mean Squared Deviation
SOLEMI	Solar Energy Mining database
UNEP	United Nations Environmental Programme
UTC	Universal Time Coordinated

8 Annex A – AERONET stations

Tab A.1: 147 European and African stations as used in the study (in the Meteosat field of view)

latitude [°N]	longitude [°E]	station height [m]	number of coincidences	station name
25.5	53.15	24	83	Abu_AI_Bukhoosh
24.48	54.33	7	4	Abu_Dhabi
15.35	-1.48	305	316	Agoufou
-15.58	-47.66	1100	0	Aguas_Emendadas
37.12	-3.23	2103	0	Ahi_De_Cara
43.7	0.25	80	0	Aire_Adour
24.25	54.55	40	0	Al_Dhafra
24.16	55.1	192	100	Al_Khaznah
24.13	53.03	5	44	Al_Qlaa
-9.92	-56.02	175	186	Alta_Floresta
69.28	16.01	379	0	Andenes
37.13	-3.24	691	0	Armillia
-7.98	-14.41	30	217	Ascension_Island
43.93	4.88	32	264	Avignon
38.53	-28.63	50	76	Azores
26.21	50.61	25	0	Bahrain
13.54	2.66	250	325	Banizoumbou
13.17	-59.5	0	0	Barbados
51.84	20.79	190	150	Belsk
-2.65	-54.95	70	81	Belterra
-28.25	28.33	1709	0	Bethlehem
43.48	-1.55	0	0	Biarritz
14.06	-2.45	0	0	Bidi_Bahn
36.51	2.88	230	220	Blida
16.88	18.55	179	0	Bodele
11.85	-3.75	0	0	Bondoukoui
44.79	-0.58	40	0	BORDEAUX
-0.83	-46.64	55	0	Bragansa
-15.92	-47.9	1100	0	Brasilia
44.45	26.52	44	0	Bucarest
51.97	4.93	-1	0	Cabauw
38.78	-9.5	140	193	Cabo_da_Roca
30.03	31.21	50	52	Cairo_University
16.73	-22.93	60	59	Capo_Verde
45.76	2.96	1464	0	Clermont_Ferrand
48.79	2.44	57	0	Creteil
-15.5	-56	250	0	Cuiaba
-15.73	-56.02	210	75	CUIABA-MIRANDA
23.72	-15.95	12	0	Dahkla
14.39	-16.96	0	219	Dakar
24.5	52.33	0	161	Dalma

31.1	35.45	410	0	Dead_Sea
24.48	54.38	15	203	Dhabi
25.51	56.33	81	161	Dhadnah
9.76	1.6	400	136	Djougou
51.03	2.37	0	65	Dunkerque
37.1	-6.73	0	302	EI_Arenosillo
37.61	15.02	736	40	ETNA
-19.17	15.91	1131	0	Etosha_Pan
38.57	-7.91	293	266	Evora
48.41	2.68	85	106	Fontainebleau
35.33	25.28	20	272	FORTH_CRETE
46.68	13.91	1900	0	Gerlitz
57.92	18.95	10	8	Gotland
37.16	-3.61	680	3	Granada
58.59	17.47	25	0	Gustav_Dalen_Tower
53.57	9.97	105	115	Hamburg
22.97	54.3	209	183	Hamim
54.18	7.89	33	40	Helgoland
77	15.55	0	0	Hornsund
13.28	-5.93	285	195	IER_Cinzana
51.35	12.44	125	129	IFT-Leipzig
8.32	4.34	350	66	Ilorin
39.91	8.5	10	0	IMC_Oristano
36.56	34.26	3	235	IMS-METU-ERDEMLI
-26.04	32.9	73	0	Inhaca
45.44	12.33	20	209	ISDGM_CNR
45.8	8.63	235	200	Ispra
28.3	-16.5	2367	0	Izana
24.06	55.78	1059	83	Jabal_Hafeet
-26.19	28.03	1736	0	Joberg
-14.86	24.83	1230	0	Kaloma
-14.79	24.8	1179	0	Kaoma
49.09	8.43	140	0	Karlsruhe
-10.17	31.18	1300	0	Kasama
12.92	-7.53	0	0	Katibougou
35.53	23.78	0	0	Kolimbari
43.58	4.82	32	0	La_Crau
47.48	8.35	735	125	Laegeren
35.52	12.63	45	111	Lampedusa
40.33	18.1	0	219	Lecce_University
50.61	3.14	60	71	Lille
78.22	15.65	30	30	Longyearbyen
24.7	54.66	10	56	MAARCO
53.33	-9.9	20	5	Mace_Head
43.28	5.38	100	0	Marseille
-19.9	23.55	940	0	Maun_Tower
23.15	53.78	204	124	Mezaira
-13.26	31.93	550	0	Mfuwe
53.92	27.6	200	88	Minsk

44.63	10.94	56	70	Modena
47	28.82	205	190	Moldova
-15.25	23.15	1107	238	Mongu
55.7	37.51	192	165	Moscow_MSU_MO
48.21	11.26	520	18	Munich_Maisach
48.57	11.57	533	0	Munich_University
24.37	54.47	10	75	Mussafa
-11.74	24.43	1430	0	Mwinilunga
-12.99	28.66	1270	0	Ndola
31.92	34.79	40	299	Nes_Ziona
45.43	12.38	13	10	Nicelli_Airport
51.22	2.92	23	0	Oostende
48.7	2.21	156	139	Palaiseau
41.99	-4.52	750	258	Palencia
48.87	2.33	50	7	Paris
36.93	-3.22	1252	0	Pitres
-11	-48	210	0	Porto_Nacional
50.37	-4.15	0	0	Rame_Head
43.49	5.38	208	0	Realtor
44.23	-77.59	0	0	Rochester
41.84	12.65	130	66	Rome_Tor_Vergata
48.33	7.62	167	0	Rossfeld
31.63	-8.16	420	158	Saada
24.83	55.31	84	111	Saih_Salam
-2.43	-54.75	70	0	Santarem
-23.56	-46.74	865	198	Sao_Paulo
30.85	34.78	480	310	SEDE_BOKER
-16.11	23.29	1025	0	Senanga
-17.48	24.3	951	0	Sesheke
25.22	54.23	10	60	Sir_Bu_Nuair
-24.99	31.59	150	279	Skukuza
-24.97	31.59	293	0	SKUKUZA_AEROPORT
24.25	55.61	250	55	SMART
24.25	55.61	250	58	SMART_POL
58.58	16.15	0	25	SMHI
24.91	46.41	650	284	Solar_Village
-12.17	26.36	1333	0	Solwezi
54.45	18.57	0	0	Sopot
-20.53	26.07	900	0	Sua_Pan
5.8	-55.2	0	0	Surinam
-22.66	14.56	250	0	Swakopmund
43.25	0.08	350	0	Tarbes
28.03	-16.63	10	0	Tenerife
35.55	8.68	1091	0	THALA
52.11	4.33	18	73	The_Hague
58.26	26.46	70	139	Toravere
43.58	1.37	150	176	Toulouse
-3.72	-49.68	100	0	Tukurui
-18.9	-48.28	850	0	Uberlandia

25.53	55.66	20	135	Umm_Al_Quwain
45.31	12.51	10	230	Venise
43.68	7.33	130	235	Villefranche
43.71	5.76	304	0	Vinon
-26.34	28.22	1775	0	Wits_University
57.04	59.54	300	68	Yekaterinburg
-13.53	23.11	1040	0	Zambezi

Tab A.2: 22 Asian AERONET stations used in the study

latitude [°]	longitude [°]	station height [m]	number of coincidences	station name
36.54	126.33	47	143	Anmyon
21.29	106.23	15	59	Bac_Giang
39.98	116.38	92	271	Beijing
23	120.22	50	120	Chen-Kung_Univ
13.74	100.53	115	94	Chulalongkorn
43.58	104.42	1470	240	Dalanzadgad
20.71	116.72	5	0	Dongsha_Island
33.28	126.17	0	140	Gosan_SNU
35.13	126.5	60	185	Gwangju_K-JIST
51.8	103.09	670	35	Irkutsk
26.45	80.35	142	161	Kanpur
6.78	73.18	0	20	MCO-Hanimaadhoo
16.61	104.68	166	216	Mukdahan
24.97	121.19	138	0	NCU_Taiwan
34.65	135.59	50	219	Osaka
15.18	102.56	220	60	Pimai
33.69	135.36	10	240	Shirahama
25.03	121.5	26	65	Taipei_CWB
56.48	85.05	130	119	Tomsk
43.7	132.16	280	13	Ussuriysk
39.75	116.96	36	87	XiangHe
61.66	129.37	118	69	Yakutsk